Dissertation
submitted to the
Combined Faculties for the Natural Sciences and for Mathematics
of the Ruperto-Carola University of Heidelberg, Germany
for the degree of
Doctor of Natural Sciences

presented by
Dipl.-Phys. M.Phil. Norman Sieroka
born in Bremervörde
Oral examination: 26.05.2004

# Neurophysiological Aspects of Time Perception

Referees:
Prof. Dr. Hans Günter Dosch / Prof. Dr. Hans-Joachim Specht
Prof. Dr. Michael Scherg

**Neurophysiologische Aspekte der Zeitwahrnehmung.**

In magneto- und elektroenzephalographischen (MEG/EEG) Experimenten wurde die Quellenstruktur und die Amplitude evozierter Felder bzw. Potentiale, die beim Erfüllen einer Aufgabe zur Diskrimination von Zeitintervallen auftreten, untersucht. Um deren Abhängigkeit von der Sinnesmodalität zu untersuchen, wurde die Aufgabe mit Tönen, Tonpausen, Bildern und Bildpausen durchgeführt. Hierbei zeigten sich aufmerksamkeitsspezifische Unterschiede in den evozierten Feldern der beiden sensorischen Areale und insbesondere bezüglich einer parietalen Hirnaktivität. Um zusätzliche, modellunabhängige Evidenz für den Ort und die Ausdehnung dieser Aktivierung zu gewinnen, wurde ein Teil der Aufgaben auch mittels funktioneller Kernspinresonanz (fMRI) untersucht. Weiterhin wurde der Zusammenhang zwischen Elektrophysiologie und Psychometrie untersucht. Bezüglich beidem spielte der Ton-Versuch eine herausragende Rolle. Hier war die parietale Hirnaktivität am stärksten ausgeprägt und korrelierte signifikant mit der individuellen Diskriminationsfähigkeit, die ihrerseits signifikant höher als bei allen anderen Aufgaben ausfiel. Weiterhin kovariierte für alle Aufgaben die Diskriminationsfähigkeit mit der rhythmischen Musikbegabung. Den Rahmen der Arbeit bildet ein Abriß neurophysiologischer und -psychologischer Untersuchungen zu den Themen Zeit- und Musikwahrnehmung. Dieser Abriß ist eingebettet in wissenschaftstheoretische Überlegungen, welche ihrerseits das Thema Zeit betreffen sowie die Aussagekraft psychophysischer Korrelationen (Leib-Seele-Problem).

**Neurophysiological Aspects of Time Perception.**

In magneto- und electroencephalographic (MEG/EEG) experiments the source structure and the amplitudes of the evoked fields and potentials recorded during the fulfillment of an attentional task on discriminating durations were investigated. This was done for tones, tone pauses, pictures and picture pauses to investigate the dependence upon sensory input and modality. The attention-specific differences found include primary sensory responses and a parietal activation in particular. The tone and tone pause tasks were also examined using functional magnetic resonance imaging (fMRI) to gather model-independent evidence for the location and extension of the parietal network. Further, the relation between electrophysiological and psychometric data was explored, where the study on tones played a crucial role. Here the strength of the parietal activity was largest, the individual discriminative abilities were highest and the two variables were found to be significantly correlated. Finally, the discriminative ability for all tasks covaried with the individual rhythmic musical aptitude. The frame of this work is given by a sketch of neurophysiological and -psychological findings on the perception of time and music; findings which get embedded into philosophical considerations on time and on psychophysical correlations (mind-body-problem).

For those who matter most: PMS, SLS, TJS

# Contents

# List of Figures

# List of Tables

# Chapter 1

# Introduction

This thesis tries to shed some light onto neurophysiological and behavioural processes involved in human time perception. The first motivation for such an enquiry is, of course, its intrinsic scientific interest. Second, however, there is also a more conceptual or philosophical interest, given that time plays a crucial role within our daily life and was tried to be understood long before we were equipped with whole-head magnetoencephalographic systems and magnetic resonance imaging scanners. Thus, this introduction sketches some main aspects of those different ways to investigate time.

A brief survey of the different domains or scales found in human time perception will be given by means of psychological findings. These will be added by neurophysiological results which attempt to reveal the concrete implementation of time perception mechanism inside our heads. The main underlying philosophical issues when engaging in such a work are the philosophy of time and, since relations between psychological and neurological states are concerned, the mind-body-problem. Hence, we will briefly introduce those themes. This will be done not only for matters of completeness. Indeed a reconsideration of philosophical positions after gaining scientific insights—and vice versa—can sometimes be fruitful (and for the given case of time perception we will witness such a prolific interaction). Finally, in this chapter the course of the thesis will be outlined.

## 1.1 The Perception of Time

> *Quid est ergo 'tempus'? Si nemo ex me quaerat, scio; si quaerenti explicare velim, nescio.* ([3], p. 628)
>
> St. Augustine, *Confessiones*

Some major findings within the psychology of time must be presented, before persuasive conjectures about its neurophysiological implementations can be made.

A 'time sense' is already reported about more than one-hundred years ago in the work of Ernst Mach; and around the turn of the nineteenth towards the twentieth century famously James, Wundt and others were investigating time perception (for an overview see [7], [86]). The first huge monograph to appear was Vittorio Benussi's 1913 *Psychologie der Zeitauffassung* [5]. Afterwards, however, the psychology of time was largely neglected, an exception being the French-speaking world as can be seen by the works of, e.g., Bergson, Bachelard, Piaget (for further references see [86]). In 1957 then, Paul Fraisse's epochal monograph *Psychologie du temps* put the topic back onto the world stage [28].

As a first attempt to describe the nature of time as experienced, one could state with John Michon:

> *Time is the conscious experiential product of the processes which allow the (human) organism to adaptively organize itself so that its behavior remains tuned to the sequential (order) relations in its environment.* [85]

The thing to notice is that time is not only a dummy parameter describing input-output relations; that is, it is not an epiphenomenon of our experiencing of the world. It is information itself and we can react discriminatively to stimuli that differ only in duration. Indeed the latter is what the main part of this thesis is about. To motivate the time scale on which we investigated duration discriminations, we first have to introduce the three prominent temporal domains found in the psychology of time as derived from experiments on time estimation, (re-) production and discrimination (for a comprehensive overview see [27]; we will also come back to the different time scales in the conclusion).

First, according to Fraisse [28] we have phenomena occurring on a time scale of about below 100 ms (the literature gives values between about 30–150 ms) which

are related, e.g., to the perception of stimulus features like pitch or loudness in the auditory domain. Second, we have the so called specious present which concerns longer lasting sensory input up to a duration of about 5 s (the literature gives upper limits of 2–8 s [7]; note that we do not follow the definition of the specious present as the minimum threshold for order perception which is also sometimes found in the literature). Third, we have the domain of larger temporal intervals which are related to memory processes (retrieval of stored information). This differs functionally from the specious present which is not related to processes of conscious retrieval but to the simultaneous processing of sensory information concerning an extended window in time. Thus, as we will see below, temporal awareness given to us by means of the specious present is of major importance for sense gathering in language and music; and it is this temporal domain which our neurophysiological experiments will investigate.

The psychological literature disagrees with respect to the differences between the modalities as, for instance, between the auditory and the visual system ('[...] the study of modality effects on perceived duration has had a checkered history [...]', [100]). However, there is a general tendency to assume the auditory modality to be 'the modality of time'. More on this will be reported in Chapter 6 when discussing our own data which also show auditory sensory input to play a distinctive role in discriminating durations. Further, the close connection between the auditory domain and the different temporal domains from above can be seen by looking at the main ingredients of music. A temporal regularity of an auditory stimulus with a time constant of less than 30 ms corresponds to the perception of pitch, followed by the perception of rhythm for stimuli with a greater time constant. For time constants of 1 s and more this turns into interval perception, whereas for temporal patterns of more than about 5 s the corresponding perception is that of musical architectural structure. Thus, pitch, rhythm and musical structure are reflected by the three temporal domains mentioned above—a fact also known in music theory (see the later work of the eminent jazz musician and composer George Russell, famous for his [114]; more specific literature on auditory stores is given by [16], [80]). There is also a microsecond scale which is responsible for sound localisation by processing interaural delays, but which we shall not consider any further.

There are, of course, further psychological issues involved in the analysis of time. The relation between time perception and production, for instance, is addressed in [110]. Further, many accounts on time estimation were brought forward as, e.g., a recent one by Glicksohn [34]. Assuming a constant pool of attention (an idea already prominent in the work of William James and Franz Brentano), he

separates external from internal attention. The more attention is paid to external phenomena the less our 'inner clock' is attended to. This in turn leads to smaller subjective time units the number of which increases with the level of arousal. Such a model accounts, for instance, for the common experience that exciting football matches appear short, while sitting in a dentist's waiting room appears to be endless. There are other models which try to implement retrospection phenomena in a similar way, since when looking back, the exciting football likely appears to have been lasted longer than the waiting for the dentist. However, many things have been criticised about such models and it is obvious that a complex interaction of several factors—as, e.g., the contents of that time period, the activities during that period and any time-related behaviour or judgements—takes place in the perception, production and estimation of time [7].

## Clock Mechanisms and Subcortical Systems

As already mentioned, the main concern of this thesis is the investigation of neurophysiological processes involved in time perception on the scale of the specious present. That indeed the different temporal domains are not only found in the psychological literature but are also reflected within neurophysiology, will be shown now. For an introduction into neurophysiological evidence for these matters as well as their anatomical implementations see, e.g., [10].

Many phenomena suggest the existence of an internal timing system. Different mechanisms have been proposed that form the basis for temporal information processing [54], [32]. Although differing with respect to details, they can be put into two major camps. First and more traditionally, temporal codes are assumed to rely upon endogenous oscillatory processes. According to Treisman the temporal pacemaker is composed of two parts: an oscillator and a calibration unit. The former produces an output at a constant frequency, which is re-scaled by the latter as a function of external influences and task demands—for further details see [138], [139]. We leave aside all speculations about the value of this constant frequency and how it relates to oscillatory brain activity like $\alpha$- and $\gamma$-band oscillations (see above) as found in the work of Treisman and in the time quanta approach proposed, e.g., in [31]. The brain areas where this timing mechanism is assumed to be neurophysiologically instantiated are the cerebellum and the basal ganglia [54], [32], [92]. These subcortical structures may form an integrated circuit with their respective roles yet to be defined. However, some of the literature suggests those areas to operate on different time scales; the cerebellum on the level of the millisecond processing and the basal ganglia on

the level of seconds [107]. This would, of course, challenge the idea of a single underlying oscillatory process, but could be coped with by the second type of timing systems. According to these so called network models, time is distributed across a set of neural elements, with the differing elements providing an interval-based representation. The representation of time might then be distributed across a set of interval timers, each with a particular processing cycle so that long and short intervals would be represented by distinct mechanisms. In this view, the exact elements recruited in the representation of time would be task-dependent. This network model as opposed to a single internal oscillatory clock is vindicated by several studies like, e.g., [55].

Very little is known about further *cortical* implementations of timing mechanisms, though monkey studies revealed single neurons within the parietal cortex to represent time [65]. Thus, the present investigations will concern the participation of cortical areas in the processing of time. This will be done in particular by recording electrophysiological responses like primary auditory evoked fields and the contingent negative variations, which reflect the processing of sensory features and perceptual expectancy, respectively. That this type of investigation should indeed be most fruitful, is also suggested by Michon, who maintains that ...

> *[...] there is little evidence for a relation between timing and such conspicuous periodical phenomena like the brain's alpha rhythm. Rather it seems that certain event related cortical responses, viz. the contingent negative variation [...] correspond somehow to the ways in which a person is coping with the temporal requirements of the environment.* [85]

Further, this type of electrophysiological response itself occurs on the time scale of the specious present (using stimuli on the scale of one second, the corresponding contingent variation will be of about the same duration); and, as we will see now, it is the specious present which also philosophically seems to be the most interesting time scale.

## 1.2 Philosophical Concerns: Time and the Mind-Body-Problem

> *I soon discovered that the 'problem of time' is rivaled only by the 'mind-body problem' in the extent to which it inexorably brings into play all the major concerns of philosophy.* ([126], p. 527)
>
> Wilfrid Sellars, *Time and the World Order*

The term 'specious present' was first introduced by the nineteenth century psychologist E.R. Clay. Its best known characterisation is due to William James, who in his *The Principles of Psychology* describes the specious present as follows:

> *In short, the practically cognized present is no knife-edge, but a saddle-back, with a certain breadth of its own on which we sit perched, and from which we look into two directions into time.* ([56], p. 609)

Indeed this concept of an extended present which is perceived all at once became very prominent around the time of James and can in different elaborations be found in the work of, for instance Wilhelm Wundt, Franz Brentano, Carl Stumpf and Edmund Husserl. For our purposes the conceptual analysis of the latter will be the most important one and we will come back to it shortly.

Besides, a philosophical investigation of specious present must not be confused with holding a so called presentist view of time. According to such a view only those parts of time exist which are present to us. This means that the past only exists in so far as it is still present to us or we remember it now. Something similar holds for the future as anticipated. Such a position was, e.g., held by St. Augustine in his *Confessiones* [3]. Notably, in his *De civitate Dei* Augustine relates time to the other main topic pertinent to our studies, viz. attention. For Augustine there is no such thing as attention in god, because god inhabits a divine omnipresent point of view. We human beings, however, lacking such a perspective on time, can only perceive parts of it (i.e. intervals) by focussing on them; i.e. by paying attention.

To see the conceptual importance of the specious present for human life, consider the way we understand an utterance like 'One-day cricket matches are exciting'. We somehow still have in mind the words 'one-day', 'matches', 'cricket' and

'are' when the speaker comes to say 'exciting' (together with a perception of their temporal succession). If that was not the case, we would not be able to understand the sentence or to distinguish it from other sentences ending with the same word (like 'Football matches are exciting'). Further, we are not consciously retrieving the previously uttered words to get the meaning at the end of the sentence; we do not think 'well, he said "matches" before and before that he said "cricket" ...' when hearing the word 'exciting'. Thus, the conclusion to be drawn is that meaning is largely ensured by our ability to perceive a temporally extended phenomenon at once; i.e. by the specious present. That this is generally true not only of speech but also of music is obvious, because similar arguments can be brought forward for the recognition of 'Frère Jacques' and for our ability to distinguish it from 'Happy Birthday' etc. [131].

Famously, such an account on inner time-consciousness and on the way we understand sentences, was held by the aforementioned German phenomenologist Edmund Husserl [52], [53]. Husserl, who talks of a 'Zeithof' (time halo) instead of a 'specious present' emphasises its *presentative* character. This means that the specious present integrates incoming phenomenological data to give a single impression or conceptual state. Notably, this does not involve processes of imagination, long-term memory or conscious retrieval. How far this distinguishes Husserl from other philosophers of that area, gets discussed in [131]. An interesting more recent and analytic elaboration on the specious present and on how to get from sensual to conceptual states can be found in the work of the American philosopher Wilfrid Sellars [127].

Thus, also on the level of conceptual states involving speech and music the fact that our interactions stay tuned with our environment follows in part from our inner-time consciousness as given by the specious present. This can be nicely illustrated further by means of a prominent distinction drawn in analytic philosophy. Going back to the work of J.M.E. McTaggart, A-times are commonly separated from B-times [83]. While the first are ordered according to the past-present-future relation, the latter are ordered by means of the earlier-later relation. Thus, while B-times can be presented by a time bar, A-times are tensed. If we introduce the corresponding beliefs it becomes apparent that A-beliefs are closely related to the specious present and essential for our daily life. This is because A-beliefs like 'There is a car coming from the right now' are very helpful when crossing a street. Whereas the corresponding B-belief that 'There is a car driving north through Dossenheim on the B3 at 3.12pm' would help very little as long as I have no (accurate) clock or do not know whether the street in front of me is the B3 or not. Thus, notorious discussions within analytic philosophy concern

the priority of A- over B-times. However, the fact that we *perceive* a specious present which is crucial for crossing the street and to our gathering of linguistic and musical meaning does not show its metaphysical priority. Indeed other than for the perceptual and epistemic level, B-times become extremely helpful in matters of metaphysics, for it is not easy to see how there could be tensed facts including indexical expressions like 'now' which make certain beliefs true [84]. For instance, one might believe 'There is a car coming from the right now' on two different occasions, where once it is true and the other time it is false. Two separate facts about different B-times could easily account for this: (i) 'It *is* the case, that there is a car driving north through Dossenheim on the B3 *at 3.12pm*'; (ii) 'It *is not* the case, that there is a car driving north through Dossenheim on the B3 *at 4.25pm*'. Two tensed facts about A-times, however, could not account for this, for they would have to state (i) that there *is* a car coming from the right *now* and (ii) that there *is not* a car coming from the right *now*. But this would be a contradiction.

Thus, the difference between A- and B-times partly reflects the difference between inner or psychological time and objective or physical time. This leads us to the famous distinction between primary and secondary qualities, where the former are linked to physical properties and the latter to perceptual experience. Note that sensory qualities do not characterise material objects according to their external properties. What we perceive are tones, not sound pressures. Or take the colour circle as an example: going from blue to violet will led one to red next, whereas there is no continuity in the wavelength going from violet to red. Thus, the internal relations (dimensions) between the perceived secondary qualities differ from those between the primary qualities of the (unprocessed) physical stimuli. In a recent highly respected habilitation thesis, Peter Lanz used this difference in internal dimensions as an argument for the intractability of the mind-body problem [62]. However, as we will see now by using recent findings on auditory perception of our group, (i) this difference in internal dimensions is questionable, but (ii) does not bother the persistent mind-body problem anyway.

Rupp et al. [113] investigated neuromagnetic responses in answer to auditory stimuli designed to excite the whole basilar membrane synchronously (so called 'chirps') and their time reversed counterparts (called 'anti-chirps'). Although the physical stimuli hence agree in their physical duration, their perceived compactness differs, i.e. it seems that one lasts longer than the other. Thus, the time reversal of the sound pressure definitely does not result in a temporal inversion of the perception. So far this seems to be grist to the mills of Lanz—now even providing evidence with respect to the dimension of time itself. However, the

problem with all the examples given is that so far we compared perceptions to *unprocessed* physical stimuli like the sound pressure curve of the chirps outside the human head. Yet, as soon as the processing of the chirps on the basilar membrane and in the auditory pathway is taken into consideration, the apparent differences between mental and physical states vanish. By using models for the inner ear and the auditory nerve and by looking at magnetoencephalographic recordings, which all present physical features of the processed stimulus, correlations to the perceptual differences between chirps and anti-chirps are found. In particular, for the given example the compactness of the stimuli as perceived 'is mirrored' in the neural excitation pattern of the different auditory channels.

Thus, the study by Rupp et al. illustrates that the claim by Lanz about the difference in internal dimensions between physical and perceptual states can become questionable as soon as sensory and cortical processing is taken into account. That, however, this finding does not really bother the mind-body problem is already seen from the simple fact that the correlation between perceptual experience and neural excitation pattern does not entail that the excitation pattern *is* the perception. A difference between mental and physical states is not explained by a correlation. In particular, famously one cannot read off causes and effects from a (probabilistic) 'constant conjunction'. Thus, it is rather the other way round that any amalgamation of neurophysiological and psychological findings asks for a justification. A rather naive one would be the identification of those two types of states by saying that, e.g., what seems to be a psychophysical correlation is really just evidence for the fact that mental states ultimately *are* physical states. Within philosophy there are, of course, more elaborate positions on, for instance, supervenience, which (though differing in details) maintain that there can be no change in mental states without a change in physical states.

Also within the neurophysiological literature these underlying problems have gained some interest, though the discussions widely differ in their level of philosophical sophistication—see, for instance, [101], [109], or [149]. On the one hand, there are rather naive conclusions like those about the non-existence of a free will drawn from a readiness-potential experiment by Libet et al. [68], or those about the neurophysiological 'counterpart' of a conscious state as given by $\gamma$-band oscillations as, e.g., in [21], [71] or [135] (for some more details on the philosophical relevance of these discussions see [129]). On the other hand, there are discussions like the one initiated through *Descartes' Error* by Antonio Damasio [17]. Damasio emphasised the role of affects and emotions in neurophysiological cognition processes, a theme fruitfully employed in scientific research—especially, in recent investigations on the psychology and neurophysiology of time perception and

episodic memory [1], [78], [111]. Further, *Descartes' Error* also had considerable influence upon quite revealing philosophic investigations on the role of emotions and affects in human cognition [46], [108].

The fact that the present work encompasses the search for psychophysical correlations in Chapter 7 is in part guided by examples like the work of Damasio which inspired a fruitful interaction between neurophysiology and philosophy. Further, the summary of our neurophysiological and psychometric findings in Chapter 8 will illustrate the appeal of one theory covering both the sensation and the perception of time, although the status of this theory itself is not so easy to judge upon. Before we can say something about such a possible theory, however, some empirical work has to be done. So here is what this thesis aims to investigate concerning neurophysiological aspects of time perception:

## 1.3 Thesis Outline

In the following Chapters 2–4 we will explore the neurophysiological activation during the performance of an auditory duration discrimination task. This will be done by means of magnetoencephalographic (MEG) recordings and functional magnetic resonance imaging (fMRI). The combination of these two methods will allow for gaining both spatial and temporal high resolution data sets. The two methods together with their respective advantages and disadvantages are explained in the Appendices A & B. The dependence upon auditory sensory input will be investigated by comparing a task where subjects are asked to discriminate tone durations (which are 'interrupted' by pauses) with the inverse task; i.e. a task, where subjects are asked to discriminate the durations of pauses which are 'interrupted' by tones. Next, we will investigate the modality-specificity of the neurophysiological activations by MEG recordings on visual duration tasks (Chapter 5). Again, tasks with and without sensory input to be discriminated will be applied (picture task and picture pause task). Apart from their brain responses, the subjects' performances during all MEG experiments will be evaluated to learn about (i) the relation between the performances over the different tasks and their relation to the individual musical aptitudes, and (ii) the relation between performances and neuromagnetic responses (Chapter 6 & 7). The methods employed are introduced in Appendix C (together with an alternative way of analysing the test on musical aptitude). Finally, a brief summary of the results and the implications for the philosophical issues raised in this introduction will be given in Chapter 8.

# Chapter 2

# MEG-Study on Discrimination of Tone Durations: Fitted Model

## 2.1 Introduction

Long-duration acoustic stimuli elicit a so-called sustained potential (SP) or sustained field (SF) measurable by electro- and magnetoencephalography. The sustained field is a primary sensory response that must be distinguished from the contingent negative variation (CNV), which reflects higher cognitive processes of expectancy. Sustained fields (potentials) can even be recorded during sleep as shown in 1978 by Picton et al. [102], whereas a CNV is generally assumed absent during sleep [102]. It is known from several studies that the sustained field is generated in the area of the auditory cortex (cf., e.g., [119], [96] or [97]). Picton et al. [102] also found that the amplitude of the sustained field is increased when subjects were given an attentional task in an oddball paradigm where the task consisted of differentiating tone bursts of 1.2 s (deviants) and 1.0 s duration (standards). This attentional effect, presented as a single EEG channel waveform (vertex against right mastoid) by Picton et al. [102], could be due to an enhanced activation of the generators of the sustained field or could be a CNV equivalent; i.e., a slow wave stemming from some cortical area other than the auditory cortex. Näätänen [90] conjectured that this increase in amplitude may result from a superimposition of a CNV type of wave rather than from a stronger activation of the generator mechanism of the sustained potential.

The present study focuses on whether and to what extent the effect found by Picton et al. [102] is due to the generators of the sustained field or to a CNV

equivalent. The former would suggest that the enhancement of activation elicited by attention is mainly of sensory auditory origin while the latter points to a different (higher) cognitive processing. A CNV equivalent should also be distinguishable from a sustained field by its slow increasing source waveform. This work also investigated the relationship between the subjects' performance in a duration discrimination and their neuromagnetic responses.

## 2.2 Material and Methods

The amplitude and latency of the components of the auditory evoked fields and potentials as recorded during the performance of a duration discrimination task were compared with those from a 'non-attend' condition. All experimental procedures were approved by the local ethics committee (Faculty of Medicine, University of Heidelberg).

### Stimuli and Tasks

An oddball paradigm with sinusoidal tones of 500 Hz was used. The standard tones which lasted for 1.0 s were interspersed with slightly longer deviants (1.2 s duration) in 20% of all cases (310 standard, 63 deviant tones). The tone sequence was pseudorandomised and presented with an interstimulus interval (ISI) of 1.35–1.40 s. The procedure was constrained in that the beginning of each sequence was marked by three standard tones and two deviants were never consecutive. Subjects were informed about these constraints to ease the task.

The tones were presented at a level of 65 dB SPL (measured by a Brüel & Kjær 2 CC Coupler). They had a 10 ms ramp at their start and end (Hanning window) and were generated digitally with a sampling frequency of 44.1 kHz. Digital-to-analogue conversion was done using a Soundblaster AWE-64 soundcard (Creative Labs Inc.) connected to a PC. The sounds were presented diotically using shielded transducers (Etymotic Research ET-3) equipped with 90 cm plastic tubes and foam ear pieces. In the 'attend' condition subjects were asked to press the button of a computer mouse in answer to a deviant while in the 'non-attend' condition they watched a silent movie of their choice. The order of the conditions was reversed for 8 of the 17 subjects to assess the effect of habituation.

## Subjects

Twenty subjects with no history of peripheral or central hearing disorders participated in the experiments after having given informed consent. Data from three subjects were rejected as one showed ocular artefacts accounting for more than 75% of the entire variance of the data while for two others the signal-to-noise ratio was too low to render a source model possible. The remaining group consisted of 11 right-handed male subjects with a mean age of 32 years (range 24–65 years) and of 6 female subjects, 5 of whom were right-handed, with mean age 31 years (range 25–37). The handedness was determined using the standard Edinburgh questionnaire [2].

All subjects participated in a magnetoencephalographic (MEG) recording for both 'attend' and 'non-attend' conditions while six of them took part in an extra session where MEG and EEG were co-registered.

## Recording and Data Processing

MEG data were acquired with a Neuromag-122™ whole head system housed in a magnetically shielded room (IMEDCO, Switzerland). Recordings were made at a sampling rate of 1000 Hz with application of a bandpass filter from 0.01 to 250Hz. EEG data were acquired using a 32 channel cap and a Synamp amplifier (Neuroscan Inc.). For the MEG-EEG co-registration the sampling rate was reduced to 769 Hz and only an online low-pass filter with cutoff frequency of 250 Hz was used. For the EEG data an offline bandpass filter from 0.1 to 15 Hz was applied (zero-phase shift, Butterworth filter, 6 dB/oct).

The data were analysed using the BESA2000® software package (MEGIS Software GmbH). Auditory evoked fields were averaged offline over an epoch from 500 ms before to 2300 ms after tone onset. Abrupt changes in amplitude with gradients of more than 800 fT/cm per sample were discarded automatically resulting in about a 5% rejection rate. The baseline was calculated over the 300 ms interval prior to tone onset.

## Source Analysis

All reported data are based on responses to standard tones; the resulting high number of tone bursts improved reliability.

The data were analysed with a spatio-temporal source model comprising one equivalent dipole near the expected location of the auditory cortex in each hemisphere. To estimate the source strength of the sustained field [120], a low-pass filter of 20 Hz (Butterworth filter, zero-phase shift, 12 dB/oct) was utilised and the dipole pair was fitted to the epoch 500–1050 ms post-stimulus onset without further constraints on location or orientation. This selection of epoch was guided by the end of the P200 wave and the decay of the sustained field after stimulus offset. The two-dipole model was adapted for each individual from the 'non-attend' condition and held fixed as a spatio-temporal filter for both the 'attend' and 'non-attend' condition.

A further analysis was carried out by including a further dipolar source fitted without constraints over the epoch of 500–1300 ms post-stimulus onset in the 'attend' condition. The lower boundary of this epoch was chosen to avoid an overlap with the P200 deflection, the upper boundary ensured that the slow increase and maximum of the source activity of the third dipole was covered for all subjects.

The source strength of the sustained field was assessed by calculating the mean dipole moment over the epoch 500–1050 ms post-stimulus onset which covered exclusively the plateau of the waveforms. The source strength of the third dipole was calculated over its maximum; i.e., the epoch 750–1200 ms post-onset.

Ocular artefacts were accounted for by a spatial filter [6]. For this purpose, a template was defined in the raw data starting from an artefact with high signal-to-noise ratio. The data were then scanned for further artefacts applying a correlation threshold of $r > 0.75$. To account for those artefacts in the spatio-temporal model, a principal component analysis (PCA) was computed. The first PCA component always explained more than 90% of the variance and hence was identified with the ocular artefact and included as a spatial component. To estimate the slow magnetic artefacts inherent in a recording with low cut-off frequency of 0.01 Hz, a PCA was computed for each average condition over the epoch 2100–2300 ms post-stimulus onset; i.e., 1100–1300 ms post-stimulus offset. The PCA component explaining the majority of the variance was included in the spatial filter for each experimental condition.

For twelve subjects individual anatomical T1-weighted 3D-MRI scans were available. The dipole locations were mapped onto the standard stereotactic space of Talairach and Tournoux [137] using the BrainVoyager® software (Brain Innovation B.V.).

### Statistics

The effect of attention was tested using an analysis of variance with repeated measurements performed with the dependent factors *source strength* (dipole moment of sources 1 to 3) and *attention* ('attend' vs. 'non-attend'). The influence of habituation was evaluated by the introduction of the additional independent factor order indicating which measurement condition subjects underwent first.

To investigate further descriptive and inferential statistics on the residual variances for all four combinations of models and conditions (two and three-dipoles; 'attend' and 'non-attend'), the percentage values were transformed using the standard arcsine function. An ANOVA with two dependent factors (*dipole number* and *attention*) was computed.

Due to the small number of subjects in the EEG experiment, all statistical evaluations on EEG data were based on Friedman's non-parametric analysis of variance. Statistical procedures were computed with the programme package SAS® (version 8).

## 2.3 Results

### EEG Data

The grand average for the channel waveforms as recorded from vertex (Cz electrode) against right mastoid was calculated (Fig. 2.1a). The main difference between the waveforms of the 'attend' and 'non-attend' condition is a significantly enhanced amplitude of the sustained potential (SP) when subjects performed the duration discrimination ($F_{1,5} = 6.00, p < 0.05$). The successive increase of the SP amplitude in the 'attend' condition was assessed by comparing its mean over the first half to that of the second; i.e., for the epochs 500–775 ms and 775–1050 ms. This increase was also found to be significant ($F_{1,5} = 6.00, p < 0.05$).

### MEG Data

The grand average source waveforms based on the individual two-dipole fits are depicted in Fig. 2.2. As in the EEG channel waveform, an increased amplitude of the sustained response is visible in the 'attend' condition. The statistic evaluation showed a significant effect of attention (significant increase in

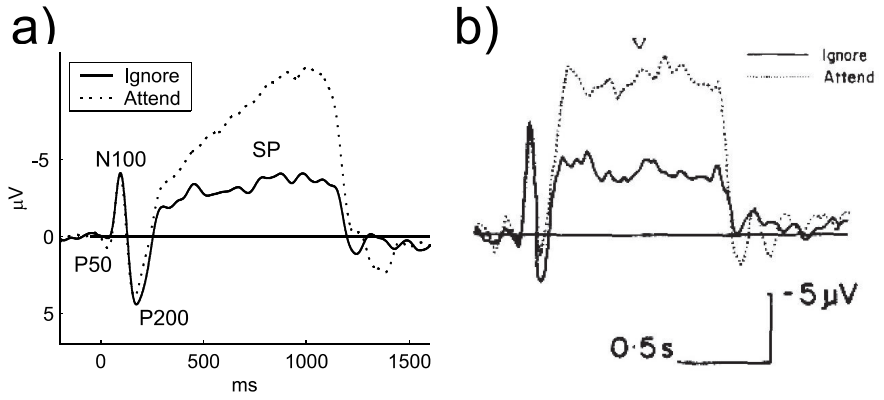


***Figure 2.1:*** *EEG Data: Auditory evoked potentials as recorded from vertex to right mastoid (a) in the present study (for N=6 subjects) and (b) by Picton et al. [102] for a single subject. The waveforms of both studies exhibit a significant enhancement of amplitude for the sustained potential (SP) in the 'attend' condition.*

dipole strength), but no significant interaction between attention and hemisphere (*attention*: $F_{1,16} = 7.27, p < 0.05$; *hemisphere* × *attention*: $F_{1,16} = 0.18, n.s.$). This model had an arcsine transformed mean residual variance of 30% (transformed SD: 4%; Range: 8–74%) for the 'attend' and 29% (transformed SD: 2%; Range: 7–50%) for the 'non-attend' condition over the epoch 500–1050 ms covering the plateau of the sustained field.

The grand average of the source waveforms for the three-dipole model are depicted in Fig. 2.3. We found both a significantly increased dipole moment for the attend condition as well as a significant interaction between attention and sources (*attention*: $F_{1,15} = 11.20, p < 0.01$; *attention* × *source*: $F_{2,30} = 4.41, p < 0.05$). Our analysis considered the effect of habituation during the two measurement conditions, but no significant influence was found (*attention* × *order*: $F_{1,15} = 0.00, n.s.$). Elementwise comparisons for each source yielded an approximate value for their contributions to the overall effect. In agreement with the results of Fig. 2.2, the largest effect was found for the third source ($F_{1,15} = 26.40, p < 0.001$). A smaller but still significant effect was also determined for the left sustained field ($F_{1,15} = 4.67, p < 0.05$) while the right lacked significance ($F_{1,15} = 1.24, n.s.$).

The top view in Fig. 2.4 for the difference between the channel waveforms for the 'attend' and the 'non-attend' conditions revealed a pattern of activation above the parieto-occipital region. Its slow linear increase over the epoch 500–1200 ms differs from the channel waveforms recorded by the sensors above the auditory cortices. The introduction of a third dipole could account for this residual ac-

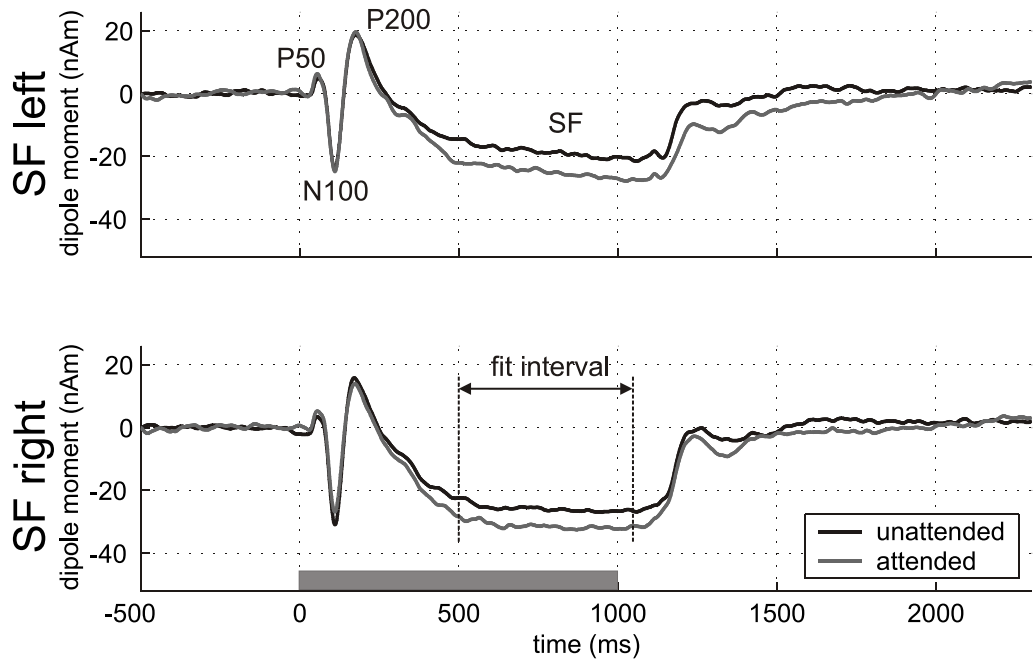


***Figure 2.2:*** *MEG Data: Grand average source waveforms for the 17 subjects in the two-dipole model. An attentional effect on the sustained field in terms of an increased amplitude is seen in both hemispheres. The gray bar indicates the temporal position of the standard tone. The spatio-temporal model is based on the epoch 500–1050 ms.*

tivation. The three-dipole model had a mean residual variance of 19% (SD: 2%; Range: 7–47%) for the 'attend' and 24% (SD: 2%; 5–44%) for the 'non-attend' conditions over the epoch 500–1050 ms. Compared to the two-dipole model this was a highly significant decrease in residual variance (*dipole number*: $F_{1,16} = 41.29, p < 0.0001$). The interaction between the different models and the attentional condition, which tests for the specific decrease in residual variance over the attentional conditions by introducing a third dipole, was highly significant (*dipole number* $\times$ *attention*: $F_{1,16} = 36.48, p < 0.0001$).

Using the individual 3D MRIs available for 12 of the 17 subjects we calculated the coordinates for the third source according to Talairach and Tournoux [137]. The average values were found to be $x = -5$ (SE: 7), $y = -50$ (3), $z = 37$ (7). All individual as well as the mean Talairach coordinates are presented in Fig. 2.5, which also shows an individual MRI scan for which the average and individual coordinates agree well. The mean is located in the area of the precuneus (PCu); however, due to the large standard error of means, the location of the third source cannot be separated from the posterior cingulate gyrus (postGC), which builds the dorsal boundary of the precuneus.

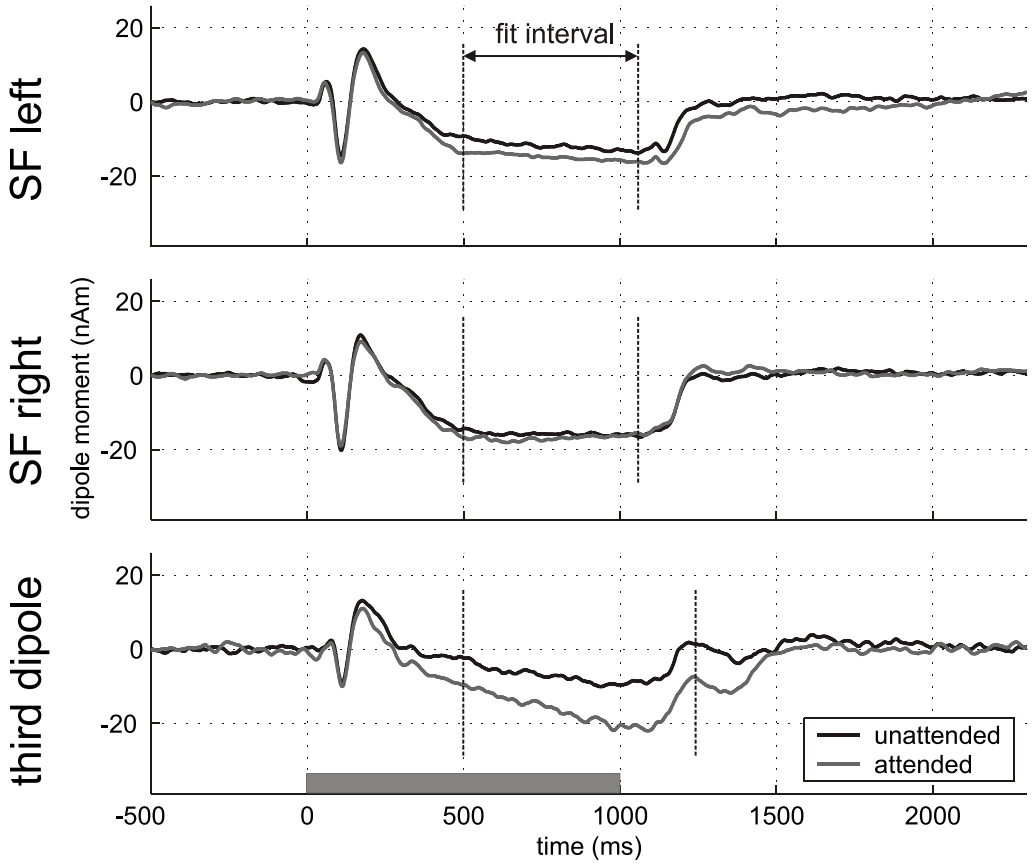


***Figure 2.3:*** *MEG Data: Grand average source waveforms for the 17 subjects in the three-dipole model. The major difference between conditions is seen in the waveforms of the third source. The left sustained field shows only a slight amplitude augmentation in the 'attend' condition while the right exhibits no substantial difference between conditions.*

### Transient Responses

The most prominent transient responses in the MEG, that is the P50, N100, and P200, were analysed with a spatio-temporal source model comprising one equivalent dipole near the expected location of the auditory cortex in each hemisphere. The dipoles were then fitted without further constraint over the respective epoch of the transient's maximum. However, in contrast to the sustained field, no significant attentional effect was found:

P50: *attention*: $F_{1,15} = 1.88, n.s.$;
N100: *attention*: $F_{1,15} = 0.23, n.s.$;
P200: *attention*: $F_{1,15} = 0.14, n.s.$

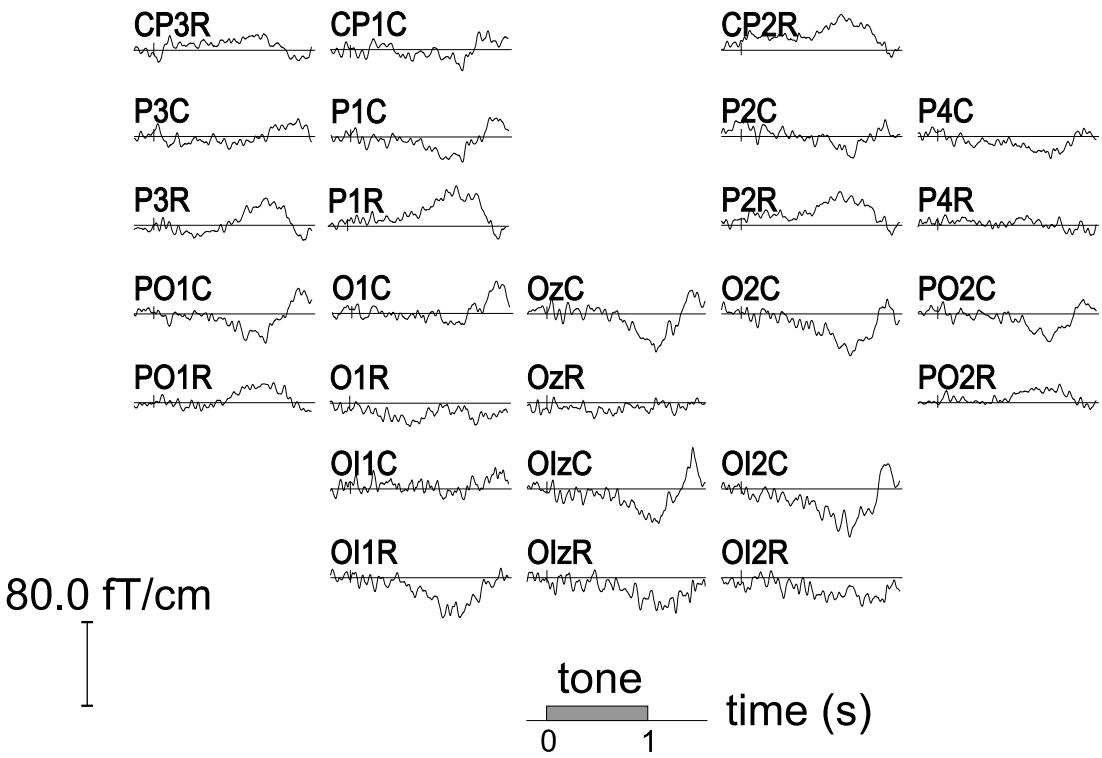


***Figure 2.4:*** *A subset of the MEG channel waveforms showing the sensor data above the parieto-occipital region. The difference between the channel waveforms for the 'attend' and the 'non-attend' conditions is shown for a single subject. The location of this activation as well as its linear increase over time differs from the auditory sustained field.*

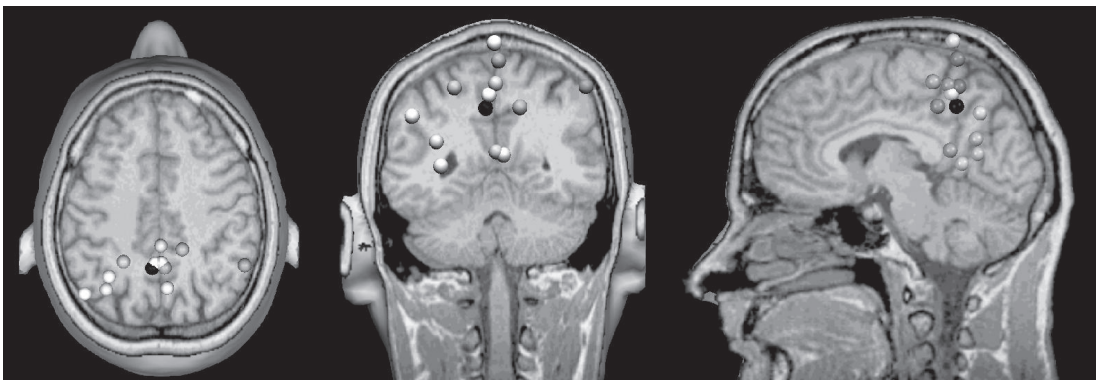

***Figure 2.5:*** *Location of the third source which accounts for the attentional effect in duration discrimination. The white balls represent the individual Talairach coordinates of the twelve subjects for whom a 3D-MRI data set was available. The black ball gives the mean Talairach coordinates* $x = -5$ *(SE: 7),* $y = -50$ *(3),* $z = 37$ *(7), which lies in the area of the precuneus (PCu). To illustrate the location, an individual MRI scan was chosen for which the average and individual coordinates agree well.*

## 2.4 Discussion

The aim of this study was to investigate the generator structure of the attentional effect found by Picton et al. [102]. When subjects were asked to discriminate tones of different duration, the sustained potential was increased by around 150% for the 'attend' condition (cf. Fig. 2.1a). This result is confirmed by our EEG (Fig. 2.1b).

A systematic comparison of the MEG data with respect to the transient components P50, N100, and P200 reveals no significant attentional effect; again, this is in perfect agreement with Picton et al. [102]. Whether these findings stand in opposition to those of Woldorff and Hillyard [144], will be discussed in Chapter 5, for only then will we be able to fully appreciate the difference in the attention-specific behaviour of auditory and visually evoked transient responses.

Two models (two and three dipoles) were investigated to account for the sustained responses. According to the two-dipole model with one dipole in the auditory cortex of each hemisphere (Fig. 2.2), the attentional effect was caused by an augmented activation of the sustained field generators. The statistical evaluation revealed a significant effect of attention with no significant interaction between attention and hemisphere. However, the magnitude of the attentional effect was much smaller in the MEG than in the EEG data. These results emphasised the inadequacy of the two-dipole model for the MEG data. The three-dipole model was significantly supported by our data. Though the decrease in residual variance when including an additional dipole is trivial, the highly significant interaction between the number of dipoles and the experimental condition is not. If the third dipole modelled only noise, then the decrease in the residual variance would be expected to be the same for the 'attend' and the 'non-attend' conditions. However, the much larger decrease in the 'attend' condition showed that the third dipole in the attend condition modelled source activation. Further, the top view of the difference between the 'attend' and the 'non-attend' conditions revealed an additional activation above the parieto-occipital region with a different waveform morphology (Fig. 2.4).

The location of the third dipole, estimated by calculating the mean Talairach coordinates, was found to be the precuneus or the posterior cingulate gyrus.

In contrast to the two-dipole model, the introduction of the third source resulted in an even smaller attentional difference in the waveforms reflecting activation in the auditory cortices. The prominent attentional effect was thus due to the third dipole (Fig. 2.3), the amplitude of which was increased by about 150% in the

'attend' condition. The magnitude of the attentional effect was thus the same as in the EEG data where vertex vs. right mastoid was measured. This differed from the MEG two-dipole configuration where the magnitude of the attentional effect was considerably smaller (see Fig. 2.2).

Our findings correlate with other studies in electrophysiology and functional imaging. The fact that the third source showed an increasing attentional effect fits well with a further experiment performed by Picton et al. [102]. They presented 1000 Hz sinusoidal tones, which endured for eight seconds and were interrupted by a pause of either 1.5 s (standard) or 2.0 s (deviant), for discrimination between the different pause durations. They recorded an 'attend' and an 'ignore' condition and found an increasing potential in response to the pauses of the 'attend' condition (vertex vs. right mastoid). Since pauses are not acoustic stimuli, duration discriminations correlate with an increasing potential which is not auditory-specific. This is exactly the result found with respect to the third source of the current study. It showed an increasing activation with the same waveform morphology as to be seen in the EEG channel data of the pause experiment by Picton et al. [102]; and it did not lie within the auditory cortex and might well be involved in discriminating pauses. Recent fMRI and PET studies found the precuneus and the posterior cingulate gyrus, proposed here as locations of the third source, to be involved in tasks on pitch discrimination [103], [70], auditory-verbal memory [38] and deaf-hearing [22]. In addition, the precuneus is known to be activated during processes of imagery and retrieval [25], [26] which led Satoh et al. [115], who found an activation in that area in musicians asked to listen to the altopart of a motet, to maintain that subjects were 'writing tones on a mental score'.

An attention-dependent response known to be related to the cingulate gyrus is the 'contingent negative variation' or CNV [82], [141]. The standard CNV paradigm consists of a warning stimulus S1 followed by an imperative stimulus S2; some attentional task is to be performed in answer to S2 with an interstimulus interval of the order of a few seconds [51]. The electrophysiological response between S1 and S2 is a successively increasing negative deflection or 'expectation-wave' [51]. The standard CNV paradigm itself is implicitly related to any attentional task involving duration discrimination as in the present study. In our experiments subjects heard the beginning of an ongoing sound, had to 'measure' it until its end, and then had to decide whether it was a standard or a deviant. Thus, the tone onset was equivalent to a warning stimulus S1 and the tone offset resembled an imperative stimulus S2, showing the close connection between a CNV paradigm and the present study. Furthermore, the morphology of the source

waveform of our third source which depicted a CNV-type slow wave can be considered an 'expectation-wave'. This agrees with the view of Picton et al. [102] in that the increase in amplitude is related to auditory expectancy and supports Näätänen's [90] conjecture that the difference in activation is due to a superimposition of the sustained field and the CNV and not to an enhanced sustained field alone. We were able to locate this 'expectation-wave' in the area of the precuneus or the posterior cingulate gyrus.

A functional explanation for the activation of the third dipole and the enhanced left sustained field can be proposed. Some type of duration templates become encoded in the precuneus or the posterior cingulate gyrus. As soon as a new tone is presented, a comparison mechanism begins since the subject must decide whether the duration of the actually presented tone agrees with his or her template. The fact that the enhancement in the sustained field was only significant for the left hemisphere may be explained by the work of Zatorre and Belin [147] who found that temporal processing, and hence the processing of encoded and actual duration, predominantly takes place in the left hemisphere whereas spectral processing is assumed to be more prominent in the right hemisphere.

Although our data is in very good agreement with the literature, further direct evidence for the location of our third source as well as for its functional role is searched for. First, to see whether the location of our third source can be replicated in an model-independent way, the discrimination task was implemented in a fMRI-study (cf. Chapter 3). Second, to learn more about the functionality of the additional source—its need for auditory input, in particular—also the discrimination of pause durations got examined both in a fMRI- and a MEG-experiment (cf. Chapters 3 & 4). The investigation on functionality was rounded off by looking at the discrimination of filled and empty durations within a further modality; namely vision (cf. MEG-experiments in Chapter 5).

# Chapter 3

# fMRI-Study on Discrimination of Tone & Tone Pause Durations

## 3.1 Introduction

In Chapter 2 we found strong evidence for an additional parieto-occipital activation in a tone duration discrimination task. However, since any MEG dipole analysis suffers from the non-uniqueness of the inverse problem, it is desirable to access and locate duration-specific brain activation in a model-independent way. For this purpose we turned the stimulation of the MEG study in Chapter 2 into a block design to allow for a functional magnetic resonance imaging (fMRI) experiment using sparse imaging.

The second aim of the present experiment concerns the attentional effect within the auditory cortex. In our MEG study we found an attention-specific enhancement for the left sustained field. Though the time course of the MEG source waveforms clearly separates this effect from the parieto-occipital activation, it is of major interest to see whether the auditory blood oxygen level-dependent (BOLD) responses exhibit this effect as well (cf. the brief discussion on sensitivity of fMRI and MEG in Appendix B).

We conducted a fMRI experiment focussing on our target regions, i.e. the auditory cortices and parieto-occipital regions including the following Brodman areas: BA 7, 19, 39 and 40. To avoid time-consuming whole brain imaging we thus left out other areas known to be involved in time perception; i.e. basal ganglia, cerebellum and prefrontal areas. For a brief introduction of the subcortical networks

see Chapter 1, the prefrontal areas will be discussed to some extent at the end of this chapter.

An immediate follow-up question, when investigating the discrimination of tone durations, is whether and to what extent the attention-specific activations depend on sensory input. Hence, a further fMRI experiment was conducted where subjects had to attend intervals which lack sensory input; i.e. the original fMRI block stimulation was inverted and subjects had to discriminate pause instead of tone durations (in the discussion of Chapter 2 we already mentioned an EEG experiment on pause durations conducted by Picton et al. [102]).

## 3.2 Material and Methods

### Stimuli and Tasks

Three sessions were conducted in the following order: a tone discrimination task, a control recording and a pause discrimination task. Each session consisted of 96 scans.

The general design of the sessions is given in Fig. 3.1. For the tone discrimination task the stimuli were 500 Hz tones lasting for 1.0 s (standards) and 1.2 s (deviants). There were five conditions in the experiment: four sound conditions and one silent baseline (condition 5). The sound conditions—also shown in Fig. 3.2—all contained three tones, either two standards and a deviant at the first, second or third position (conditions 1–3), or three standards (condition 4). Conditions 1–3 each occurred 8 times, together matching the 24 repetitions of condition 4. All sound conditions taken together matched the number of silent baseline conditions (48). Subjects were asked to press one of two buttons after each sound condition (i.e. within the scanning interval); one if they thought a deviant had occurred, the other if not. The sound conditions were presented in randomised order, and each one was followed by a silent baseline condition. Subjects were informed about this constraint to ease the task (providing them a better 'orientation').

The pause discrimination task used the exact inverse of the sound conditions of the tone discrimination task; i.e. pauses of 1.0 s (standards) and 1.2 s (deviants) were separated by 500 Hz tones, condition 4* only entailed standard pauses etc. Again, the silent baseline condition was used 48 times. The duration of all pauses and tones within the sound conditions was balanced so that there was no net difference in the stimulation for the tone and the pause discrimination task.

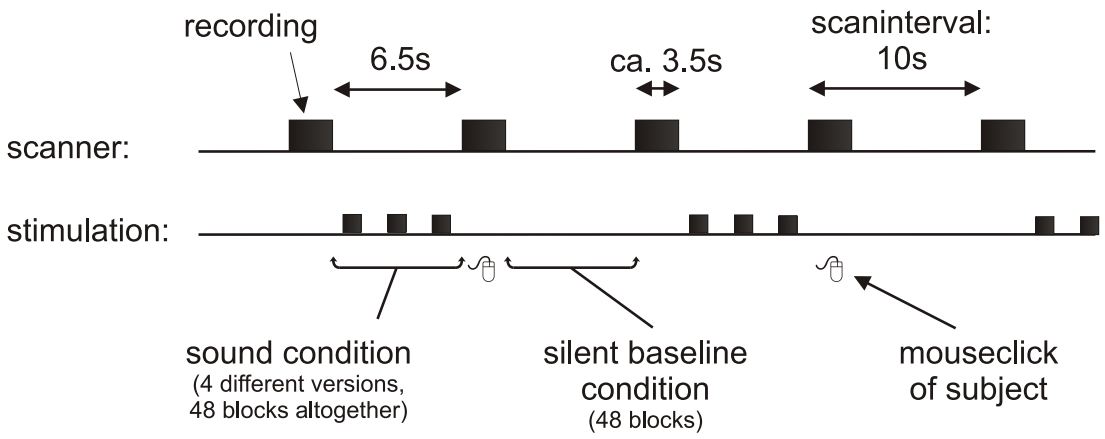


***Figure 3.1:*** *General design of the tone and the pause discrimination task. Sparse imaging allowed for investigating the BOLD signal in response to the stimuli and the attentional task rather than to the scanner noise. The control session only differed in so far as two different sound conditions instead of four were used (but still making up 48 blocks altogether).*

The control recording consisted of silent baseline conditions (48 scans) and of standard sound conditions (24 times condition 4 and 24 times condition 4*). Subjects were asked to press a button after each sound condition. This was done to avoid net effects stemming from motor responses when computing contrasts between the task sessions and the control recording. Since subjects were informed about the alternation of sound and silent baseline conditions, the attentional load of the control recording was negligible as compared to the task sessions.

## Subjects

Six subjects (taken from the MEG sample of Chapter 2) with no history of peripheral or central hearing disorders participated in the experiments after having given informed consent. The group consisted of a 26 year old female and 5 male subjects. The latter had a mean age of 37 years (range 25–67 years). All subjects were right-handed as determined by the standard Edinburgh questionnaire [2] and participated in all three experimental sessions mentioned above.

## Data Acquisition

Sparse imaging was used to enable examination of activation due to the stimuli and the attentional task in the absence of the effect of scanner noise. This

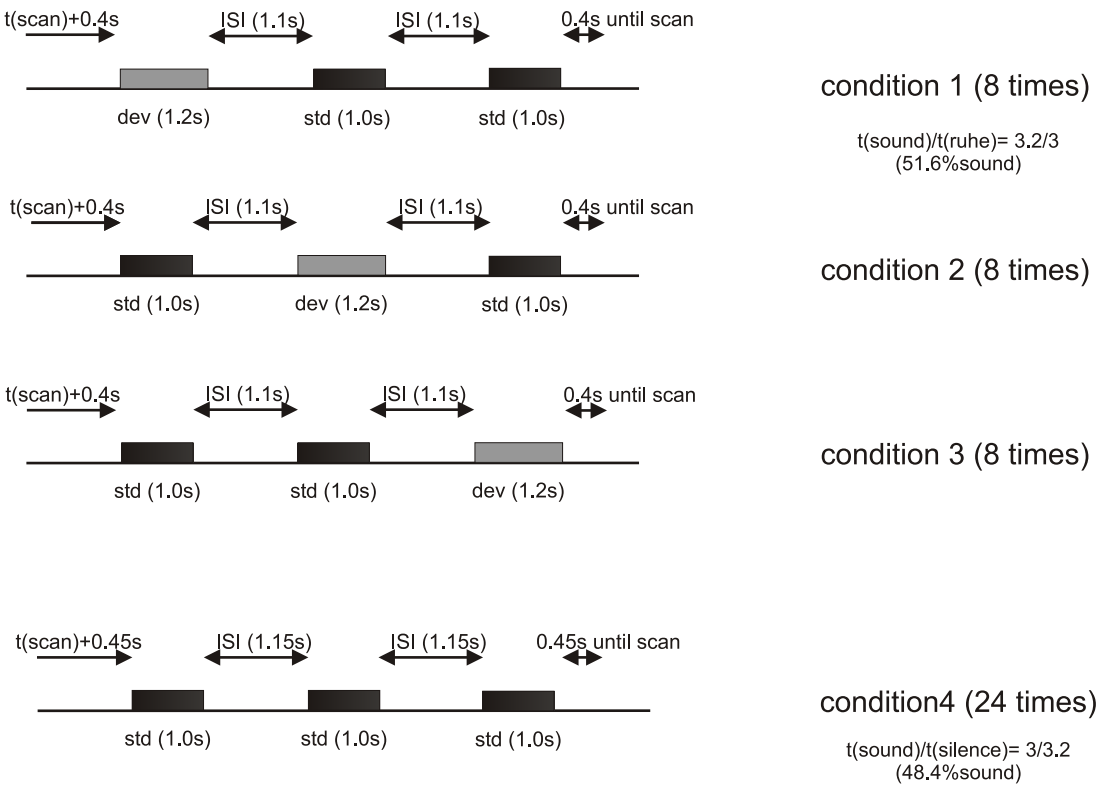


***Figure 3.2:*** *Different sound conditions of the tone discrimination task. Sound and pause intervals were balanced to avoid net differences as compared to the pause discrimination task, which employed the exact inverse of the conditions shown; i.e. pauses were replaced by sounds and vice versa.*

is achieved through the acquisition of brain images just after lengthy periods of stimulus presentation and task performance, during which there is no image acquisition and, hence, no noise generated by the scanner. Thus, it uses the sluggishness of the BOLD response—cf. Fig. B.4 in Appendix B. Sparse imaging is a commonly used method for the investigation of sound processing [42], [99].

Sound stimuli were presented to both ears at a level of approximately 65 dB SPL. BOLD contrast image volumes were acquired using a 1.5 T MRI scanner (Siemens, SONATA, Erlangen) with gradient-echo-planar-imaging (TR= 10,000 ms; TE= 77 ms). A total of 21 slices were acquired covering the temporal, parietal and occipital regions of interest ($3 \times 3 \times 3\,\mathrm{mm}^3$). A T1-weighted high-resolution ($1.4 \times 1 \times 1\,\mathrm{mm}^3$) structural image was collected from each subject on the same MRI system to allow for rendering BOLD activation onto individual anatomy.

## Data Processing and Analysis

All structural and functional data were processed and analysed using SPM2 (`http://www.fil.ion.ucl.ac.uk/spm`). Each BOLD and the structural time series was realigned to its first image and then normalised using affine nonlinear spatial transformations. The template used for the BOLD series was the standard SPM EPI template, for the structural data it was the standard SPM T1 template. Finally, the functional data were smoothed with a Gaussian filter of 5 mm (full width at half maximum). The location of the significant BOLD responses, given in MNI space, were transformed into Talairach coordinates. The transformation matrix together with some further discussion on common brain spaces is given in Appendix B (equation B.6).

Fixed-effects analysis was carried out on individual (288 scans) and group data (1728 scans) using the SPM general linear model. The significance level for group activation was $p < 0.05$ corrected for multiple comparisons across the whole volume. This corresponded to a height threshold of $T > 4.95$. Thus, the group contrasts presented only show highly significant activations with very few false detections. In contrast, the presentation of the individual data is much less conservative as to illustrate the inter-individual variability (in particular for the attention-specific activities). The significance level for the individual data was set to $p < 0.001$ (uncorrected), which corresponded to a height threshold of $T > 3.13$. More on the motivation and definition of corrected and uncorrected significance levels is presented in Appendix B.

The following four (kinds of) contrasts were calculated:

- 'sound-silence': the responses to the silent baseline conditions were subtracted from those to the sound conditions (48 vs. 48 scans) for each session—in the following the resulting contrast for the second (control) session is called 'sound-silence control';
- 'attention sound': 'sound-silence control' was subtracted from the sound-silence contrast of the tone discrimination task;
- 'attention pause': 'sound-silence control' was subtracted from the sound-silence contrast of the tone pause discrimination task;
- 'attention pause-sound': to assess attention-specific differences between discriminating pause durations and tone durations, 'attention sound' was subtracted from 'attention pause';

- 'attention standard sound': to estimate possible differences between BOLD responses to deviants and standards, the 'attention sound' contrast was also calculated using only standards; that is, only condition 4 (and not 1–3) was used for the evaluation of sounds in session 1.

## 3.3 Results

### Control Condition

The contrast 'sound-silence control' revealed activation spread over auditory sensory and premotor areas. The occurrence of the latter was due to the fact that subjects were asked to press a button after each sound conditions (to avoid net effects due to motor responses when it comes to the attention-specific contrasts). The areas activated were the left and right premotor area (PreMA) being localised above the auditory cortices (this is also where the index finger is represented) and the pre-supplement motor area (Pre-SMA) in the medial frontal gyrus (BA 6 and 32).

The auditory activation showed a prominent substructure for both hemispheres consisting of three 'hotspots' with an extension of about 5 mm in each direction. Here the fronto-lateral one was the most prominent. All Talairach coordinates are given in Table 3.1. The group and the individual data are shown in glass brain representation in Fig. 3.3 & 3.4. As mentioned above, individual data are presented with a much lower significance threshold to illustrate the inter-individual variability, rather than the very robust effects we are interested in when analysing the whole group. However, the strong inter-individual variability of the auditory responses as seen in the glass brain representation of Fig. 3.4 is largely explained by individual anatomical differences. Rendering the BOLD responses onto individual structural MRI data reveals that for all individuals the main activations stemmed from the auditory cortices—cf. Fig. 3.5. If posterior duplications are considered to be proper parts of the individual Heschl's gyri (cf. S6 in particular), we can even claim that all major responses stemmed from Heschl's gyri.

Further, the three prominent BOLD responses found in the auditory cortex were compared to average anatomical landmarks and locations of MEG source analyses. Here the anatomical standard map by Leonard et al. [66] showed a certain tension as compared to our data—cf. Fig. 3.6. It suggested that only a little part of the BOLD responses stemmed from the individual Heschl's gyri, which appeared disputable when looking at the individual functional-anatomical compar-

| auditory activation | Talairach coord. $x_{\mathrm{Tal}}$ | $y_{\mathrm{Tal}}$ | $z_{\mathrm{Tal}}$ | $T$-value |
|---|---|---|---|---|
| right medial | 39 | -25 | 7 | 6.53 |
| left medial | -32 | -34 | 3 | 15.04 |
| right fronto-lateral | 56 | -18 | 8 | 13.00 |
| left fronto-lateral | -50 | -21 | 2 | 19.53 |
| right dorso-lateral | 52 | -31 | 3 | 13.88 |
| left dorso-lateral | -47 | -32 | 7 | 14.85 |

***Table 3.1:*** *Talairach coordinates for the three most prominent BOLD responses stemming from the left and right auditory cortex respectively.*

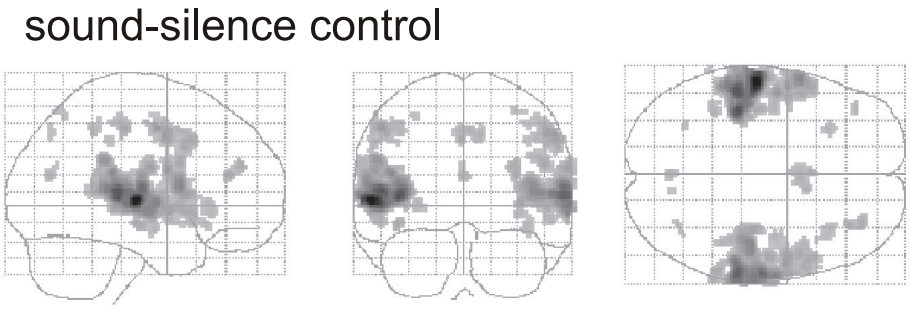


***Figure 3.3:*** *Group Data: Contrast between sound conditions and silent baseline conditions for the control recording ('sound-silence control'). The activation of the auditory sensory areas consists of three core regions. The fronto-lateral one is the most prominent. Since subjects were asked to press a button after each sound condition, also preparatory motor responses occur (left and right premotor area, pre-supplement motor area). Conservative statistics with a corrected significance level of* $p < 0.05$ *(corresponding to a height threshold of* $T > 4.95$*) were used to present only highly significant activations with very few false detections.*

isons in Fig. 3.5. Knowing about the inter-individual variability of Heschl's gyri, we then used a map provided by Peter Schneider (personal communication) into which also the anatomical landmarks of our six subjects had entered. Indeed this map turned out to be more in accord with our individual functional-anatomical comparisons, for now most of the BOLD signal appeared to originate from Heschl's gyrus. This can be seen in Fig. 3.7, which also provides a comparison to the locations of prominent auditory responses as found by recent MEG studies. To make such a comparison even more immediate, Fig. 3.8 shows MEG source localisations only of those subjects who participated in the fMRI experiment.

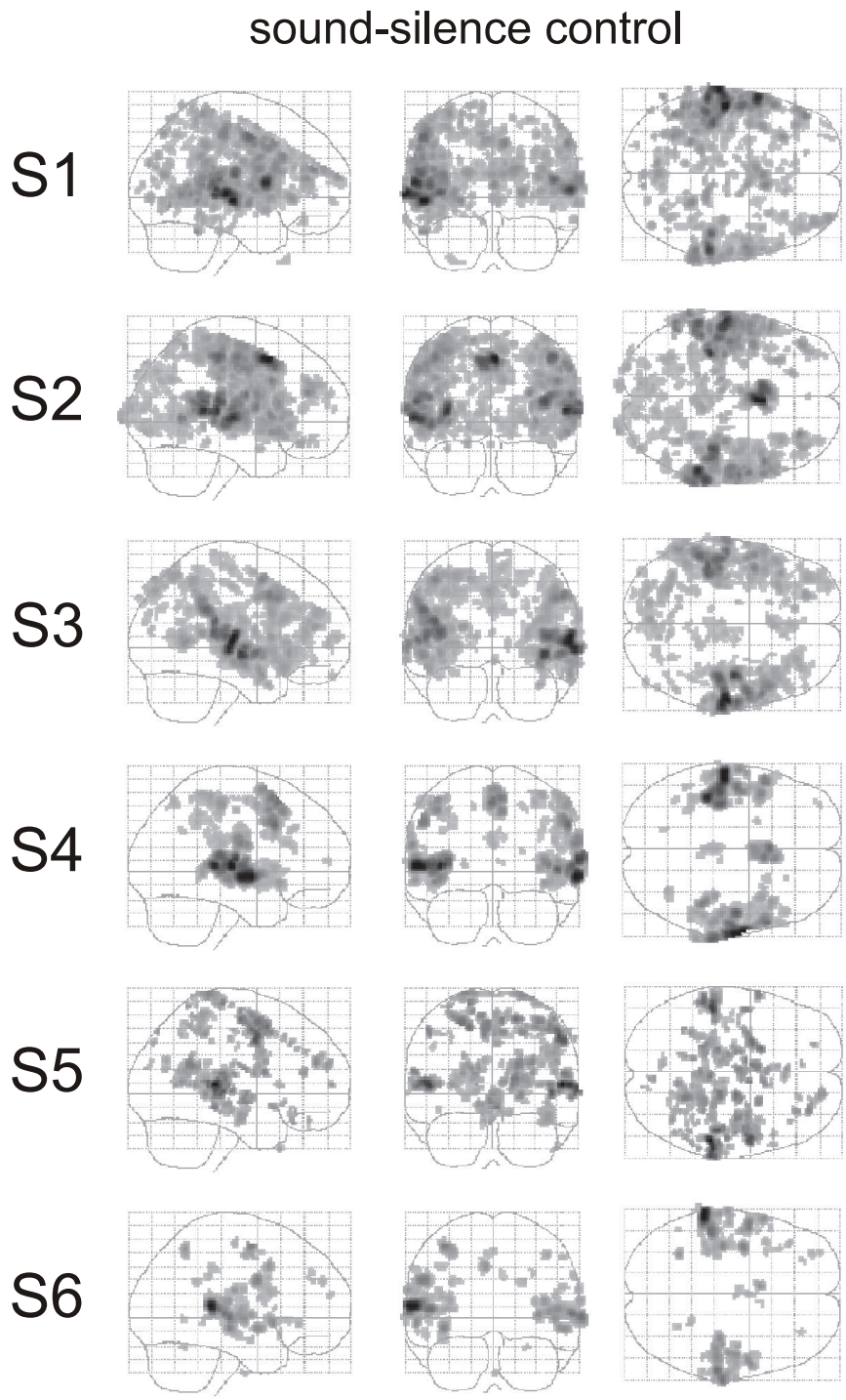


***Figure 3.4:*** *Individual Data: Contrast between sound conditions and silent baseline conditions for the control recording ('sound-silence control'). In contrast to the presentation of the group data, here a less conservative statistic was used to illustrate the inter-individual variability—and again preparatory motor responses are seen as well (cf. Fig. 3.3). An uncorrected significance level of* $p < 0.001$ *was applied, which corresponded to a height threshold of* $T > 3.13$.

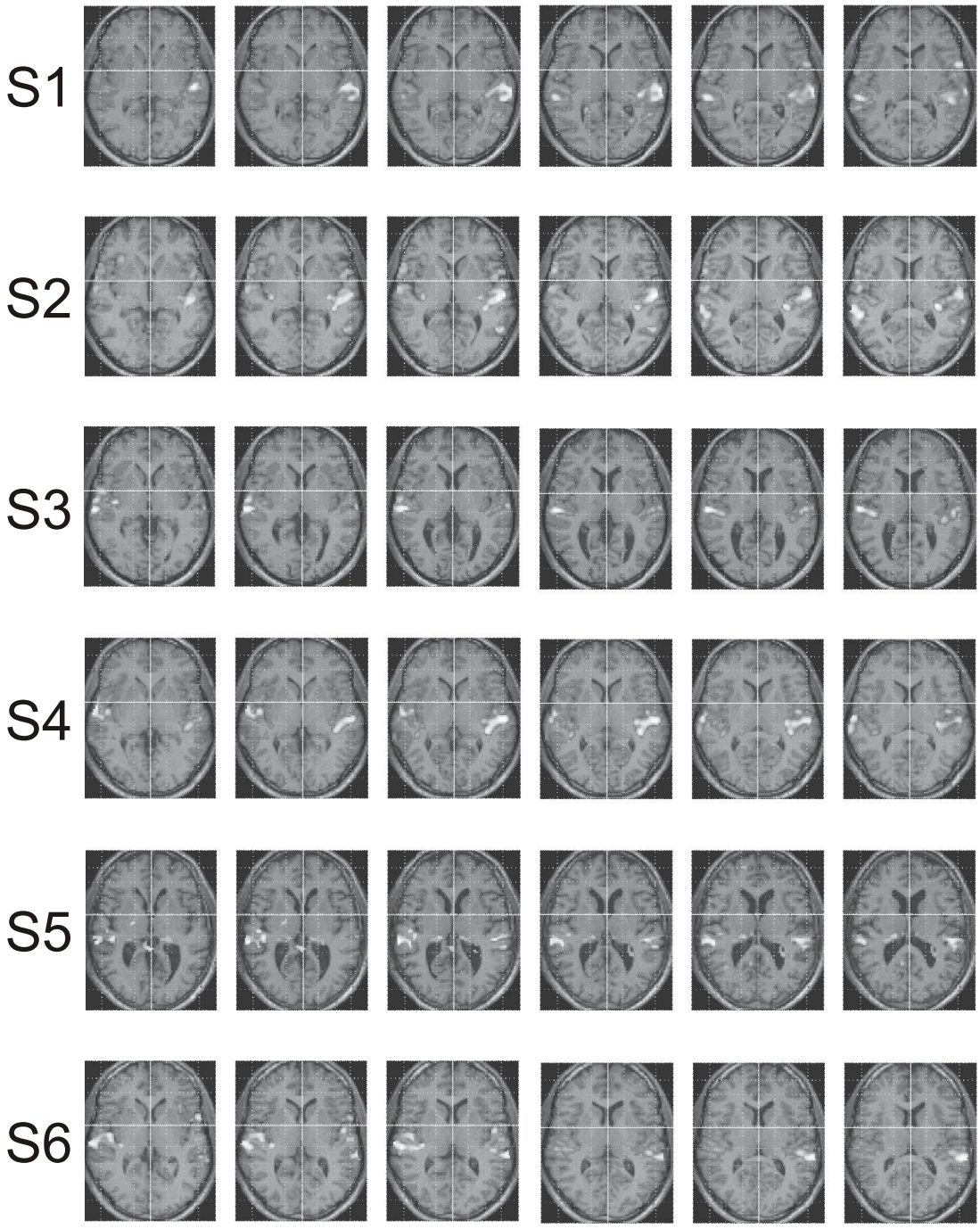


***Figure 3.5:*** *Individual Data: Contrast between sound conditions and silent baseline conditions for the control recording ('sound-silence control') as projected onto the individual structural data of the high resolution anatomical MRI scan (in axial steps of 2 mm starting from $z = -2$ for S1 to S3 and $z = 0$ for S4 to S6). The strong inter-individual variability of the auditory responses as seen in the glass brain representation of Fig. 3.4 is explained by the variability of the individual anatomy. All major responses locate very well into the individual Heschl's gyri (assuming posterior duplications to be proper parts of it as well—cf. activation found in S6).*

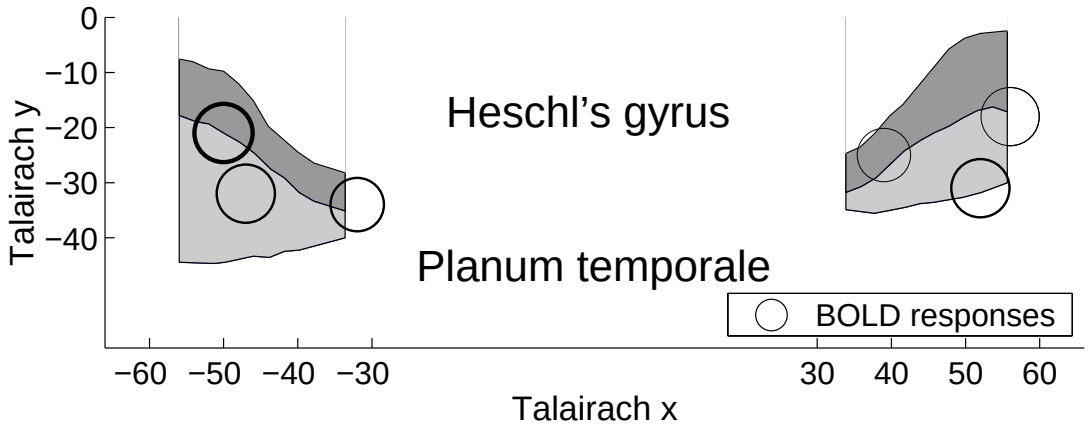


***Figure 3.6:*** *The three prominent auditory BOLD responses of the present fMRI study as projected onto the map by Leonard et al. [66]. Their strength and extension is roughly indicated by the line width and the radius of the circles. The figure gives the impression that only very little of the BOLD signal stems from the Heschl's gyri, which—given the individual functional-anatomical comparisons of Fig. 3.5—appears to be disputable.*

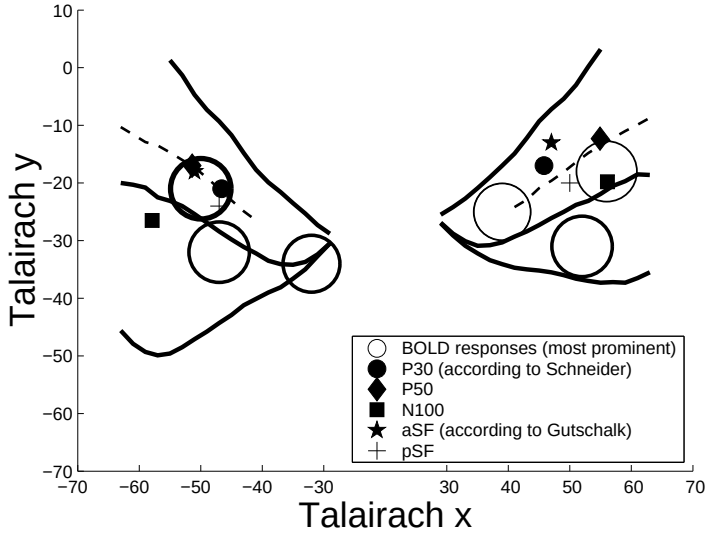


***Figure 3.7:*** *Comparison of fMRI ('sound-silence control') with recent MEG studies. The MEG localisations for the transient responses were kindly supplied by Peter Schneider (personal communication), for the sustained fields they were taken from Gutschalk et al. [44]. The standard errors of the MEG data are about 2–5 mm in both directions. Nearly all MEG localisations agree best with the fronto-lateral BOLD response of our fMRI experiment. The underlying map giving the borders of Heschl's gyrus and Planum temporale was kindly supplied by Peter Schneider (personal communication) and is in better agreement with the individual functional-anatomical comparisons of Fig. 3.5 than the map by Leonard et al. [66] used in Fig. 3.6.*

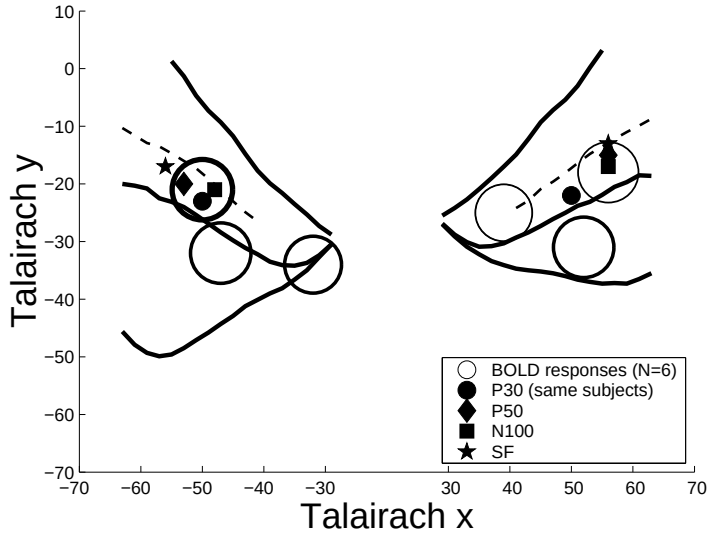


***Figure 3.8:*** *Comparison of fMRI data ('sound-silence control') with MEG data of the same subjects. Again the standard errors of the MEG data are not indicated for matters of clarity. Given that they are about 5 mm here, all MEG localisations agree very well with the fronto-lateral BOLD response.*

## Attention Conditions (Against Control)

The group analysis of the two attentional tasks (tone and pause duration discrimination) against the control condition are shown on the top and in the middle of Fig. 3.9. Both contrasts lack significant BOLD responses stemming from the auditory cortices. This is also true on the level of the individual uncorrected contrasts (not shown). A parietal activation was found for both tasks, which differed, however, with respect to its extension. Whereas for the sound discrimination it was sharply localised in the superior temporal lobe (SPL), it was more widespread for the pause discriminations. This finding is supported by the second order attentional contrast given at the bottom of Fig. 3.9. Here the difference between the pause-specific and the tone-specific attention activation is depicted and again the widespread parietal network is present. In terms of Brodman areas, the parietal activation was by and large restricted to BA 7 for both tasks.

Further, in the $yz$-plane the location of the third dipole in our MEG analysis of Chapter 2 agreed excellently with the focussed parietal BOLD response of the 'attention sound' contrast. Additionally, both tone and pause discriminations gave rise to a frontal BOLD response stemming from BA 44 and 45, including Broca's area, which in some individuals extended into the insula. However, looking at the bottom row of Fig. 3.9, where the attention-specific difference between the pause and the tone task is shown, the frontal activation is considerably diminished.

Fig. 3.10 gives the individual 'attention sound' and 'attention pause' contrasts with the low significance threshold from above. Again, although many inter-individual differences were seen, a common pattern for the strongest signals was visible. For instance, all subjects showed a significant activation in the parietal but not in the occipital cortex. The dorsal-most activation in S5 (to take an extreme example), is located in the posterior cingulate gyrus and thus still in the parietal cortex (as could be seen by rendering the BOLD activation onto the individual structural data—not shown here). Note also that, e.g., S6 exhibits activation both in the left and right superior temporal lobe and more medial in the precuneus (all within BA 7). Thus, the differences between the individual BOLD responses reflected those of the fitted MEG dipole analysis in Chapter 2.

Finally, the 'attention sound' contrast for standard stimuli only is given in Fig. 3.11. Notably, the pattern of activation is exactly the same as at the top of Fig. 3.9 where all stimuli (standards and deviants) were evaluated. This can also be seen from Table 3.2 where the $T$-values for the four most prominent BOLD responses are compared. Again, for the parietal activation this fits with the MEG analysis of Chapter 2, where we fitted the third dipole in answer to standards only.

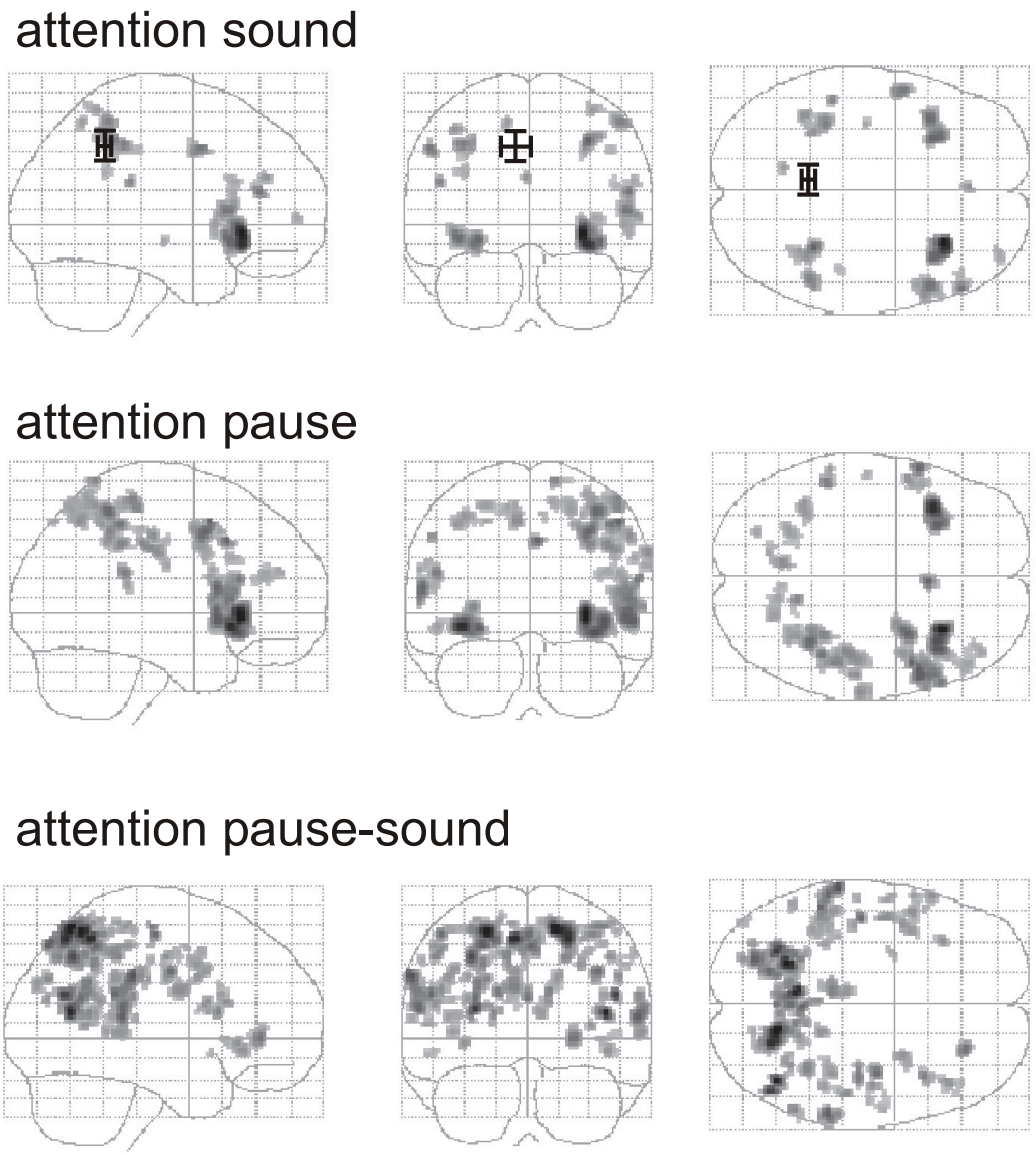


***Figure 3.9:*** *Group Data: Attention-specific activation in the tone and the pause duration discrimination (top: 'attention sound'; middle: 'attention pause'). Both contrasts lack activation in the auditory cortex but show activation in the inferior frontal gyrus (IFG; BA 44 and 45, including Broca's area) and in parietal regions. For 'attention sound' the latter is rather sharply localised in the superior temporal lobe (SPL; BA 7), while 'attention pause' exhibits a widespread parietal network. The errorbars in the top row indicate the location of the third dipole as reported in Chapter 2. Note the excellent agreement in the yz-plane. The bottom row gives the specific activation in the tone pause duration discrimination as compared to the tone duration task ('attention pause-sound'). Here the prominent frontal activations of the other two contrasts vanishes to a large extent. Further, this second order contrast strongly underpins the more widespread parietal activation during the discrimination of pauses as compared to tones.*

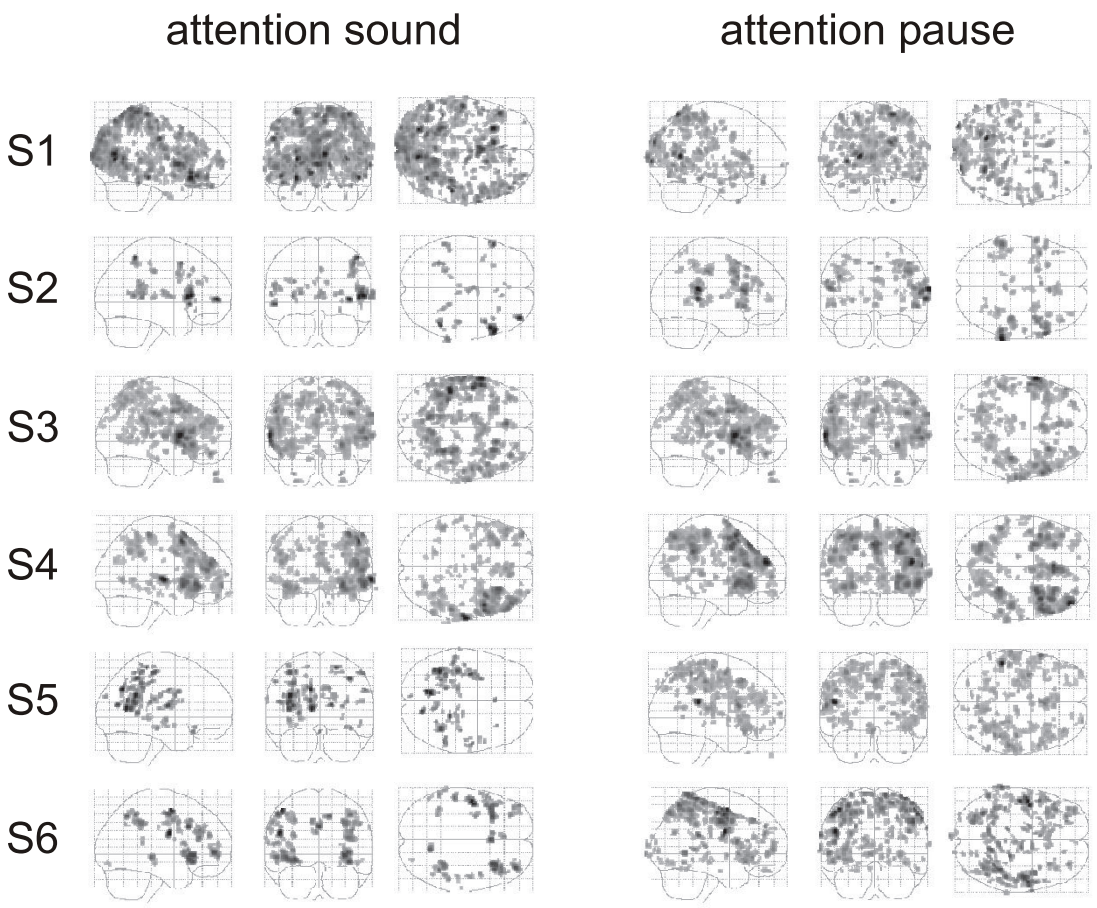


***Figure 3.10:*** *Individual Data: Attention-specific activation in the tone and the pause duration discrimination (left: 'attention sound'; right: 'attention pause'). A low significance threshold was applied to illustrate the inter-individual differences (but remember that partially these differences are due to the large number of independent individual false positives followed by such a threshold). Apart from those differences, however, also several communalities over the individual BOLD responses can be seen. This is particularly true for the parietal and frontal activations also prominent in Fig. 3.9. Further, note that for both tasks several individuals show an enhanced activation in the precuneus and the posterior cingulate gyrus, as suggested by the MEG analysis in Chapter 2.*

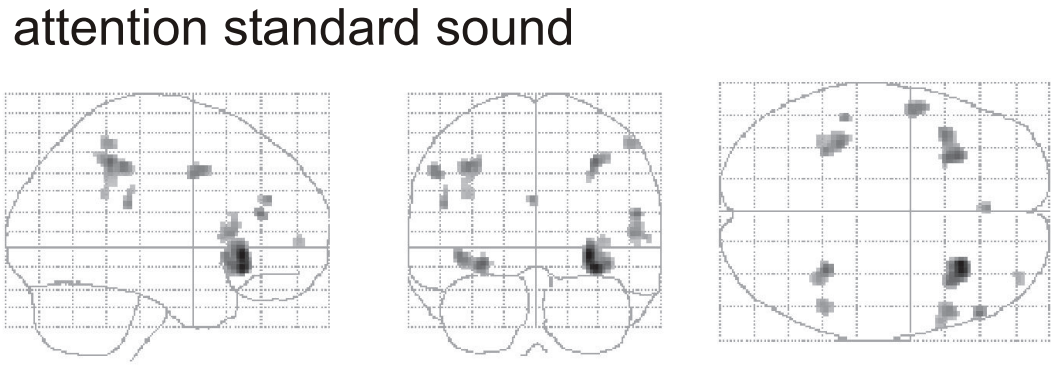


***Figure 3.11:*** *Group Data: Attention-specific activation for the tone task in answer to standards; i.e. sound condition 4, which contained no deviants, but not conditions 1-3 were used for evaluation. The pattern of activation is the same as in Fig. 3.9 (top row: 'attention sound'), where all stimuli were used for evaluation. The very slight differences are likely due to the lower signal-to-noise ratio here.*

| | Talairach coord. | | | $T$-values for | |
|---|---|---|---|---|---|
| area of activation | $x_{\mathrm{Tal}}$ | $y_{\mathrm{Tal}}$ | $z_{\mathrm{Tal}}$ | std & dev | std only |
| right IFG | 24 | 22 | -3 | 11.13 | 9.44 |
| left IFG | -25 | 16 | -6 | 8.63 | 7.74 |
| right SPL | 27 | -46 | 38 | 8.70 | 7.58 |
| left SPL | -32 | -40 | 37 | 7.77 | 7.03 |

***Table 3.2:*** *$T$-values for the four most prominent BOLD responses of the contrast 'attention sound' when using all stimuli versus using standards only. The decrease in the $T$-value is about the same for all activations and presumably mainly due to the lower signal-to-noise ratio when using only standards. Thus, although the reduction is strongest for the right frontal activation, no BOLD response seems to be specific to targets (i.e. duration deviants). This fits with our MEG data of Chapter 2 which found the parietal activation for an evaluation of the standards only. With respect to the frontal sources we will discuss this issue again when looking for their electrophysiological counterpart in the next chapter.*

## 3.4 Discussion

### Auditory Cortex

Since the present fMRI study was the first auditory sparse imaging investigation conducted with the given scanner, we had to somehow validate the accuracy of our results. Here the 'sound-silence control' contrast turned out to be a good starting point, for we know from other studies where to expect activation. Indeed the individual BOLD responses projected onto the individual anatomy showed the expected activation in the auditory cortices—cf. Fig. 3.5

Going into more detail, the group analysis of the control session revealed three prominent activations within left and right auditory cortex—cf. Fig. 3.3. The location of the fronto-lateral-most could be identified with that of the most prominent MEG responses (P30, P50, N100, SF)—cf. Fig. 3.8. Looking at the same figure, it seems as if the dorso-lateral activation stems from the Planum temporale. This, however, was not straightforwardly confirmed by comparing individual activation with individual anatomy, as it was done in Fig. 3.5. The data suggest that subjects with a prominent posterior duplication of the Heschl's gyrus have their strongest BOLD responses coming from there rather than from the anterior Heschl's gyrus. The present study, which comprised data of only six subjects, cannot settle this issue. However, it should be added that for S6, which had the most distinguished posterior duplication of the subjects, the location of a free fitted P50 within MEG data agrees well with the localisation of the dorso-lateral BOLD response. (The compatibility between BOLD and MEG responses assumed in this paragraph will be discussed in more detail later; namely in Appendix B on a more theoretical basis and in Chapter 4 on the basis of our empirical data.) The medial-most auditory BOLD activation could not be related to MEG responses which suggests that it is linked to early auditory activity for which MEG is blind. This would correspond to the time course of auditory processing which goes from medial to lateral areas of the Heschl's gyrus. This separation into a prominent medial and a lateral auditory BOLD response seems to be a general phenomenon and can also be found in other fMRI studies like [99].

Apart from auditory activation the 'sound-silence control' revealed preparatory motor responses which are due to the fact that subjects were asked to press a button after each sound condition. This pattern of activation in the left and right premotor cortex and pre-supplement motor areas agrees well with the literature. For detailed analyses of those areas and their involvement in preparation and execution of movements see [64], [132], [128].

Further, the auditory cortex revealed no attentional difference for the task sessions. This is true for both the group analysis and the individual data (the latter employing rather non-conservative statistics). This finding is in accordance with a lot but not with all of the literature—cf. [57]. However, a look at the literature allows the claim that if there is an attentional effect than it is at least not a robust one as the parietal one we shall discuss now. The fact that the MEG study of the previous chapter revealed an attentional effect in the auditory cortex (the left sustained field was enhanced) does not contradict our fMRI results given that the sensitivity of BOLD and MEG responses is not the same—cf. Appendix B.

## Attention-Specific Parietal Network

The main intention of the present study was the model-independent assessment of the parieto-occipital activation we found in the MEG study of the previous chapter. Indeed it is strongly supported by the fMRI experiment on tone discrimination, which revealed activation within the superior parietal lobe (Brodman area 7). The agreement between the BOLD response and the fitted dipole location in the $yz$-plane is excellent, the standard errors of the MEG dipole localisations and the extension of the BOLD responses nearly match exactly. Only the $x$-direction differs in so far as the BOLD responses suggest a bilateral activation, while the dipole fitting favoured a single medial source—cf. top row of Fig. 3.9. However, on the individual level some fMRI data sets showed activation in the precuneus and the posterior Cingulate gyrus like in the MEG modelling (cf. S5 and S6, in particular). The fact that the parietal BOLD responses were found to be not target-specific (cf. Fig. 3.11 and Table 3.2) is also in line with MEG data of Chapter 2, for there we analysed standards only.

Further, we investigated in how far this attention-specific activation is depending on sensory input. This was done by a pause discrimination task; i.e. by using the inverted paradigm, so that subjects had to attend to the intervals lacking sensory input. Again a parietal activation was found; this time much more widespread, but still by and large restricted to BA 7—cf. middle row of Fig. 3.9. The difference in the network extension can also be seen from the contrast 'attention pause-sound' (bottom row of Fig. 3.9), which gives the specific-difference between discriminating pauses and discriminating tones. Thus, the extension of the network is related to estimating durations when a sensory input is missing. The fact that the parietal activation is much more focussed in 'attention sound' than in 'attention pause' suggests that an auditory sensory input is of great assistance in discriminating durations; i.e. it allows to estimate durations without 'forcing

into the recruitment of widespread cortical areas'. Notably, the individual discriminative performance is also much better for the tone duration task than for the pause duration task, as we will see in Chapter 6.

As partly discussed in the previous chapter, several other studies find an activation in BA 7 as well. Satoh et al. [115], who found the precuneus to be activated (cf. Chapter 2), also report on more lateral responses from the superior parietal lobe. All these activations lie within BA 7 and strongly resemble our data of, for instance, S6. The same is true for the attention-specific activation in deaf-hearing people [22]. In general, the superior parietal lobe is supposed to have two major functions: first, the integration of multimodal sensory information; second, providing guidance to motor operations [29].

The question in how far the parietal network is duration-specific is hard to answer. From our fMRI data we cannot draw any firm conclusion since we did not contrast the duration task with other tasks. However, also other studies do not leave a consistent picture. There are several studies emphasising the key role of larger parietal network involved in auditory spatial and attentional functions—cf. [106], [12], [115]. More specifically Rao et al. [107], who did an auditory study somehow similar to our pause duration task, claim that the activation they found in the superior parietal lobe is not duration-specific, since they observed it also in a pitch task. The same is true for Ferrandez et al. [24], who used a visual duration task which roughly parallels our tone duration task. They compared it to an intensity task and maintain that the parietal activation reflects a general network for matching-to-sample tasks, no matter which property has to be discriminated. However, other studies from the same group do not agree in all details—cf. [77], [105]. Additionally, and this is presumably more pressing, monkey studies using implanted electrodes found single neurons representing time within the parietal cortex—see, e.g., [65]. We will come back to this issue of duration-specificity when re-analysing our MEG data in the next chapter. There the time course of the electrophysiological activation will provide further insight.

## Further Attention-Specific Networks

The data acquisition was such that our areas of interest (i.e. the parietal network and the auditory cortices) were included, while we left out other regions; e.g. subcortical areas, which are known to be involved in the processing of time—cf. Chapter 1. Cortical areas often claimed to be related to time perception include large parts of the prefrontal cortex and premotor areas [124], [107] [24]. The

medial premotor pathway is presumably important for internal representation of time [4]. However, these areas were not systematically included in our investigation. For instance, the pre-supplementary motor area is more prominently included in the fMRI data recorded for S2 than in those of S6 (cf. Fig. 3.10).

However, one further attention-specific network was found in the fMRI data (and happened to be included in all individual data); namely a frontal one for both the tone and the pause duration task—Fig. 3.9. It stemmed from the inferior frontal gyrus (BA 44 and 45) including Broca's area and the insula. For the slight individual differences see Fig. 3.10. However, most of this activation vanished in the contrast 'attention pause-sound' (bottom row in Fig. 3.9). Thus, other than the more extended parietal network seen in this contrast, the frontal BOLD response is not specific to pause discriminations.

The fact that it is presumably not even specific to duration discriminations is suggested by the literature which reports frontal activation in many different contexts. For instance, PET studies reported right inferior frontal gyrus (BA 45) activation for duration and intensity discrimination [77]. Rhythm tasks involving precuneus activation are also reported to show activation in the left Broca's area, with extension into the neighbouring insula; and also the aforementioned study on deaf-hearing [22] found activation in BA 45. Also the fMRI study by Rao et al. [107], which already agreed with our results with respect to the parietal network, found activation in right and left BA 44 and 45. There are several studies reporting on different functional roles played by different frontal subregions [24], [105]. However, these studies partially contradict each other, and our fMRI data do not suggest a separation into functionally differing frontal subregions.

Most of the literature just cited was already discussed in the context of the parietal network. Indeed there are several other studies reporting a simultaneous activation of both areas, which include a PET study on automatic processing of auditory duration deviants and studies involving prospective memory tasks (ongoing tasks with superimposed task unrelated to retrieval context), [18], [11]. Finally, the hemispheric asymmetry for the frontal and the parietal activation which is sometimes reported, could not be seen in our data—and notably the literature differs with respect to the direction of these asymmetries [15], [48], [140], [26].

## Conclusion

The fMRI experiment offered further evidence for an attention-specific activation in the parietal cortex as already suggested by the fitted MEG model of Chapter 2. However, the BOLD responses were bilateral and less medial, so that perhaps the dipole analysis revealed the centre of activation. Additionally, the experiment showed that the parietal activation is more extended for the pause duration task than for the tone duration task. This suggested that the more difficult task 'forces into the recruitment of more widespread cortical areas'. Further, there was no attention-specific BOLD response stemming from the auditory cortex. This differs from our MEG data for the left auditory cortex and likely reflects the difference in sensitivity between fMRI and MEG. Finally, an attention-specific frontal activation was found. Since it was similar for both task, this response is not specific to the discrimination of pause durations.

Given these results, there are several questions coming up with respect to our electrophysiological data of Chapter 2. Hence, the next chapter will include a re-analysis of them to see, for instance, whether a bilateral parietal activation can be supported by electrophysiology. Moreover, frontal sources will be included in the re-analysis to investigate the time course of the electrophysiological activation there—and to learn why we did not model it in Chapter 2. Finally, the different time-courses for the parietal and the frontal response will also provide evidence for a functional separation of those activations.

# Chapter 4

# MEG-Study on Tone & Tone Pause Durations: Seeded Model

## 4.1 Introduction

The aim of this chapter is a further analysis of the attentional networks associated with duration discrimination tasks; i.e. a deeper insight into the functional differences underlying the parietal and the frontal BOLD responses found in the last chapter. Here a re-analysis of the electrophysiological data of Chapter 2 using a seeded model gathered from the fMRI data is the method of choice, for it combines the spatial accuracy of the fMRI with the high temporal resolution of the MEG and EEG data (cf. Appendix B). The time course of the gained source waveforms might then enable us to separate executive from monitoring or evaluative activation; i.e. rather short activation linked to subsequent behavioural response from sustained activation 'measuring' the rather long-enduring task-relevant input.

Further, we conducted a MEG experiment on pause duration discrimination, which will also be evaluated in a seeded model gathered from the fMRI data. Again, as in Chapter 3, the question to be answered by this experiment is whether and to what extent the attention-specific activations depend on sensory input.

Implicitly, this chapter will obviously tell us more about the compatibility between electrophysiological and functional magnetic resonance data (more on the theoretical background of their compatibility is given in Appendix B).

## 4.2 Material and Methods

The amplitudes of the auditory evoked fields and potentials as recorded during the performance of two duration discrimination tasks (tones and pauses) were compared with those from the respective 'non-attend' conditions. All experimental procedures were approved by the local ethics committee (Faculty of Medicine, University of Heidelberg).

### Stimuli and Tasks

For the tone duration tasks stimuli and tasks were the same as in Chapter 2.

A second oddball paradigm was designed for the discrimination of pause durations basically by 'inverting' the tone duration task. Sinusoidal tones of 500 Hz with a 10 ms ramp at their start and end (Hanning window) were used to 'fill' the randomised interstimulus intervals (ISIs) of 1.35–1.40 s. 'Standard stimuli' now were pauses enduring for 1.0 s which were interspersed with slightly longer deviants (1.2 s pauses) in 20% of all cases (310 standard, 63 deviant pauses). All other parameters (sound pressure level, sampling rate etc.) were kept the same as in the tone duration task—cf. Chapter 2. As with the tone discrimination, the procedure was constrained in that the beginning of each sequence was marked by three standards and that two deviants were never consecutive. Subjects were informed about these constraints to ease the task. In the 'attend' condition subjects were asked to press the button of a computer mouse in answer to a deviant.

In both procedures the order of the conditions was reversed for half of the subjects to avoid effects of habituation in the grand average.

### Subjects

Subjects for the tone discrimination task were the same as in Chapter 2. Since a seeded model was applied, this time no subject was excluded; i.e. the MEG data of all twenty subjects of Chapter 2 were used.

Ten of those twenty subjects participated in the tone pause experiment after having given informed consent. The group consisted of 6 right-handed male subjects with a mean age of 37 years (range 25–66 years) and of 4 female subjects, 3 of whom were right-handed, with mean age 33 years (range 26–38). The handedness was determined using the standard Edinburgh questionnaire [2]. All ten subjects

participated in a magnetoencephalographic (MEG) recording for both 'attend' and 'non-attend' conditions.

## Recording and Data Processing

Recording and data processing was the same for both tasks (i.e. as described in Chapter 2) except for that the tone pause discrimination task was recorded DC.

## Source Analysis

The fMRI results of Chapter 3 were used to gather a six-source model for both the tone and the pause duration experiment. The seedings followed the most prominent BOLD activations. For the auditory cortices, which both exhibited a triad structure as discussed in Chapter 3, the arithmetic mean in all three directions was computed and used as a seed—see Fig. 4.1. Further, the BOLD responses stemming from the left and right superior parietal lobe (SPL) and inferior frontal gyrus (IFG) were taken as seeds—see Fig. 4.2 & 4.3.

The orientation of the auditory and parietal dipoles was fitted over their sustained responses. This analysis was guided by Chapter 2 from which we knew the activation's time course. Hence, for the tone task the orientation of the auditory sources was fitted to the epoch 500–1000 ms after tone onset in the 'non-attend' condition. Afterwards the parietal dipoles were fitted over the epoch 750–1200 ms post-stimulus onset in the 'attend' condition. Lacking further knowledge about the kind of activation in the inferior frontal gyrus, regional sources were used and their activation was assessed by calculating the root-mean-square of the two resulting dipole moments. Ocular artefacts were accounted for by a regional source.

This six-source MEG model was gathered for the standard stimuli of the tone discrimination task. It was held fix and applied to the deviant stimuli of the same task. It was also used to evaluate the EEG data. Here a bandpass filter of 0.1–5 Hz was applied and the frontal sources were turned into single dipoles and their orientations were fitted over the epoch 1100–1600 ms post-stimulus onset.

A second MEG model omitted the frontal sources and thus resulted in a four-dipole model for the standards of the tone discrimination task. The model was also applied to the standard stimuli of the pause discrimination task. Here the baseline, which for the tone discrimination task was always calculated over the

300 ms interval prior to tone onset, had to be readjusted for the auditory dipoles (for the parietal dipoles it was assumed to be right, since no duration task-specific activity should occur before the pause starts off). Two definitions baselines were used, both indicated in Fig. 4.10. First, we used a 'transient baseline', where the individual mean over the epoch 1000–1300 ms post-pause onset was subtracted from the whole time course data; i.e. the source waveforms were renormalised to the auditory transient responses P50, N100 and P200. This procedure is legitimised by the fact that these responses show no attentional difference—cf. Chapter 2. Further, this definition allows for a statistical evaluation over the same intervals as for the tone discrimination task (cf. below). Second, a 'no-input baseline' was applied subtracting the individual mean over the epoch 500–1000 ms post-pause onset. This definition was guided by the assumption that the auditory cortex lacks a sustained response in answer to a pause. Since by definition there will thus be no attentional effect over the epoch 500–1000 ms post-pause onset, we used this baseline to check for a difference in the auditory sustained field which occurs in answer to the tones about 1500–2300 ms post-pause onset—also indicated in Fig. 4.10. The evaluation of the parietal sources was untouched by the different baselines for the AC sources.

For each of the four experimental conditions the slow magnetic artefacts inherent in a recording without low cut-off frequency was separately modelled. This was done by computing a principal component analysis (PCA) for each average condition over the epoch 2100–2300 ms post-stimulus onset; i.e., 1100–1300 ms post-stimulus offset. The PCA component explaining the majority of the variance was included in the spatial filter for each experimental condition. (The computation of a PCA is explained in detail in Appendix A.)

## Statistics

Due to the small number of subjects in the EEG experiment, its statistical evaluation was based on Friedman's non-parametric analysis of variance. The source strength of the frontal dipoles were assessed by determining the maximum amplitude over the prominent transient response occurring 1100–1600 ms post-onset.

For the MEG data all attentional effects were tested using an analysis of variance with repeated measurements. The source strength of the sustained field in the tone discrimination task was assessed by calculating the mean dipole moment over the epoch 500–1000 ms post-stimulus onset which covered exclusively the plateau of the source waveforms. The source strength of the parietal dipoles was

calculated over their maximum; i.e., by the mean dipole moment over the epoch 750–1200 ms post-onset.

The tone pause discrimination task was evaluated over the same intervals for the 'transient-baseline'; that is the auditory sources were investigated over an interval lacking sensory input. The additional 'no-input baseline' model (only differing for the auditory responses) was used to compare the strength of the auditory sustained field. This was done over the epoch 1500–2300 ms post-pause onset, where the source waveforms showed their plateau—cf. Fig. 4.10.

The mean latency and the $t$-interval of the parietal slow-wave offset in the tone task was estimated by means of bootstrapping. The offset latency was defined by the maximum of the source waveform's first derivative between 1000–1300 ms (for standard stimuli) and 1200–1500 ms (for deviant stimuli). One-thousand samples were drawn to extract robust $t$-intervals.

Bootstrapping was done by using MATLAB. All other statistical procedures were computed with the SAS® package (version 8).

## 4.3 Results

### Model Gathering

The localisations for the auditory sources—as gained from calculating the mean position of the three prominent auditory BOLD responses—are shown in Fig. 4.1. The locations of the four attention-specific sources for the tone task, which lie in the superior temporal lobe (SPL) and the inferior frontal gyrus (IFG), are indicated in Fig. 4.2, which also gives the location and standard error of the third dipole fitted in the MEG analysis of Chapter 2. For the parietal and frontal sources, positions exhibiting the highest $T$-value within the activation clusters were chosen as seeds. The Talairach coordinates of all six seed locations are given in Table 4.1.

For the tone pause discrimination the locations were kept the same. While for the auditory sources this is evident, the legitimisation for retaining the other four source locations can be read off Fig. 4.3. While the frontal BOLD activations completely agreed in their location for both tasks, at least the centre of the widespread parietal network found in the pause discrimination task was well approximated by the superior parietal lobe (SPL) activation of the tone task. Indeed this strategy of modelling the parietal centre of activation is much more

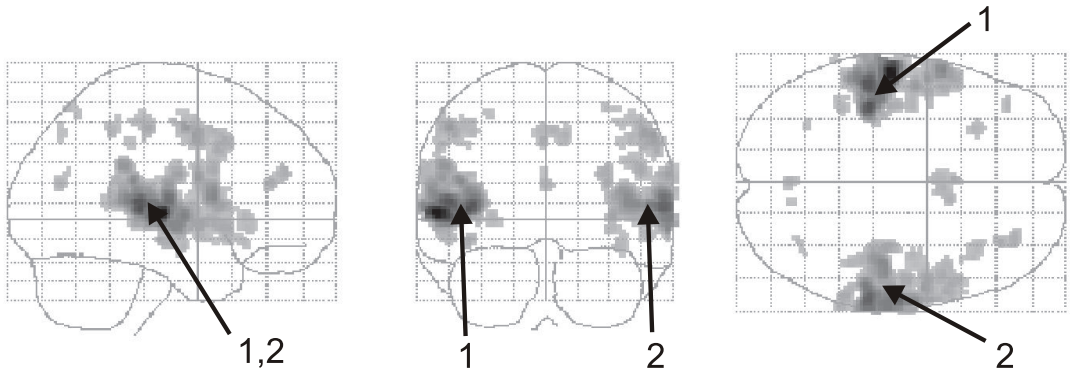


***Figure 4.1:*** *Model Gathering: The tips of the arrows indicate the seeds for the auditory sources. The locations were gathered from the depicted fMRI data of the last Chapter and then used for a (re-)analysis of the MEG and EEG data of Chapter 2.*

| area of activation | Talairach coord. $x_{\mathrm{Tal}}$ | $y_{\mathrm{Tal}}$ | $z_{\mathrm{Tal}}$ | $T$-value |
|---|---|---|---|---|
| 1: left auditory cortex (AC) | -45 | -30 | 3 | (16.5) |
| 2: right auditory cortex | 50 | -26 | 5 | (11.1) |
| 3: left superior parietal lobe (SPL) | -32 | -40 | 37 | 7.77 |
| 4: right superior parietal lobe | 27 | -46 | 38 | 8.70 |
| 5: left inferior frontal gyrus (IFG) | -25 | 16 | -6 | 8.63 |
| 6: right inferior frontal gyrus | 24 | 22 | -3 | 11.13 |

***Table 4.1:*** *Talairach coordinates of the six source locations as gathered from the fMRI experiment and as to be used for (re-)analysing the MEG and EEG data. The $T$-values for the auditory cortex activation were put in brackets since they give the respective mean of the three major auditory BOLD responses from which the seeding location was gathered. The numbering of the sources (1–6) is the same as in Fig. 4.1–4.3.*

adequate than seeding several parietal sources near each other. The latter would inevitably lead to disturbing cross-talks between sources, while our main interest lies in the overall time course of the parietal activation and its separation from auditory (and frontal) activation. Thus, parsimoniousness of the pause task model is searched for and achieved by using only the two parietal seeds from the tone task. Moreover, using the same seeding locations for both tasks allows for a direct comparison between source strengths.

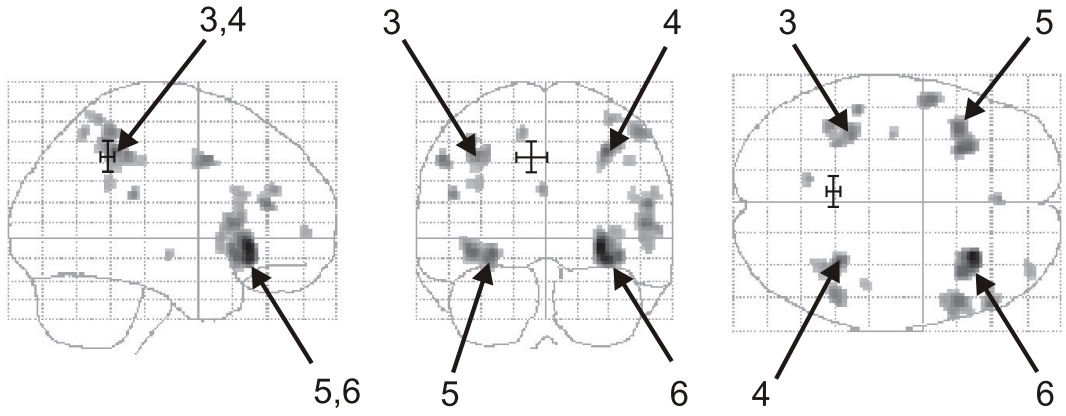


***Figure 4.2:*** *Model Gathering: The tips of the arrows indicate the localisations for the seeds of the attention-specific sources in the superior temporal lobe (3 & 4) and the inferior frontal gyrus (5 & 6). The locations were gathered from the depicted fMRI data of the tone task and afterwards used for re-analysing the MEG and EEG data of Chapter 2. The errorbars indicate the location of the third dipole fitted in the MEG source analysis of Chapter 2. In the yz-plane (left column) this location agrees excellently with the parietal BOLD response.*

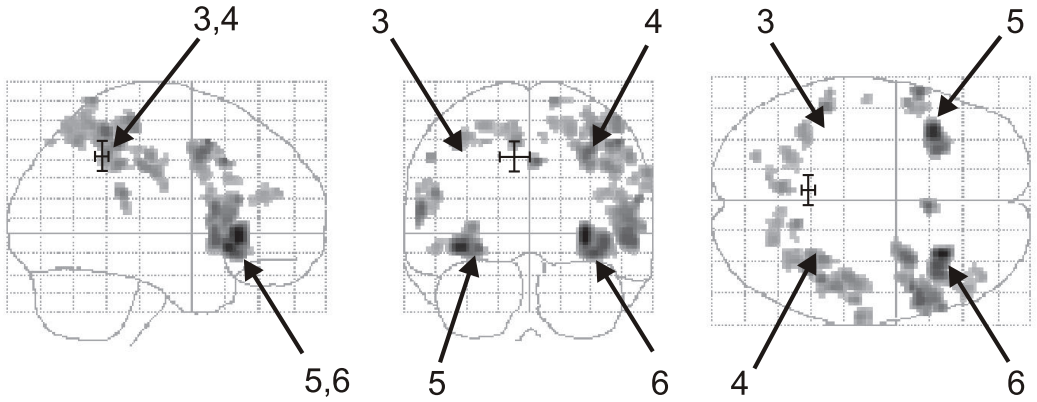


***Figure 4.3:*** *Model Gathering: The tips of the arrows indicate the localisations for attention-specific sources in the superior temporal lobe (3 & 4) and the inferior frontal gyrus (5 & 6) as used for the tone task—cf. Fig. 4.2. The depicted fMRI data, however, are taken from the pause task. The figure suggests that all seeding locations used for the tone task can also be applied to the pause task. Indeed the frontal activations agree in their location for both tasks. Further, the widespread parietal network observed in the pause discrimination can also be modelled by using the seeds of the tone task, since their locations approximate the centre of the parietal activation and thus ensure the attempted parsimoniousness of the model. The latter is important to avoid disturbing cross-talks between sources, which would have been an inevitable consequence of seeding several parietal sources near each other.*

## MEG Six-Source Model

The four auditory and parietal sources exhibited a significantly increased dipole moment for the 'attend' condition of the tone task (*attention*: $F_{1,19} = 21.34, p < 0.001$). Elementwise comparisons for each source yielded an approximate value for their contributions to the overall effect. Here the mean of the parietal sources and the left auditory cortex showed a significant effect—the individual data are listed in Table 4.2. This is all in agreement with the corresponding grand average source waveforms for the standard stimuli as depicted in Fig. 4.4 (all MEG source waveforms presented in this chapter got bandpass-filtered from 0.01–20 Hz using a zero phase shift Butterworth filter with 12 dB/oct). Further, the frontal sources were tested over the complete averaging epoch and also revealed an attentional difference—cf. Table 4.2. However, visual inspection of the source waveforms in Fig. 4.4 suggests that this difference is most prominent around 1500 ms post-stimulus onset.

The neuromagnetic responses to the deviant stimuli exhibited a similar pattern. The statistical evaluation also revealed an overall attentional effect for the auditory and parietal sources (*attention*: $F_{1,19} = 16.31, p < 0.001$). Again the elementwise comparison showed a significant attention-specific enhancement for the mean dipole moment of the parietal sources. The values are listed in Table 4.2 and Fig. 4.5 gives the grand average source waveforms. Also the frontal sources exhibit the same pattern of activation with the most prominent attentional enhancement occurring around 1500 ms post-stimulus onset (see Table 4.2 and Fig. 4.5).

| area | | epoch (post-tone onset) | $F_{1,19}$-value for standard stimuli | | deviant stimuli | |
|---|---|---|---|---|---|---|
| AC: | mean | 500–1000 ms | 2.75 | *n.s.* | 1.36 | *n.s.* |
| | left | | 4.92 | $p < 0.05$ | 3.07 | *n.s.* |
| | right | | 0.71 | *n.s.* | 0.12 | *n.s.* |
| SPL: | mean | 750–1200 ms | 11.46 | $p < 0.01$ | 9.23 | $p < 0.01$ |
| | left | | 10.60 | $p < 0.01$ | 3.92 | *n.s.* |
| | right | | 8.15 | $p < 0.05$ | 6.49 | $p < 0.05$ |
| IFG: | left | 0–2300 ms | 28.67 | $p < 0.0001$ | 7.36 | $p < 0.05$ |
| | right | | 17.20 | $p < 0.001$ | 13.16 | $p < 0.01$ |

***Table 4.2:*** *Elementwise comparisons for attentional effects in the six-source model. The model encompasses dipoles in the auditory cortex (AC) and the superior temporal lobe (SPL), and regional sources in the inferior frontal gyrus (IFG).*

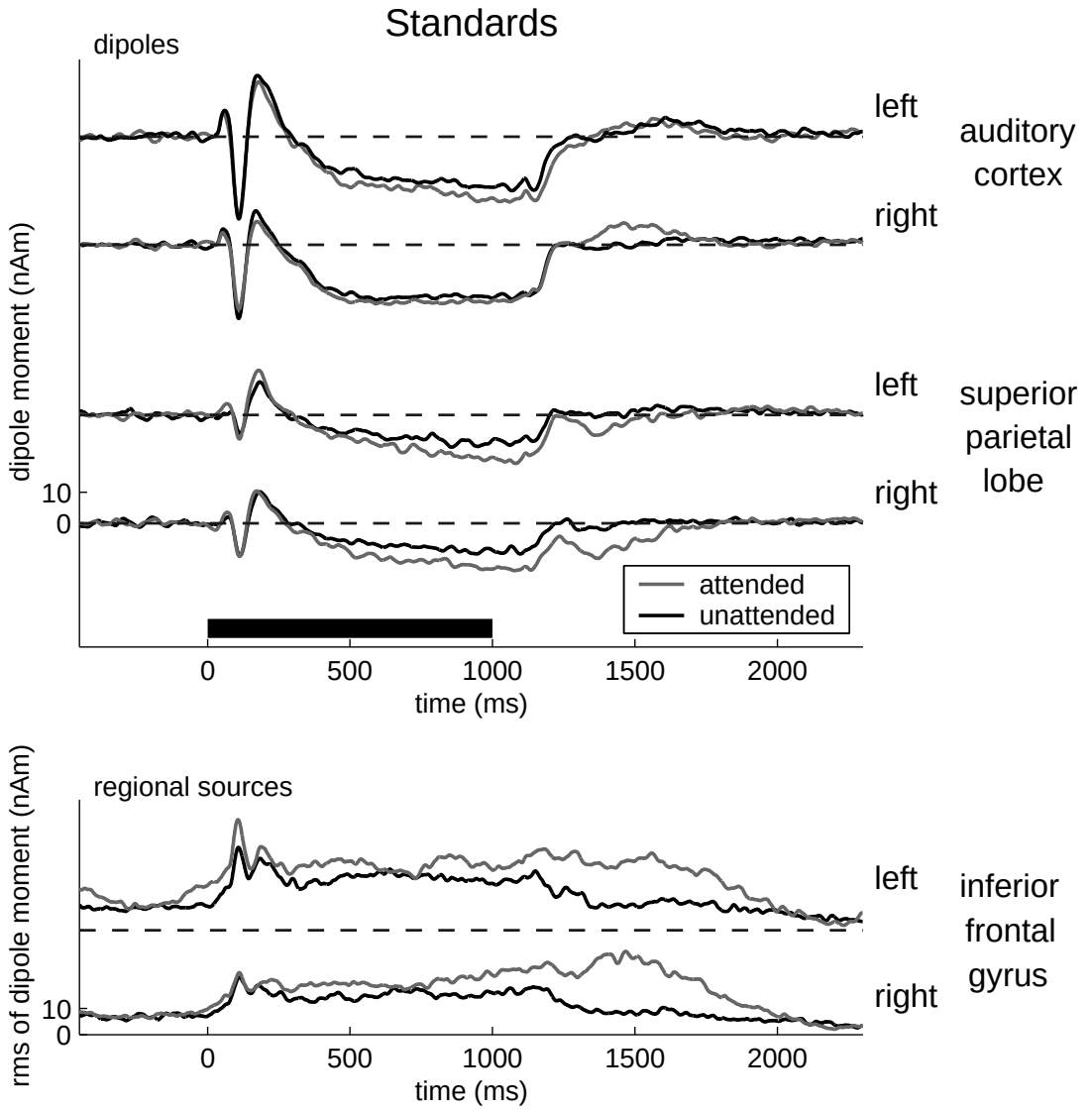


***Figure 4.4:*** *MEG Data, Tone Task: Grand average source waveforms in the seeded six-source model in answer to standard stimuli. An attentional effect in terms of an increased amplitude is seen for the sustained response of the left auditory cortex and for the parietal sources. The frontal sources exhibit no clear pattern in terms of a transient or well-defined sustained response. However, its most prominent attention-specific enhancement is seen around 1500 ms post-stimulus onset. The black bar indicates the temporal position of the tone.*

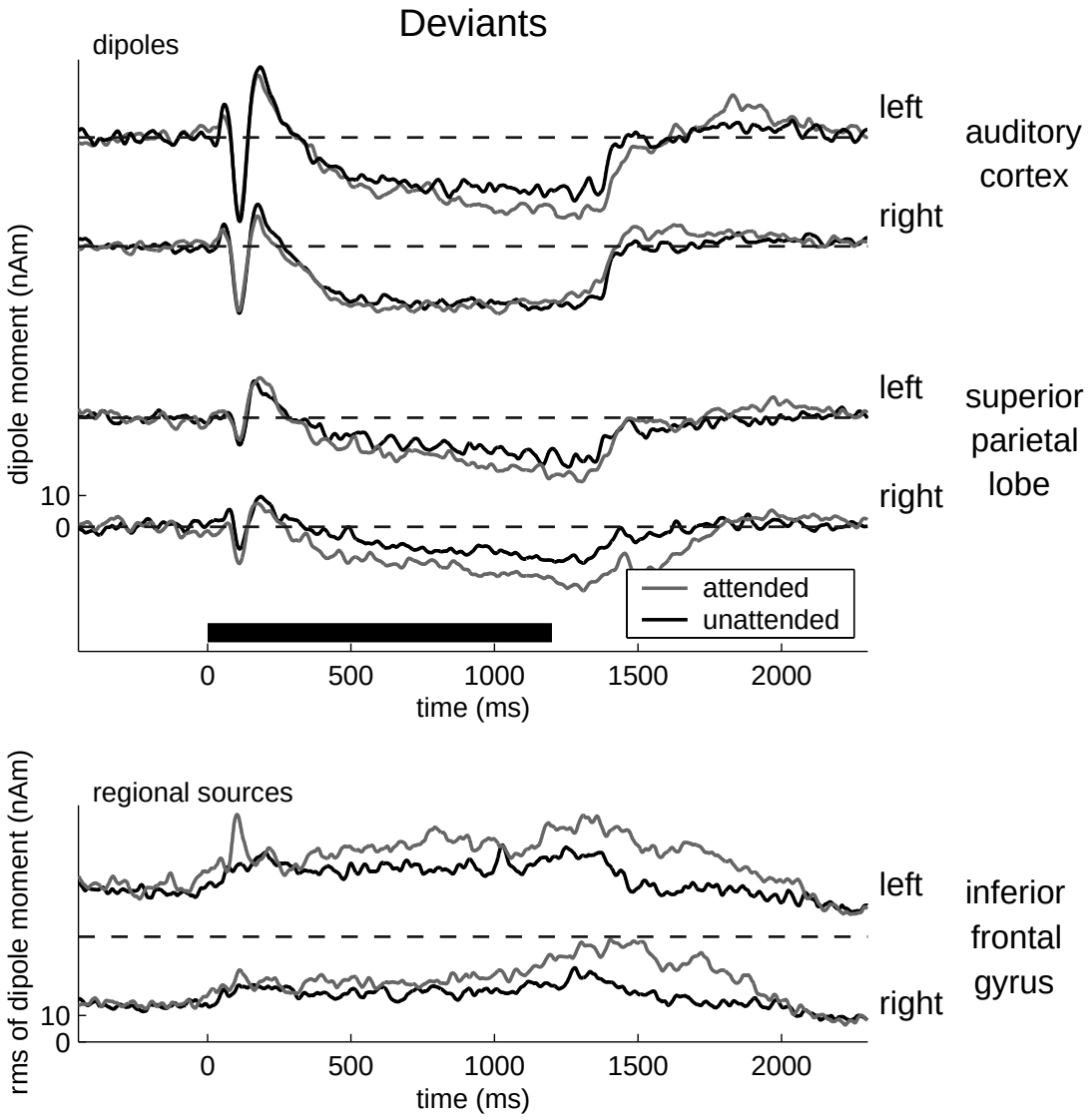


***Figure 4.5:*** *MEG Data, Tone Task: Grand average source waveforms in the seeded six-source model in answer to deviant stimuli. Note the similarity in the time course of the source waveforms as compared to Fig. 4.4. Again the left auditory cortex and the parietal sources show an attention-specific enhancement, whereas the nature of the frontal sources remains opaque.*

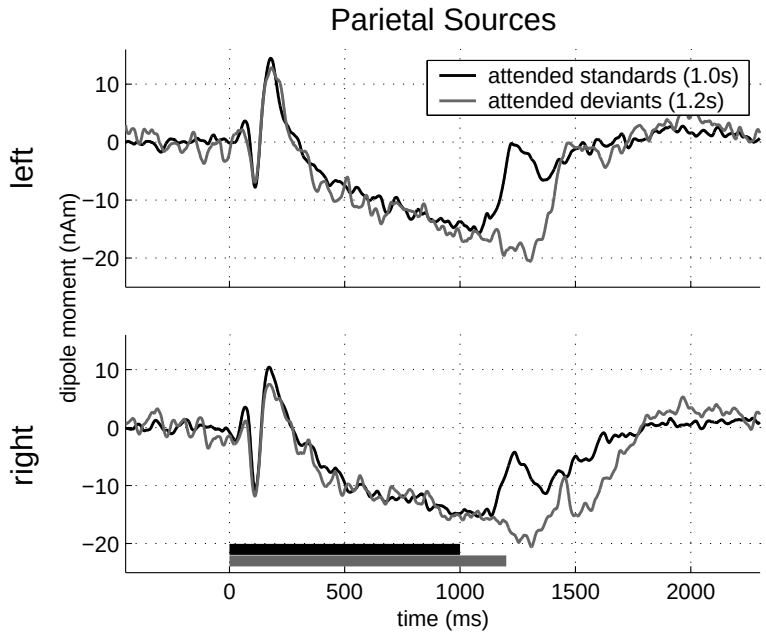


***Figure 4.6:*** *MEG Data, Tone Task: Grand average source waveforms for the parietal dipoles in answer to stimuli with differing lengths. The source waveforms in answer to the deviant stimuli agree with those evoked by the standard stimuli except for a prolongation of about 200 ms. Thus, the time course of the parietal sources is linked to the stimulus duration.*

Although implicit in Fig. 4.4 & 4.5 the time course of the left and right parietal source waveforms as evoked by standard and deviant stimuli is directly compared in Fig. 4.6. The respective mean offsets and $t$-intervals of the parietal slow wave are given in Table 4.3. Their difference of about 200 ms reflects the difference in the stimulus duration. Thus, the time course of the parietal source waveforms indicates the duration of the stimulus.

| type of stimulus | duration [ms] | hemisphere | mean latency SF offset [ms] | $t$-interval [ms] |
|---|---|---|---|---|
| standard | 1000 | left | 1192 | 33 |
| standard | | right | 1172 | 43 |
| deviant | 1200 | left | 1395 | 64 |
| deviant | | right | 1408 | 74 |

***Table 4.3:*** *Mean offsets and t-intervals of the parietal source waveforms with respect to standard and deviant stimuli. The difference in the offset latency is about 200 ms, which matches the difference in the stimulus duration.*

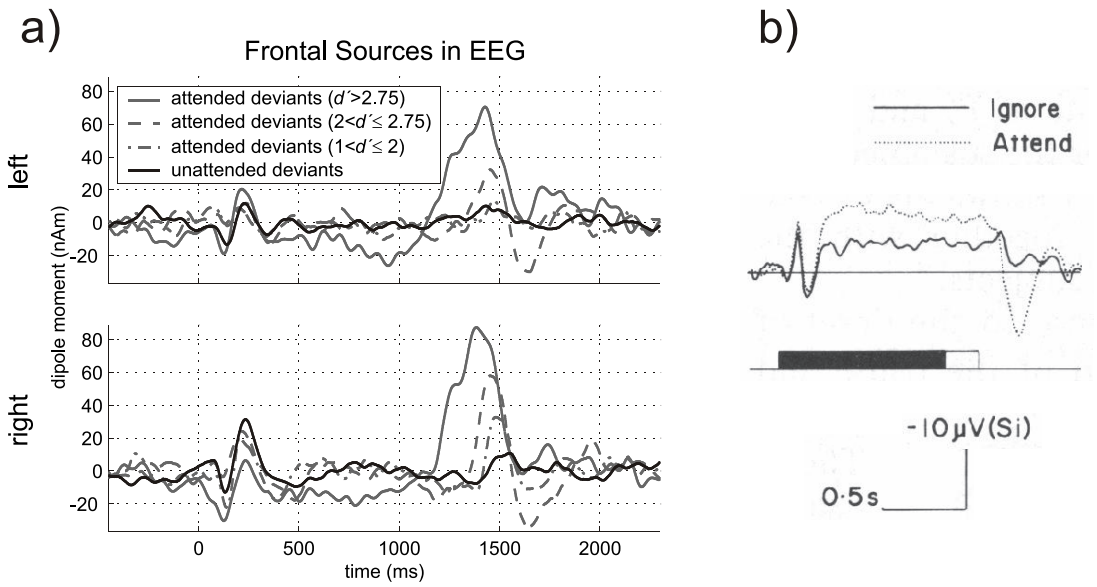


***Figure 4.7:*** *EEG Data, Tone Task: (a) Source waveforms of the two frontal sources taken from the seeded six-dipole model of the present study. Taking the six subjects pairwise according to their performance (high versus intermediate versus low d′-values) resulted in a decreasing transient deflection considered to be a P3. (b) Individual channel waveforms (vertex against right mastoid) evoked by deviant stimuli as taken from Picton et al. [102]. Both (a) and (b) exhibit a prominent P3 deflection in answer to attended deviants.*

## EEG Six-Source Model

To gain clarification about the nature of the sources seeded into the inferior frontal gyrus, the six-source model was applied to the EEG data as well. The source waveforms of the frontal sources as evoked by the deviants in the 'attend' and 'non-attend' condition are shown in Fig. 4.7a. Only the attended deviants evoked a prominent transient response about 1400–1500 ms post-stimulus onset. The amplitude of this deflection, which was considered to be a P3, was larger in those subjects which performed the task more adequately—also shown in Fig. 4.7a. Considering all six subjects the effect was significant only for the right hemisphere (right: $F_{1,5} = 6.00, p < 0.05$; left: $F_{1,5} = 2.67, n.s.$). Excluding the two subjects with the lowest discriminative ability (measured by $d'$ as introduced in Appendix C) resulted in a significant effect for both hemispheres (right: $F_{1,3} = 4.00, p < 0.05$; left: $F_{1,3} = 4.00, p < 0.05$).

## MEG Four-Source Model

All data presented in the four-dipole model are for the ten subjects only which participated in both the tone duration and the pause duration task. This was done to allow for direct comparisons between the two experiments (tones and pauses).

### Tone Discrimination Task

The grand average source waveforms for the four-dipole model applied to the tone task are given in Fig. 4.8. Again the left auditory cortex and the two parietal sources show a prominent attentional effect. This is confirmed by the statistical analysis given in Table 4.4.

| area | | epoch (post-tone onset) | $F_{1,9}$-value | |
|---|---|---|---|---|
| AC: | mean | 500–1000 ms | 2.43 | *n.s.* |
| | left | | 5.26 | $p < 0.05$ |
| | right | | 0.01 | *n.s.* |
| SPL: | mean | 750–1200 ms | 13.93 | $p < 0.01$ |
| | left | | 9.56 | $p < 0.05$ |
| | right | | 9.52 | $p < 0.05$ |

***Table 4.4:*** *Attentional effects on source strength in the four-dipole model for the tone task. The significant effects match those visible in the source waveforms of Fig. 4.8.*

### Pause Discrimination Task

As for the tone task (cf. Chapter 2), the transient auditory responses in the pause duration task revealed no significant attentional effect. The data for the mean over both hemispheres are:

P50: *attention*: $F_{1,9} = 0.27, n.s.$;
N100: *attention*: $F_{1,9} = 0.72, n.s.$;
P200: *attention*: $F_{1,9} = 0.72, n.s.$

For the auditory and parietal sustained responses we found no significant attentional effect, when using the above described 'transient baseline'. The element-wise comparisons are given in Table 4.5. Using the 'no-input baseline', element-wise comparisons for the parietal sources are, of course, the same; for the auditory

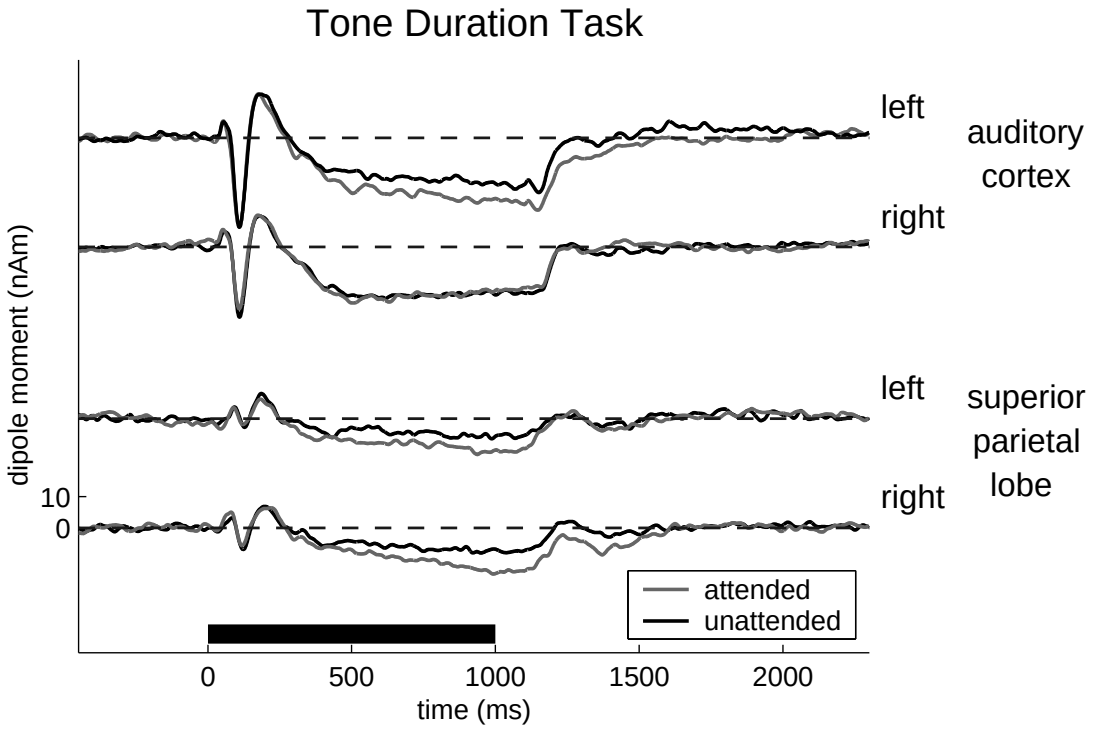


***Figure 4.8:*** *MEG Data, Tone Task: Grand average source waveforms in the seeded four-dipole model. Both parietal sources and the left auditory SF show a significantly increased amplitude for the 'attend' condition. The black bar indicates the temporal position of the tone.*

dipoles they differ and indeed revealed a significant attention-specific enhancement for the left sustained field—cf. Table 4.5. Thus, the sustained response in answer to tones is enlarged, although the target 'stimuli' for the attentional tasks are the pauses, not the tones. This is illustrated by the grand average source waveforms given in Fig. 4.9. The two different baselines for the auditory cortex get systematically compared in Fig. 4.10. As compared to the standard baseline (300 ms prior to pause-onset) used for the parietal sources, the 'no-input baseline' ('transient baseline') resulted in an offset of -13(-17) and -19(-20) nAm for the left auditory cortex in the 'attend' and 'non-attend' condition. For the right auditory cortex the offset of -8(-11) nAm was the same for both conditions.

| area | | epoch (after pause onset) | $F_{1,9}$ ('transient baseline') | | epoch (after pause onset) | $F_{1,9}$ ('no-input baseline') | |
|---|---|---|---|---|---|---|---|
| AC: | mean | 500–1000 ms | 0.11 | *n.s.* | 1500–2300 ms | 4.20 | *n.s.* |
| | left | | 1.69 | *n.s.* | | 8.58 | $p < 0.05$ |
| | right | | 0.70 | *n.s.* | | 0.68 | *n.s.* |
| SPL: | mean | 750–1200 ms | 2.13 | *n.s.* | | | |
| | left | | 2.80 | *n.s.* | | | |
| | right | | 0.66 | *n.s.* | | | |

***Table 4.5:*** *Attentional effects on source strength in the four-dipole model for pause task. With respect to the auditory responses data for the two different baseline definitions are given. Only the left sustained field showed an attention-specific enhancement.*

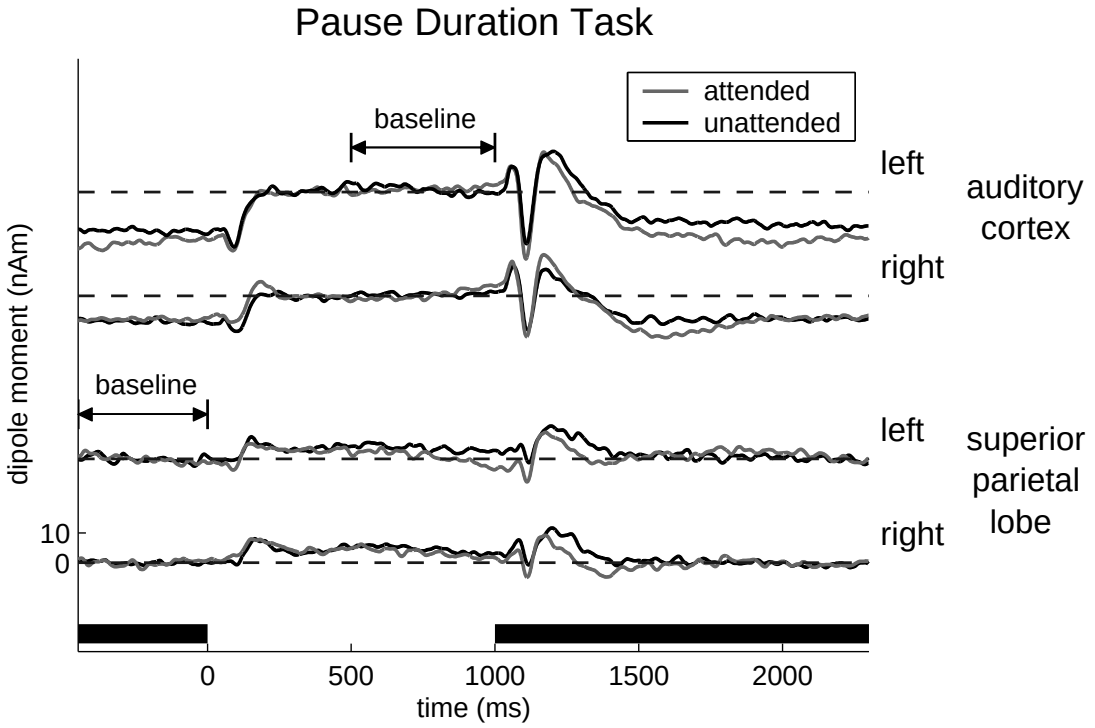


***Figure 4.9:*** *MEG Data, Pause Task: Grand average source waveforms in the seeded four-dipole model. The baseline for the parietal sources is defined over an epoch for which no attention-specific activation is assumed. The baseline for the auditory dipoles is defined over the epoch without sensory input ('no-input baseline'). For the resulting offsets see the main text. Again the black bar indicates the temporal position of the tone.*

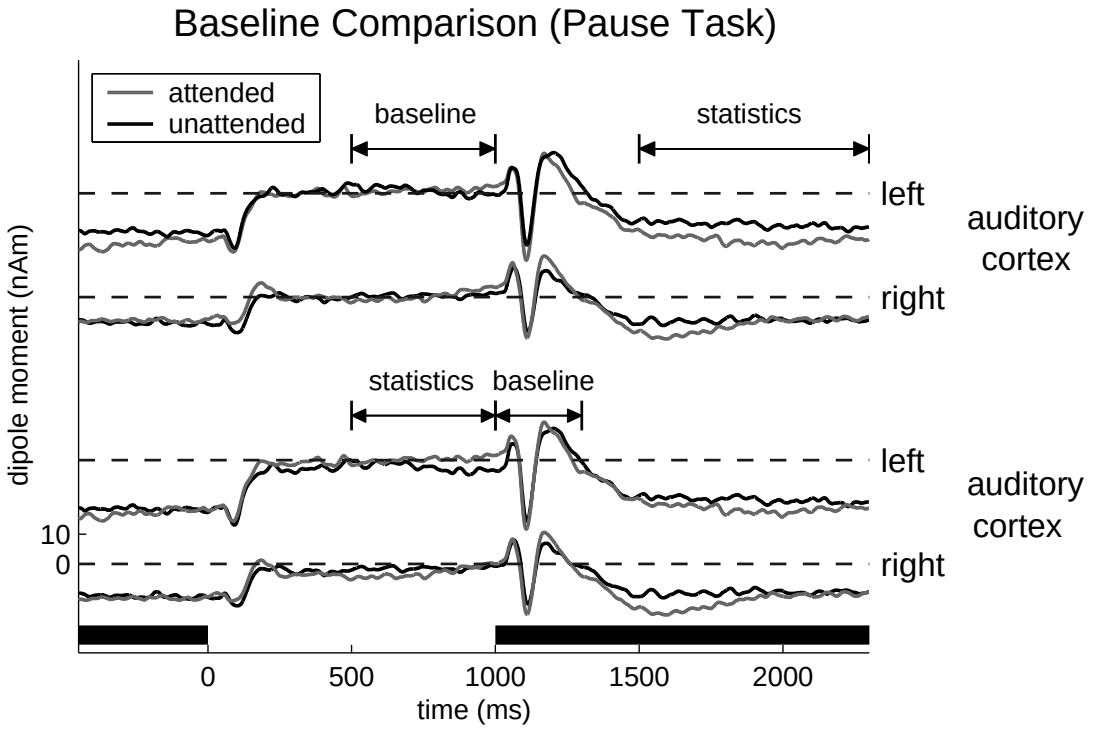


***Figure 4.10:*** *MEG Data, Pause Task: Grand average source waveforms for the auditory cortices using different baselines. Top: 'no-input baseline', defined over an interval lacking auditory stimulation (as employed in Fig. 4.9). Bottom: Since we know from Chapter 2 that the transient responses show no attentional effect, they can be used for baseline definition as well ('transient baseline'). For the resulting offsets see the main text. The intervals tested for attention-specific enhancements are also indicated.*

## 4.4 Discussion

The aim of this chapter was to investigate possible functional differences between the brain areas activated during the performance of a duration discrimination task. To gain the needed spatially and temporally highly accurate model, we re-analysed the MEG data of Chapter 2 with seeded locations as gathered from our fMRI data of Chapter 3. Further evidence for functional differences was gathered from a MEG experiment on pause discriminations which allowed for identifying the dependence upon sensory input for the different brain areas involved.

### Model Gathering

The fMRI experiment of Chapter 3 revealed a bilateral parietal activation which in the $yz$-plane agreed very well with the mean value of the third dipole fitted in the MEG data of Chapter 2 (cf. sagittal view in Fig. 4.2—something more on the agreement and the inherent errors of the different methods is said at the end of Appendix B). This strongly suggested that the activations depicted in the fMRI and MEG data originated from the same area, only that the MEG model was biased in $x$-direction by assuming one instead of two symmetric activations. (However, note that such a symmetric model could not be fitted to the majority of the individual MEG data sets.) Thus, the two fMRI seeds were used to replace the third source of Chapter 2. Since the frontal activations were very prominent in the fMRI data it seemed sensible to use them for a seeded model as well. Here regional sources were employed to estimate the whole neuromagnetic power at these sites and to learn about whether prominent patterns (transient responses or well-defined slow waves) are visible.

For the pause discrimination task seeds were kept fixed, since the location of the frontal activations completely agreed and since the widespread parietal network was well approximated by the more focussed parietal sources found in the fMRI experiment on tone discriminations (Fig. 4.3). Moreover, retaining the parietal seeds allowed for direct comparison between tasks and ensured the attempted parsimoniousness of the model (see above).

The auditory activation from the 'sound-silence passiv' contrast was used for both tasks. The exact seeding location was defined by the mean location of the three prominent auditory BOLD activations (Fig. 4.1).

## MEG Six-Source Model

The source waveforms of the two dipoles seeded into the superior parietal lobe exhibited the same time course as the third dipole in Chapter 2—cf. Fig. 4.4 & 4.5. Thus, we gained further evidence that the parietal activation is a bilateral one. Further, it was shown in Fig. 4.6 that the duration of this parietal slow wave is related to the length of the stimulus; a stimulus duration increase of 200 ms resulted in a 200 ms prolongation of the slow wave. Thus, the parietal activation does not reflect the evaluation of a 1.0 s duration template which gets compared to all incoming stimuli. It rather evaluates or monitors the incoming stimulus over its full time span.

Both the evaluation of the standards and of the deviants revealed no prominent pattern for the frontal sources. However, the largest attentional difference in the source waveforms occurred about 1300–1600 ms post-stimulus onset. Knowing that radial source activation escapes the MEG, a re-consideration of the EEG data was necessary to decide whether the frontal BOLD responses have an event-related electrophysiological counterpart or not. (See Appendix A for a derivation of the MEG's 'radial blindness'.)

## EEG Six-Source Model: P3 Effect

Indeed within the six-source model for the EEG data, the frontal activation (the regional MEG sources were now turned into dipoles) revealed a prominent transient response occurring after 1300–1600 ms post-stimulus onset for the deviant but not for the standard stimuli—see Fig. 4.7. This parallels the findings of Picton et al. [102] given in the same figure. Further, excluding subjects with poorer performance from the group analysis led to an increase in the amplitude of the transient deflection (Fig. 4.7). Thus, the latency (it occurs about 300 ms after deviant offset), the time course of the deflection and its dependence upon the accurateness of the deviant detection showed it to be a P3 response (the fact that the amplitude of the P3 is related to the accurateness of the deviant detection was repeatedly shown [104]). Further, the frontal location of the P3 generator is in accordance with, for instance, the findings of Yamazaki et al. [146]. Admittedly, there is considerable controversy about the spatial origin of the P3 and usually it is reported with a centro-parietal maximum in the EEG channel waveforms. However, the fact that there is a frontal topography contributing to the P3 is also evident. Segalowitz et al. [125] found that the ratio of the P3 amplitude at frontal versus posterior sites increases with the complexity of the task and that a

rapid decrease of the frontal P3 occurs for simple tasks. Thus, the high difficulty of the present task might account for the fact that in our data the frontal P3 generators are more prominent than possible posterior ones. Furthermore, Kiehl et al. [61] showed in an event-related fMRI study that the N2-P3 complex stems (amongst other areas) from the inferior frontal gyrus and the insula, which is where we found it to be generated.

Since the P3 is related to the accurateness of detecting deviants, one might wonder why in the fMRI data the frontal activation also occurred when only standards were evaluated (cf. Fig. 3.11 in the previous chapter). Part of the answer lies in the difference in method; that is integrating sluggish hemodynamic responses over several seconds versus measuring electric currents on a millisecond-scale—cf. Appendix B. However, there are fMRI studies saying that good task performance is correlated with enhanced BOLD activation in frontal regions [63]. And notably the individual 'attention sound' contrast of our poorest performer (S5 in Fig. 3.10) nearly showed no frontal activity at all.

## MEG Four-Source Model

Having clarified the nature of the frontal P3 response and knowing that is not visible within the MEG data, the two frontal sources were omitted in the further MEG analyses. The resulting four-source model was used to compare the tone task with the pause task.

The most striking similarity between the two tasks concerns the auditory sustained fields—cf. Fig 4.8 & 4.9. For both tasks and for all source models and baselines the attentional-effect was larger for the left than for the right sustained field; and it was statistically significant for all analyses of the standard tones in the tone task (three-dipole model of Chapter 2, four- and six-dipole model of this chapter) and for the 'no-input baseline' of the pause task. As already suggested in Chapter 2, this might be explained by the work of, for instance, Zatorre and Belin [147] who found that temporal processing, and hence the processing of encoded and actual duration, predominantly takes place in the left hemisphere whereas spectral processing is assumed to be more prominent in the right hemisphere.

The main dissimilarity between the tone and the pause task is found with respect to the activation of the superior parietal lobe. Here only the former task exhibited a significant attentional effect, which suggested that the parietal slow wave depends upon *sensory* input. Comparing Fig. 4.8 & 4.9 shows that not only

the attention-specific difference but also the separate magnitudes of the parietal activation was larger for the tone task. Both facts are in line with the EEG channel data of the aforementioned studies by Picton et al. [102]. They also found greater absolute values for the activation in both the attend and ignore condition of a tone task as compared to a pause task; and it can be seen from their data that the attention-specific difference was also larger for the tone task.

## Conclusion

The aim of this chapter was to learn more about the brain activation specific to duration discrimination and about possible functional differences between the areas involved. This was done in particular by comparing the different time courses of the attention-specific electrophysiological activation in a model seeded from our fMRI experiment. Remember that in Chapter 2 such a difference in time course already helped separating the auditory from the parietal attentional effect. While the left sustained field showed a constant enhancement in the 'attend' condition, the parietal dipole showed an increasing effect.

The different time courses of the source waveforms allowed for a functional separation of the parietal from the frontal attention-specific activation within the tone task. On the one hand, the time course of the parietal sources suggest a monitoring or evaluating activity, for the duration of the response was related to the duration of the stimulus. This is in line with the monkey studies mentioned in the last chapter, which—by using implanted electrodes—found single neurons within the parietal cortex that represent time [65]. On the other hand, the frontal electrophysiological activation was found to be a P3, depending on the accuracy of the discriminative performance. This strongly suggests the frontal activation to be an executive one related to subsequent behavioural action. It, so to speak, 'takes up the parietal evaluation' and 'says' whether it was a deviant or not. This also speaks against its specificity with respect to duration tasks which—as we have seen—is in accordance with the literature. Human studies on high-level perception also suggest that the generation and execution of a plan predominantly takes place in frontal areas, while superior parietal activation is linked to attentional and memory processing [93]. Investigations of the cingulate gyrus also separate a posterior evaluative from a frontal executive region [142]. Several other studies are at least partially in line with these findings—see, e.g., [14]. Finally, the fact that Broca's area, where our frontal dipole was located, is related to executive mechanism is also suggested by animal studies on the homologous area within macaque monkeys [30].

While the activation stemming from the parietal cortex was very prominent for the tone task, it was found to be considerably diminished for the pause task. Also the attention-specific difference now failed to reach significance. However, as for the tone task a constant attention-specific enhancement of the left sustained field evoked by the tones was found. This is the more interesting since the intervals to pay attention to were not the tones but the pauses marked by tone onsets and offsets. The conclusion to be drawn is twofold. First, attentive listening leads to an enhanced auditory sustained field, notwithstanding whether long lasting tones are attended to or tone onsets and offsets marking a pause. Second, the parietal network involved in duration discrimination depends upon sensory input; in a pause task its event-related activation is considerably decreased. One could speculate (i) whether this is in part due to a failure in synchronising attention to intervals lacking sensory input and (ii) whether this is reflected by our fMRI finding of the last chapter that a pause discrimination task 'forces into the recruitment of more widespread cortical areas'.

The obvious follow-up question is whether these differences and similarities between discriminating intervals with and without sensory input (tones versus tone pauses) are typical for the auditory system. Thus, further MEG studies on discriminating intervals with and without sensory input were conducted for a sensory modality other than the auditory one. The next chapter presents our experiments on picture and picture pause duration discrimination tasks.

# Chapter 5

# MEG-Study on Picture & Picture Pause Durations

## 5.1 Introduction

In the last chapter we investigated the communalities and differences in the processing of filled and empty acoustic intervals, that is tones and pauses. The next step to learn about time perception more generally is the examination of a further sensory modality. Thus, having discussed the general dependence of the parietal activation upon auditory sensory input in Chapter 3 & 4, we now investigated it with respect to visual sensory input. This was done by conducting two MEG experiments on the discrimination of picture and picture pause durations.

In particular, one would like to decide between the following two hypotheses: (i) the parietal network strongly depends upon sensory input but is *modality-invariant*; (ii) the parietal network strongly depends upon *auditory* sensory input. If the communalities and differences in the processing of filled and empty visual intervals reflected those of the auditory domain, the former hypothesis would be underpinned. If, however, the results of both visual tasks resembled those of the tone *pause* task, then the latter hypothesis would be vindicated; that is we would have to conclude that there is something special about the way our brain processes durations filled with sound.

Additionally, the investigation of long lasting visual stimuli (we shall again use stimuli enduring for 1.0 s and 1.2 s) is interesting because of the rarely investigated visual sustained field. Although it was first reported upon back in 1978 by Jarviletho et al. [58], there are very few studies about it (mainly [133], [76]) and

to our knowledge it was never tested for a duration-specific attentional effect like the auditory sustained field.

This chapter will proceed as follows. First, the MEG data of the picture task will be analysed similarly to the tone data in Chapter 2; i.e. by means of a fitted two and three dipole model. Second, both picture and picture pause data will be evaluated in a combined fit-seed model resembling that of Chapter 4; that is the fitted sources for the visual cortex will be combined with the two parietal sources the location of which we gathered from the fMRI experiment of Chapter 3.

## 5.2 Material and Methods

As for the auditory tasks of Chapters 2 & 4, the amplitude of the components of the visually evoked fields as recorded during the performance of two duration discrimination tasks were compared with those from the 'non-attend' conditions.

### Stimuli and Tasks

Two oddball paradigms were used with white circles presented on a screen against a black background at a visual angle of 1°. Otherwise, stimulus presentation and task were exactly the same as in the auditory tasks of Chapters 2 & 4. That is, for the picture discrimination the standard circles lasted for 1.0 s and were interspersed with slightly longer deviants (1.2 s duration) in 20% of all cases. Altogether 310 standard and 63 deviant tones were presented. The sequence was randomised and presented with an interstimulus interval (ISI) of 1.35–1.40 s. For the discrimination of the picture pauses the stimulation was inversed; i.e. a dark screen was presented for 1.0 s (80% standard) or 1.2 s (20% deviants). During the interpause interval of the randomised sequence the white circles were presented for 1.35–1.40 s.

Both discrimination tasks were constrained in that the beginning of each sequence was marked by three standards and that two deviants were never consecutive. Subjects were informed about these constraints to ease the task. In the 'attend' condition subjects were asked to press the button of a computer mouse in answer to a deviant. For both tasks the order of the conditions was reversed for 5 of the 10 subjects to avoid effects of habituation in the grand average. The 'non-attend' condition contained only standards, allowing for a higher number of averages (500). Subjects were informed about this to further prevent them from paying attention to stimuli in the 'non-attend' condition.

## Subjects

Ten subjects, after having given informed consent, participated in four magnetoencephalographic (MEG) recordings each; an 'attend' and a 'non-attend' condition for both the discrimination of pictures and of picture pauses. Subjects were the same as in the tone pause task of Chapter 4—details like mean age and handedness see there.

## Recording and Data Processing

Recordings were made with the same hardware and acquisition settings as in the tone pause task—cf. Chapter 4. The same holds for the data processing (artefact rejections, baselines etc.)

## Source Analysis

All reported data are based on responses to standard stimuli; the resulting high number of averages improved reliability. The following three models were made for the picture task.

### Two-Dipole Model (Fitted)

The data were analysed with a spatio-temporal source model comprising one equivalent dipole near the expected location of the primary visual cortex in each hemisphere. The dipole pair was fitted (without additional filtering) to the epoch 0–1000 ms post-stimulus onset to gather a sensible location for all transient and sustained responses of the visual cortex. The dipoles where constraint on location in that they were assumed to be symmetric in the $x$-direction but with no constraints on orientation. Next the orientation was re-fitted over the plateau of the sustained field 500-1000 ms post-stimulus onset. This two-dipole model was adapted for each individual from the 'non-attend' condition and held fixed as a spatio-temporal filter for both the 'attend' and 'non-attend' condition.

Ocular artefacts were accounted for a regional source. To estimate the slow magnetic artefacts inherent in DC recordings, a PCA was computed for each average condition over the epoch 2100–2300 ms post-stimulus onset; i.e., 1100–1300 ms post-stimulus offset. The PCA component explaining the majority of

the variance was included for each experimental condition. (The computation of a PCA is explained in detail in Appendix A.)

The strength of the transient response was read off their extremal amplitude over the epochs 50–150 ms (P100), 100–200 ms (N145) and 150–300 ms (P200). The source strength of the sustained field was assessed by calculating the mean dipole moment over the epoch 500–1000 ms post-stimulus onset which covered exclusively the plateau of the waveforms.

### Three-Dipole Model (Fitted)

Starting from the two-dipole model a further dipolar source was fitted without constraints over the epoch 750–1200 ms post-stimulus onset in the 'attend' condition. This paralleled the procedure of Chapter 2, where we chose the lower boundary of this epoch to avoid an overlap with the P200 deflection and the upper boundary to ensure that the slow increase and maximum of the source activity of the third dipole was covered for all subjects. Such a model could be gathered for seven of the ten individual data sets, for which the signal to noise ratio was high enough.

The source strength of the third dipole was assessed by calculating the mean over the epoch 750–1200 ms post-stimulus, which covered the deflection's maximum activation. The strength of the sustained field was assessed as for the two-dipole model.

### Four-Dipole Model (Fit-Seed Mixture)

A further analysis was carried out by adding the two parietal dipoles of Chapter 4 into the initial two-dipole model of the ten subjects. The orientation was fitted without constraints over the epoch of 750–1200 ms post-stimulus onset in the 'attend' condition. The source strength of these dipoles was calculated over the same epoch; i.e. as was the strength of the third source in the fitted model. The strength of the sustained field was assessed as above.

This four-dipole model was adapted for each individual from the picture task and held fixed as a spatio-temporal filter for the data on the discrimination of picture pauses. Only the PCA components modelling the slow magnetic artefacts were newly calculated for each condition. As compared to the tone pause task only the 'no-input baseline' was used. So the source waveforms of the visual dipoles were renormalised by subtracting their mean value over the epoch 500–1000 ms

post-pause onset. (Choosing such a baseline is further described and defended in the section 'Methods' of Chapter 4). The 'transient baseline', which we used for the tone pauses, was not applied here, for we found an attentional effect on the visual transient responses (cf. below). Thus, other than for the auditory domain, such a baseline would considerably blur attentional effects with respect to visually evoked fields.

### Statistics

All statistical procedures were carried out in the same manner and by the same software as in Chapters 2 & 4.

## 5.3 Results

### Fitted Models

The grand average source waveforms based on the individual two-dipole models are depicted in Fig. 5.1 (all source waveforms presented in this chapter got bandpass-filtered from 0.01–20 Hz using a zero phase shift Butterworth filter with 12 dB/oct). An increased amplitude for the source waveforms in the 'attend' condition can be seen for the N145 as well as for the sustained field (SF). This is in accordance with the statistical evaluation given in Table 5.1.

| response | $F_{1,9}$-value | | | | $F_{1,9}$-value | |
|---|---|---|---|---|---|---|
| P100: | mean | 0.63 | *n.s.* | left | 4.99 | *n.s.* |
| | | | | right | 0.39 | *n.s.* |
| N145: | mean | 5.94 | $p < 0.05$ | left | 6.94 | $p < 0.05$ |
| | | | | right | 3.99 | *n.s.* |
| P200: | mean | 0.24 | *n.s.* | left | 1.08 | *n.s.* |
| | | | | right | 0.08 | *n.s.* |
| SF: | mean | 13.24 | $p < 0.01$ | left | 7.60 | $p < 0.05$ |
| | | | | right | 12.25 | $p < 0.01$ |

***Table 5.1:*** *Elementwise comparisons for attentional effects in the fitted two-dipole model. The N145 and the sustained field (SF) show a significant effect which corresponds to the source waveforms in Fig. 5.1.*

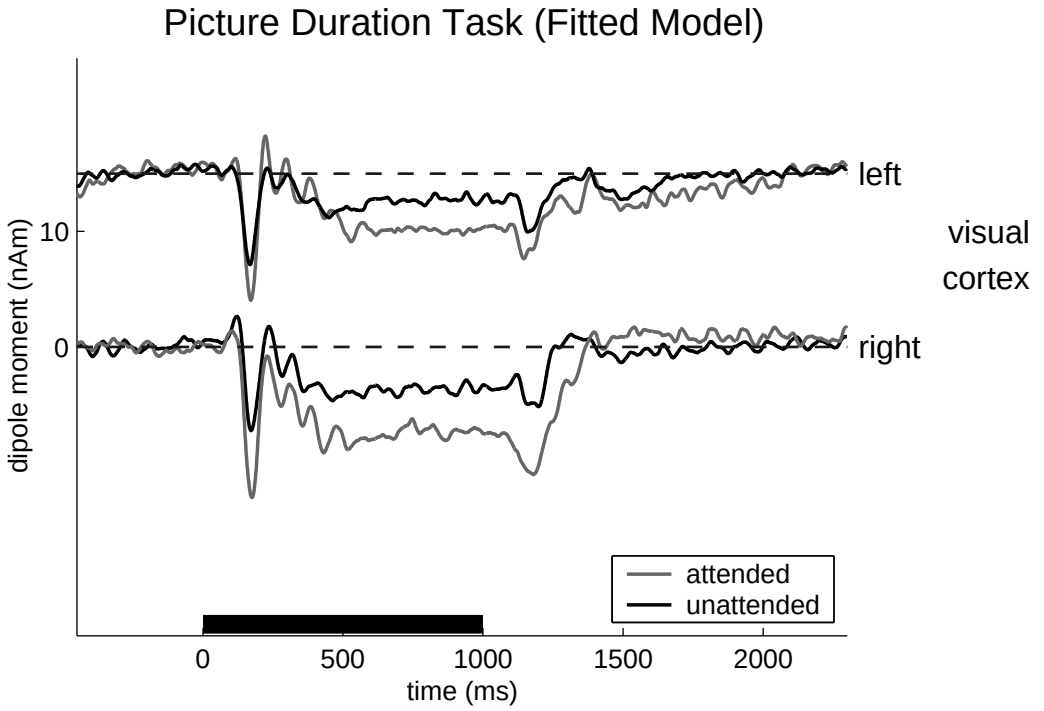


***Figure 5.1:*** *Picture Task: Grand average source waveforms for all ten subjects in the fitted two-dipole model. An attentional effect on the N145 as well as on the sustained field in terms of an increased amplitude is seen for both hemispheres. The black bar indicates the temporal position of the standard stimulus (white circle).*

This model had an arcsine transformed mean residual variance of 52% (transformed SD: 5%; Range: 21–78%) for the 'attend' and 53% (transformed SD: 4%; Range: 23–74%) for the 'non-attend' condition over the epoch 0–1500 ms.

The top view in Fig. 5.2 for the difference between the channel waveforms of the 'attend' and the 'non-attend' conditions revealed a pattern of activation above the parieto-occipital region similar to that of Chapter 2 for the tone task. A third dipole was introduced to model this activation. The resulting model had a mean residual variance of 38% (SD: 3%; Range: 17–59%) for the 'attend' and 46% (SD: 3%; 21–69%) for the 'non-attend' conditions. Compared with the two-dipole model this was a significant decrease in residual variance (*dipole number*: $F_{1,6} = 17.29, p < 0.01$). The interaction between the different models and the attentional condition, which tests for the specific decrease in residual variance over the attentional conditions by introducing a third dipole, was highly significant (*dipole number* $\times$ *attention*: $F_{1,6} = 19.06, p < 0.01$).

The grand average of the source waveforms for the three-dipole model is depicted

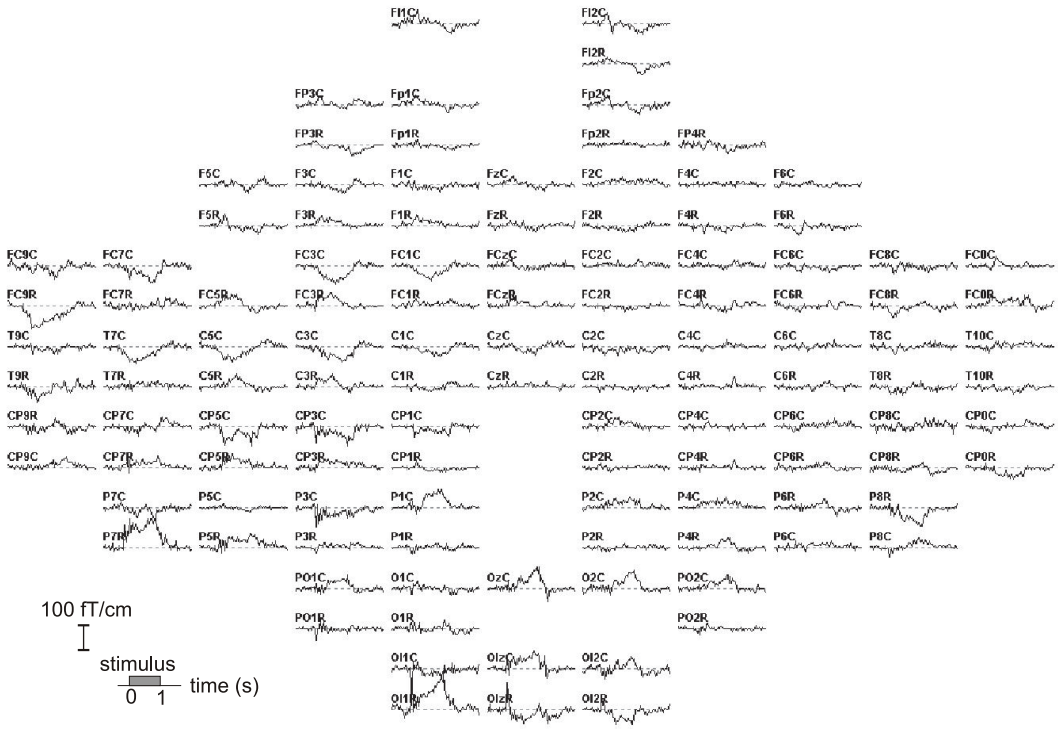


***Figure 5.2:*** *Picture Task: Individual MEG channel waveforms in top view for the difference between the 'attend' and 'non-attend' condition. The sensor data above the parieto-occipital region suggest the existence of a further attention-specific source.*

in Fig. 5.3. We found a significantly increased dipole moment for the attend condition (*attention*: $F_{1,6} = 22.95, p < 0.01$) and a significant interaction between attention and sources (visual sustained field versus third dipole; *attention* $\times$ *sources*: $F_{1,6} = 10.00, p < 0.05$). Elementwise comparisons for each source yielded an approximate value for their contributions to the overall effect. In agreement with the results of Fig. 5.3, the largest effect was found for the third source ($F_{1,6} = 16.90, p < 0.01$). A smaller but still significant effect was also determined for the two dipoles in the visual cortex ($F_{1,6} = 8.88, p < 0.05$), which mainly stemmed from the right hemisphere (right: $F_{1,6} = 10.41, p < 0.05$; left: $F_{1,6} = 1.23, n.s.$).

Using the individual 3D MRIs data sets we calculated the coordinates for the third source according to Talairach and Tournoux [137]. The average values were $x = 5$ (SE: 12), $y = -57$ (4), $z = 28$ (6). All individual as well as the mean Talairach coordinates are presented in Fig. 5.4, which shows an individual MRI scan for which the average and individual coordinates agreed best. The mean

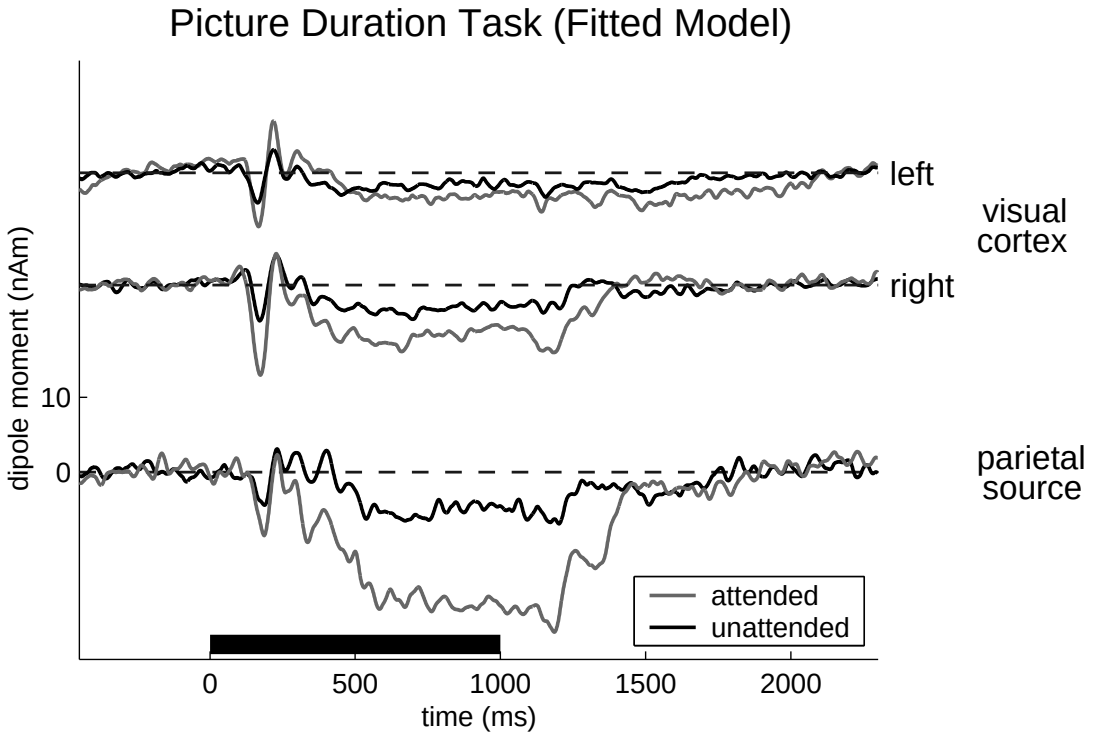


***Figure 5.3:*** *Picture Duration Task: Grand average source waveforms for six subjects in the fitted three-dipole model. The major difference between the conditions is seen for the waveforms of the third source. The right sustained field shows only a slight amplitude augmentation in the 'attend' condition while the left exhibits no substantial difference between conditions. Again the left and right N145 show a prominent attentional effect.*

is located in the area of the posterior cingulate gyrus (postGC); however, due to the large standard error of means, the location of the third source cannot be separated from the precuneus (PCu). Thus, it agrees well with the location found for the third dipole in the tone task (Chapter 2).

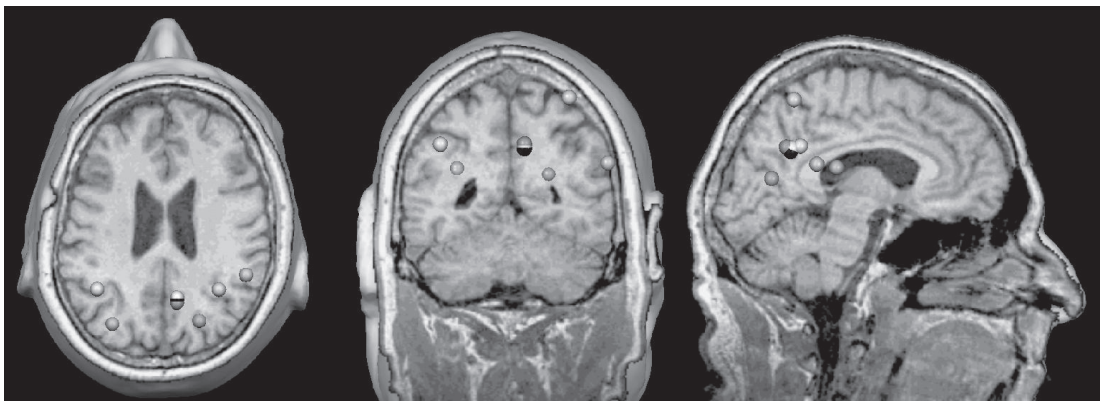

***Figure 5.4:*** *Location of the third source which accounts for the main part of the attentional effect in picture duration discriminations. The white balls represent the individual Talairach coordinates of seven subjects for which a three-dipole analysis was carried out. The black ball gives the mean Talairach coordinates* $x = 5$ *(SE: 12),* $y = -57$ *(4),* $z = 28$ *(6), which agrees well with the location of the third dipole in the tone task of Chapter 2. To illustrate the location, an individual MRI scan was chosen for which the average and individual coordinates agreed best.*

## Combined Four-Source-Models (Fitted and Seeded)

### Picture Discrimination Task

The grand average of the source waveforms for the four-dipole model of the picture duration task are depicted in Fig. 5.5. We found a significantly increased dipole moment for the visual sustained field and for the parietal responses in the attend condition (*attention*: $F_{1,9} = 17.09, p < 0.01$). This is particularly true for the right hemisphere as can also be seen from the elementwise statistical analysis given in Table 5.2. The fact that the attention-specific difference in the amplitude of the visual sustained field is more prominent for the right hemisphere is in accordance with the data for the two- and three-dipole model from above.

| area | | epoch (post-tone onset) | $F_{1,9}$-value | |
|---|---|---|---|---|
| VC: | mean | 500–1000 ms | 6.42 | $p < 0.05$ |
| | left | | 2.48 | *n.s.* |
| | right | | 6.21 | $p < 0.05$ |
| SPL: | mean | 750–1200 ms | 9.42 | $p < 0.05$ |
| | left | | 2.16 | *n.s.* |
| | right | | 18.94 | $p < 0.01$ |

***Table 5.2:*** *Attentional effects in the four-source model for the picture task. Both the source strengths within the visual cortex (VC) and the superior temporal lobe (SPL) show significant effects matching those visible in the source waveforms of Fig. 5.5.*

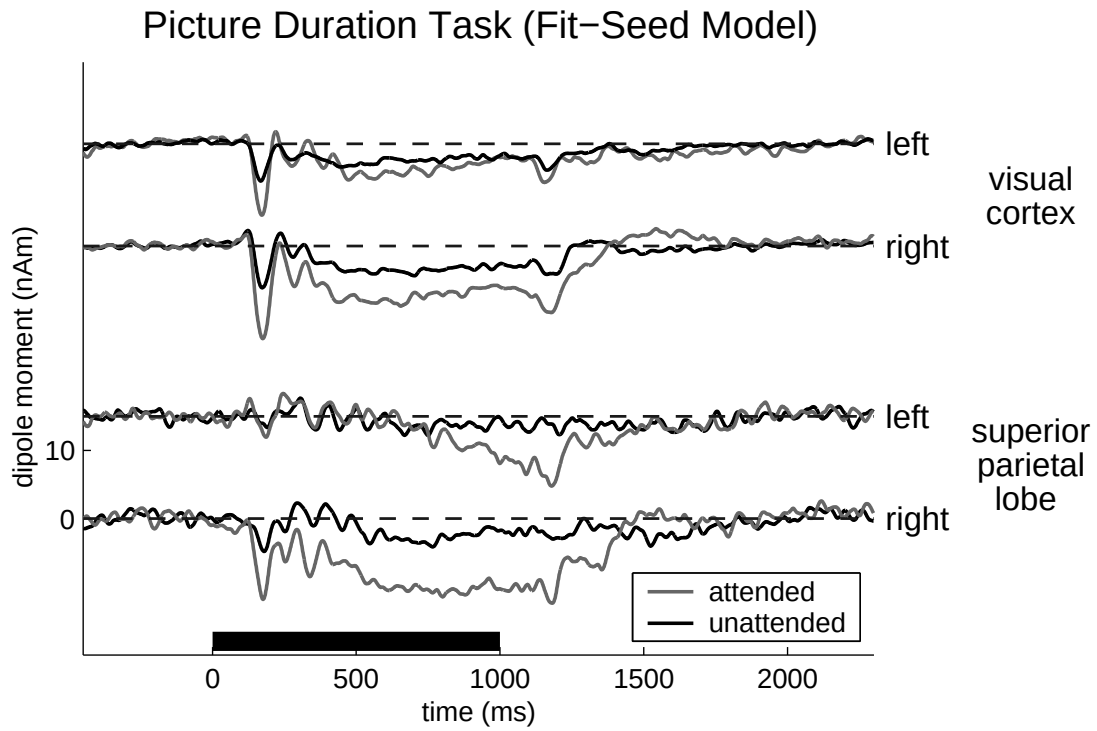


***Figure 5.5:*** *Picture Duration Task: Grand average source waveforms for the ten subjects in the combined four-dipole model (visual cortex fitted, superior parietal lobe seeded). The major difference between the conditions is seen for the waveforms of the right parietal source. However, also the right visual activation shows a significant augmentation in the 'attend' condition for the N145 and the sustained field. The black bar indicates the temporal position of the standard stimulus (white circle).*

### Picture Pause Discrimination Task

Fig. 5.6 gives the source waveforms of the combined model for the discrimination of picture pauses using a 'no-input baseline' as motivated and defined in Chapter 4. As for the picture task, the transient visual responses revealed a significant attentional effect. Here an increased amplitude for the source waveforms in the 'attend' condition was found for the hemispheric mean of the N145. Other than in the two-dipole, however, this time the effect was mainly due to the right visual cortex activation—cf. Table 5.3. Further, the visual sustained field showed an attention-specific enhancement for the left hemisphere and for its hemispheric mean—cf. Table 5.3. As for the N145, the mean effect agrees with that found for the two- and three dipole model, but the hemispheric asymmetry differs. For the other two models the augmentation was found to be biased towards the right.

The sources within the superior parietal lobe (SPL) exhibited no overall but a right hemispheric effect—cf. Fig. 5.6 and Table 5.3. Thus, as compared to the picture task the attention-specific difference is considerably decreased. A comparison of Fig. 5.5 & 5.6 also shows that the amplitudes themselves are diminished for the picture pause task. Both results match the findings of the comparison between tone discrimination and tone pause discrimination in Chapter 4.

| response | | $F_{1,9}$-value | | | $F_{1,9}$-value | |
|---|---|---|---|---|---|---|
| P100: | mean | 6.10 | $p < 0.05$ | left | 3.90 | *n.s.* |
| | | | | right | 1.67 | *n.s.* |
| N145: | mean | 15.47 | $p < 0.01$ | left | 2.83 | *n.s.* |
| | | | | right | 8.04 | $p < 0.05$ |
| P200: | mean | 1.96 | *n.s.* | left | 3.01 | *n.s.* |
| | | | | right | 0.93 | *n.s.* |
| SF: | mean | 5.96 | $p < 0.05$ | left | 6.00 | $p < 0.05$ |
| | | | | right | 3.06 | *n.s.* |
| SPL: | mean | 3.43 | *n.s.* | left | 0.37 | *n.s.* |
| | | | | right | 6.56 | $p < 0.05$ |

***Table 5.3:*** *Elementwise comparisons for attentional effects in the combined four-dipole model for the picture pause task. Two responses stemming from the visual cortex, namely the transient N145 and the sustained field (SF), show a significant enhancement due to attention. The sources within the superior parietal lobe (SPL) exhibit no overall but a right hemispheric effect.*

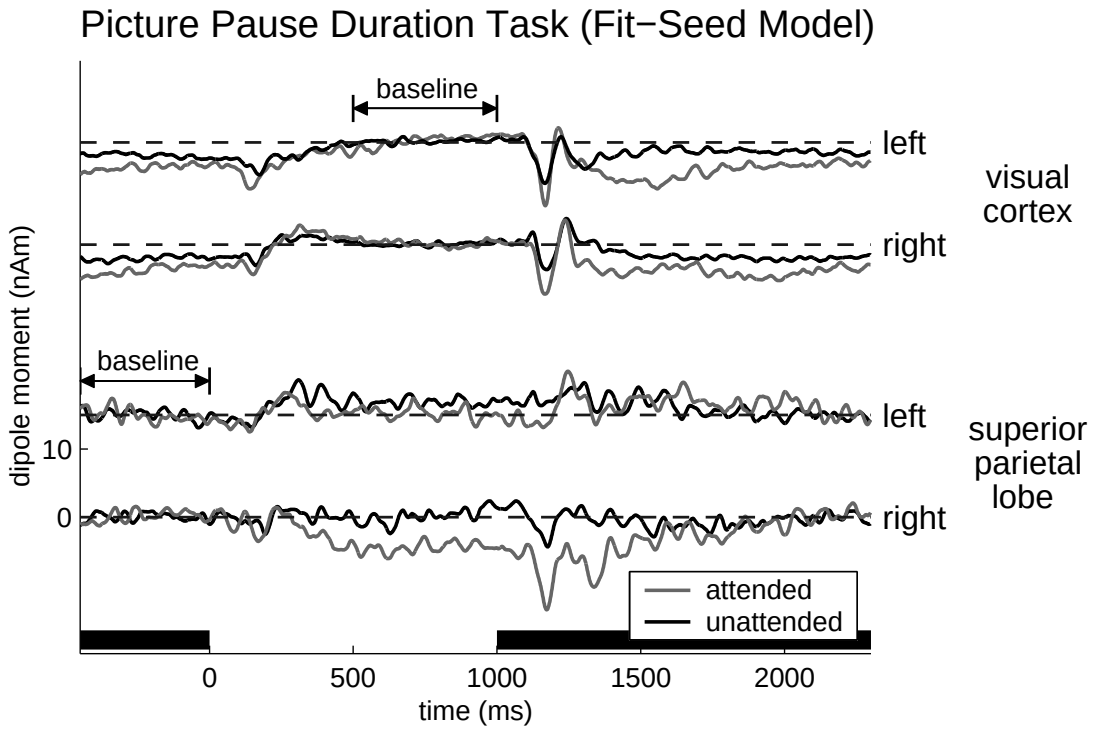


***Figure 5.6:*** *Picture Pause Duration Task: Grand average source waveforms for the ten subjects in the combined four-dipole model (visual cortex fitted, superior parietal lobe seeded). The baseline for the parietal sources is defined over the 300 ms prior to pause-onset, for which no attention-specific activation is assumed. The baseline for the visual dipoles is defined over the epoch 500–1000 ms post-pause onset, where there was no sensory input ('no-input baseline', which resulted in an offset of about -4 nAm and -2 nAm for the attend and the non-attend condition). The largest difference between conditions is seen in the waveforms of the right parietal source. However, also the visual dipole shows a significant amplitude augmentation in the 'attend' condition for the right N145 and the left sustained field. The black bar indicates the temporal position of sensory stimuli (white circles).*

## 5.4 Discussion

The aim of this study was to investigate the modality-specificity of our findings with respect to auditory duration discrimination task. This was done by investigating the amplitude and generator structure of neuromagnetic responses when discriminating visual filled and empty durations (pictures versus picture pauses).

### Transient Responses

Whereas the findings with respect to the visual and auditory sustained field agree very well (see below), they differ for the transients. The amplitude of the visually evoked N145 shows an attentional effect in all models (two-, three- and four-dipole model), while all auditory responses prior to the sustained field lack such an effect.

However, both findings are in agreement with the literature. First, our visual data fit, e.g., those of Noesselt et al. [94] who found no attentional effect on initial evoked response (60–90 ms), but on those occurring after 140–250 ms post-stimulus onset. Further, Martinez et al. [79] found an earliest attentional effect already after 70–75 ms for the extrastriate visual areas and it is only after 140–250 ms that an enhanced activity in the primary cortex can be seen. Martinez et al. [79] hypothesised that the rather late enhancement in the activation of primary areas they found is due to top-down or re-entry processes. The same conjecture about delayed feedback from higher visual-cortical areas was brought forward in Noesselt et al. [94]. Second, the fact that we found no earlier *auditory* attentional effect than for the sustained field (cf. Chapter 2), is in perfect agreement with Picton et al. [102], though it might seem as if it is in opposition to the findings of Woldorff and Hillyard [144]. The latter reported an increase in amplitude due to attention already for the auditory middle-latency components (P50 and N100). However, the paradigm of Woldorff and Hillyard differs from that employed here and by Picton et al. First, we used a diotic stimulation, i.e. the same train of stimuli (and not two different streams) was presented to both ears. Second, our single stimuli endured for one second or more, that is the presentation rate was very low as compared to that of Woldorff and Hillyard. These two major differences in stimulation might account for the difference in latency of the first change in the ERP-components due to attention (Terry Picton strongly argued for this in a personal communication).

Interestingly enough, an attention-specific enhancement of the N145 is also found for the pause discrimination. Thus, attentive looking increases the amplitude of

this deflection, never mind whether ongoing visual stimulation or stimulus on- and offsets are the relevant objects for task fulfillment.

## Sustained and Slow-Wave Responses

The visual sustained response is assumed to be related to sustained object presentation, its attention-specific behaviour during a duration task, however, is to our knowledge not established [76]. The attentional studies on the visual sustained field mainly focussed on recognition tests for words [133]. Whereas we examined the question whether the discrimination of durations forces the same kind of attentional change upon the visual sustained field as upon the auditory one.

First, a fitted two-dipole model was investigated to account for the sustained responses. According to the two-dipole model with one dipole in the visual cortex of each hemisphere (Fig. 5.1), the attentional effect is caused by an augmented activation of the SF generators. The statistical evaluation revealed a significant effect of attention with no significant interaction between attention and hemisphere.

As in Chapter 2 with the tone discrimination, we then applied a three-dipole model which proved to be more adequate for the given data. Also the top view of the difference between the 'attend' and the 'non-attend' conditions suggested an additional activation above the parieto-occipital region (Fig. 5.2). Further, though again the decrease in residual variance when including an additional dipole is trivial, the highly significant interaction between the number of dipoles and the experimental condition is not—cf. Chapter 2. The standard errors of the mean location of this additional dipole overlapped with those gained for the additional dipole in the tone discrimination experiment of Chapter 2; i.e. again the additional source was found to be located in the area of the posterior cingulate gyrus and the precuneus. Moreover, the introduction of the third source resulted in a smaller attentional difference in the sustained field depicted in the waveforms of the sources in the visual cortex. Here the prominent attentional effect was due to the third dipole (Fig. 5.3).

The fact that the generator structure is similar for auditory and visual tasks is in accordance with the literature cited in the 'Discussion' sections of Chapters 2 & 3. To briefly reiterate, both the posterior cingulate gyrus and the precuneus (lying in BA 7) are known from fMRI and EEG studies to be activated during processes of imagery and retrieval both in auditory and visual tasks (see, e.g., [25], [141]); the

parietal representation of time and the differentiation between a frontal executive and a superior parietal monitoring or evaluating activity was also not restricted to auditory paradigms (see, e.g., [65], [93]).

These communalities between the picture task and the tone task of Chapter 2 strongly suggested the usage of the seeded locations for the parietal sources as gathered from the fMRI-experiment—cf. Chapters 3 & 4. This had the further advantage of allowing a direct comparison between the magnitude of the attentional effect at the superior parietal site for different tasks (cf. Chapter 7, where the relation between neuromagnetic and psychometric data got investigated). Notably, comparing the source strength of the third dipoles here and in Chapter 2 would have been biased because of the individually differing medial depth of the fitted sources.

The four-dipole model was hence also used to evaluate the picture *pause* discrimination task. Again as with the tone pause durations, the mean dipole moment of the parietal sources did show no significant enhancement. Although the right hemispheric source taking separately did show an effect, it was considerably smaller than for the picture task. Thus, the activation of the parietal sources once more turned out to be dependent upon sensory input. Finding the same pattern of attention-specific behaviour for the visual as for the auditory domain in Chapter 4, we can now conclude that the parietal activation is not modality-specific. At least part of this result, namely the similarity between the two pause tasks, is not very surprising. After all pauses in between tones are not that different from pauses in between pictures.

Coming back to the primary sensory responses, a modality-independence with respect to attentional phenomena was found for the sustained field. As for the tone task, the picture task gave rise to an enhanced sustained field amplitude; and again this effect remained when pauses (stimulus on- and offsets) were attended to. Thus, for the visual as well as for the auditory domain, paying attention leads to an enhanced sustained field, notwithstanding whether long lasting stimuli or their on- and offsets are the task relevant objects. Notably, a consistent hemispheric asymmetry for all models as it was found in the auditory data (here the left but not the right sustained field showed a significant effect) was not present for the visual modality.

## Conclusion

The present MEG study showed an attentional effect upon the visual sustained response due to a duration discrimination. To our knowledge this is the first time such an effect is reported. Further, spatio-temporal modelling demonstrated the effect to be partially due to a source outside the primary visual cortex. The source turned out be likely the same as for the tone discrimination task. Also its pattern of activation when comparing picture discrimination and picture pause discrimination data resembled that for the auditory experiments. That is the amount of parietal activation was found to be dependent upon sensory input.

Comparing all four tasks, the sustained field always showed an attentional effect for one hemisphere, never mind the kind of sensory input (auditory versus visual) and never mind whether the target of the duration discrimination task was a sensory input (tone and pictures versus the two pause tasks). That is the auditory (visual) sustained field is increased in answer to tones (pictures) regardless of whether the tones (pictures) themselves are the events to be discriminated or whether the pauses in between are. This suggests that the enhancement is a rather general effect when a modality is paid attention to. This is made plausible by the fact that the 'key stimuli' for both auditory (visual) tasks are in some sense the same, namely the tone (picture) onsets and offsets rather than the filled or empty intervals in between. Further, also the transient responses showed a prominent pattern when comparing all four tasks. The investigated auditory transient responses (P50, N100, P200) did never show an attentional enhancement, while the visual N145 did so for both the picture and the picture pause task.

Thus, the overall conclusions to be drawn are the following. First, if attentive listening to the duration of a certain stimulus does enhance primary sensory responses, then so does attending to pauses in between those stimuli. While for the early responses a modality-specificity was shown, the enhancement of the sustained field appears to be modality-independent. Second, the parietal activation involved in duration discrimination depends upon sensory input, but is modality-independent. Thus, hypothesis (i) from the beginning of this chapter is supported, the parietal network does not depend upon *auditory* sensory input in particular. Indeed this is grist to our mills, for we conjectured already at the end of the last chapter that the parietal source might monitor time itself—notwithstanding the question what else it might monitor. Its modality-independence clearly supports such a claim, since also time itself does not rely upon a specific modality. Further, the primary sensory attentional effects are not only less dependent upon the task

(filled versus empty intervals) than the parietal one, they also occurred rather late (N145, SF). This taken together might provide interesting evidence for the notorious discussion on re-entry or top-down processes [57], [148], [37].

Having now gained a quite elaborate account on the electrophysiology of duration discrimination, an obvious question to ask is this: how does it all relate to psychophysics? Are these neurophysiological findings somehow reflected in the performance data of the subjects or not? Answering this question will be done in two steps. First, we will investigate how the gathered psychometric data relate to one another (Chapter 6). Second, in Chapter 7 we will explore their relation to our neuromagnetic responses (magnitude of attention-specific responses etc.).

# Chapter 6

# Psychophysics of Duration Discrimination

## 6.1 Introduction

Having investigated neurophysiological aspects of duration discrimination, we shall now turn to look at its psychophysics. Some general remarks on the perception of time from both a psychological and a philosophical perspective have already been made in Chapter 1. Here we shall concentrate on the evaluation of subjects' performance during the MEG experiments presented in Chapters 2, 4 and 5. This will provide further inside into the differences and communalities between the auditory and the visual modality. Additionally, we will compare the individual task performance to the subjects' musical aptitude. This will reveal whether rhythmic abilities are what is needed to discriminate durations and whether those rhythmic abilities are restricted to the auditory domain.

This (and the next) chapter will focus on the ten subjects that participated in all four MEG experiments. Although this sample is rather small for drawing firm conclusions on psychometric data, it allows for direct comparisons between the performance during the different tasks (tone, tone pause, picture, picture pause), which was considered to be of main importance in the present context.

## 6.2 Material and Methods

### Psychometric Variables

During all four MEG experiments (tone, tone pause, picture, picture pause) subjects were asked to press a mouse button in response to a deviant; i.e. the longer target signal. Their responses were recorded and evaluated using signal detection theory—a method introduced in Appendix C. This gives rise to two values; namely the discriminative ability $d'$ (d-prime) and the likelihood ratio $\beta$, where the latter gives a numerical value for the restrictiveness in the subject's response behaviour.

The individual musical aptitude was assessed by the *Advanced Measures of Music Audiation* (AMMA test; see [35]). Given that we investigate the abilities in discriminating durations, we used the test's rhythmic rather than its tonal score (i.e. $AMMA_{\text{rhythm}}$). The test is explained in more detail in Appendix C, where we also suggest and analyse an alternative way of evaluating it.

### Statistical Analysis

The difference between the task-specific $d'$-values was evaluated by the Friedman test for the non-parametric analysis of variance. The same was done for the task-specific $\beta$-values. Given a significant result, this was followed by the Holm procedure for pairwise comparisons with an adjusted $\alpha$-value.

All relations between the different $d'$-values and the AMMA score were investigated by calculating the Pearson correlation coefficients. Also a factor analysis using the VARIMAX rotation was computed to access the dimensionality of the given set of behavioural variables ($AMMA_{\text{rhythm}}$, the four $d'$-values and the four $\beta$-values). The difference in the correlation coefficients between the different evaluations of $AMMA_{\text{rhythm}}$ and $d'_{\text{tone}}$, being based on one sample, was calculated pairwise according to Olkin [95].

All statistical procedures were computed with the SAS® package (version 8).

## 6.3 Results

The individual discriminative abilities differed significantly over the different tasks; that is the task-specific $d'$-values exhibited a highly significant overall ef-

| | $d'_{\text{picture pause}}$ | $d'_{\text{picture}}$ | $d'_{\text{tone pause}}$ |
|---|---|---|---|
| $d'_{\text{tone}}$ | $p < 0.01$ | $p < 0.01$ | $p < 0.01$ |
| $d'_{\text{tone pause}}$ | $n.s.$ | $n.s.$ | |
| $d'_{\text{picture}}$ | $n.s.$ | | |

***Table 6.1:*** *The Holm procedure for the task-specific $d'$-values separates the tone task from the other three. Given are the p-values for the pairwise comparisons (adjusted $\alpha$-value).*

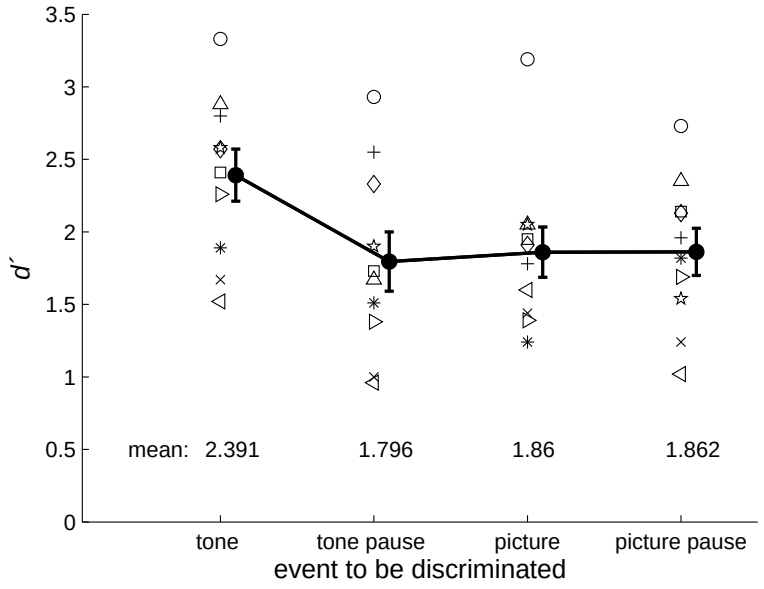


***Figure 6.1:*** *Individual data (empty and unconnected markers) and mean values (filled and connected circles) for the dependence of $d'$ upon the task as gathered from the MEG-measurements. The vertical bars indicate the standard errors of means.*

fect ($F_{3,27} = 16.68$; $p < 0.001$). The following Holm procedure revealed that $d'_{\text{tone}}$ differs significantly from the other three $d'$-values (cf. Table 6.1). For the likelihood ratio $\beta$ no significant effect was found ($F_{3,27} = 3.36$; $n.s.$).

The fact that $d'_{\text{tone}}$ differs significantly from the other three $d'$-values can also be seen from the scatter plot given in Fig. 6.1. It shows the individual as well as the mean values for the different $d'$-values. Additionally, the pairwise correlations between the different $d'$-values were all found to be statistically significant. The scatter plots for all these variables are given in Fig. 6.2.

Taking $AMMA_{\text{rhythm}}$ into account, a significant correlation to all four $d'$-values was found—cf. scatter plots given in Fig. 6.3. These five variables together with the four $\beta$-values gave rise to a rotated factor pattern with three factors,

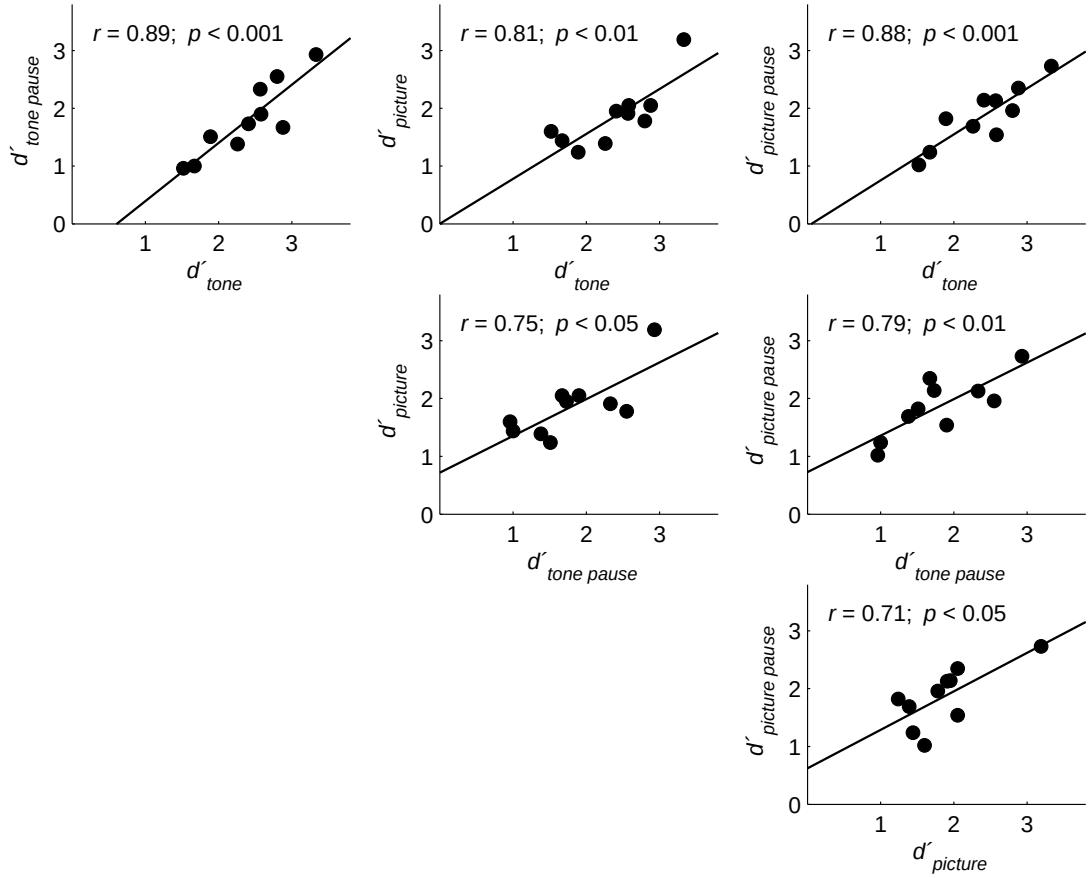


***Figure 6.2:*** *Correlations among the d′-values for the different tasks.*

which together explained 7.97 of the 9 variables—cf. Table 6.2 which gives the magnitudes of the factor loadings. All $d'$-values together with $AMMA_{\text{rhythm}}$ loaded onto the first factor which explained a variance of 3.83. Two $\beta$-values at a time loaded upon the other two factors which accounted for a variance of 2.14 and 2.00.

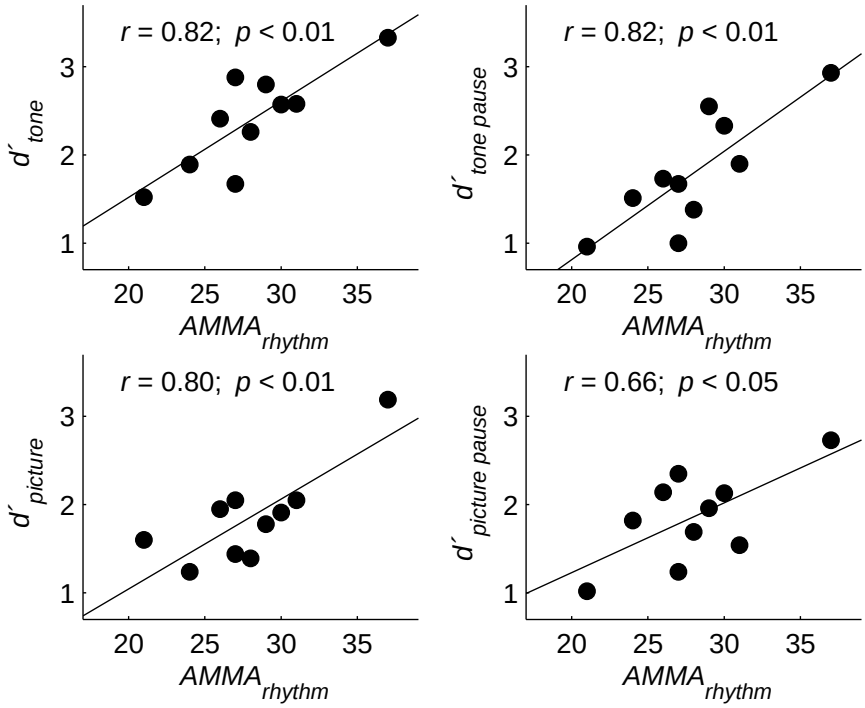


***Figure 6.3:*** *Correlations between subjects' rhythmic aptitude ($AMMA_{rhythm}$) and their task-specific d′-values.*

| | factor 1 | factor 2 | factor 3 |
|---|---|---|---|
| $d'_{\text{tone pause}}$ | **0.960** | 0.155 | 0.085 |
| $d'_{\text{tone}}$ | **0.940** | 0.070 | 0.243 |
| $d'_{\text{picture pause}}$ | **0.880** | 0.320 | 0.207 |
| $AMMA_{\text{rhythm}}$ | **0.741** | 0.148 | 0.536 |
| $d'_{\text{picture}}$ | **0.732** | 0.195 | 0.574 |
| $\beta_{\text{tone pause}}$ | 0.163 | **0.944** | 0.006 |
| $\beta_{\text{picture pause}}$ | 0.200 | **0.908** | 0.090 |
| $\beta_{\text{picture}}$ | 0.225 | 0.169 | **0.886** |
| $\beta_{\text{tone}}$ | 0.231 | 0.452 | **0.692** |

***Table 6.2:*** *The VARIMAX rotated factor analysis revealed three independent factors among the psychometric variables. Notably all discriminative measures, i.e. the four d′-values together with $AMMA_{rhythm}$, loaded upon the first factor. Thus, they strictly separated from the subjects' strategies as measured by the four β-values which loaded upon the factors two and three. Shown are the magnitudes of the factor loadings.*

## 6.4 Discussion

The aim of this chapter was the evaluation of subjects' behavioural performance during the MEG experiments and its relation to the individual musical aptitudes as given by the AMMA rhythm test.

We found that the subjects' strategies during the tasks are not correlated with their discriminative abilities; i.e. the individual $\beta$-values neither covaried with the $d'$-values nor with the $AMMA_{\text{rhythm}}$ score. On the one hand this is in agreement with signal detection theory which introduced $d'$ and $\beta$ as independent variables. On the other hand it confirms that the AMMA rhythm test measures a discriminative ability and not a behavioral attitude like restrictiveness in answering.

Let us turn towards the modality dependence of the ability to discriminate durations. Here already the rather small sample of $N = 10$ revealed a very robust effect. It turned out that $d'$ is significantly larger for tone durations than it is for the duration of pictures. This finding is in line with the literature. Already the German philosopher and psychologist Johann Friedrich Herbart (1776–1841) claimed:

> *... ein Ton hat für uns eine gewisse Dauer, da wir stets erwarten, daß er bald aufhören wird; nicht so einfach ist es hingegen bei einer Farbe, denn wir sind es nicht gewohnt, daß sie sich verändert'.* (quoted from [28])

Empirical data on the difference limen for tone and picture durations are presented, for instance, already in the famous *Grundzüge der physiologischen Psychologie* by Wilhelm Wundt [145]. Further, the decrease in discriminative abilities when going from tones to (tone or picture) pauses is reported in Paul Fraisse's standard work on the psychology of time [28]. However, some authors suppose that this difference can be overcome by training [28]. Again, the idea would be that of Herbart; namely that we are simply not *accustomed* to make judgments about the duration of pictures and pauses. However, as already pointed out, the literature is not in complete agreement here and we did not conduct any systematic investigation on training effects upon duration discrimination. We only know from our previous investigations that the reliability of $d'_{\text{tone}}$ was 0.97 (with no intercept, i.e. no offset due to training) for a sample of $N = 8$ [129].

On the one hand, the distinctiveness of discriminating tone durations suggests that there is something special about an auditory sensory input so that it allows

for this higher accuracy. On the other hand, all $d'$-values correlated significantly with one another and $d'_{\text{tone pause}}$, $d'_{\text{picture pause}}$ and $d'_{\text{picture}}$ even shared the same mean value (within their standard errors). This hints at some common core mechanism for discriminating durations. We seem to have a certain standard mechanism for processing durations with a given individual accuracy. When it comes to tones, however, some additional processing seems to be initiated by the sensory input which allows for a better performance (perhaps an auditory memory trace—cf. Chapter 8).

Assuming a standard mechanism with individual accuracy would also account for the fact that *all* $d'$-values covaried significantly with the AMMA rhythm test. If $AMMA_{\text{rhythm}}$ measured something auditory specific, then it should correlate significantly only with $d'_{\text{tone}}$, which was not the case. Thus, the results suggests that some more general ability with respect to the individual perception of time is assessed by the AMMA rhythm test. This seems very plausible at least for $d'_{\text{tone pause}}$, for one would expect that a difference in rhythmic aptitude goes along with a difference in the perception of both tones and tone pauses—last but not least, the beat given by percussion instruments does not consist of long enduring tones but of short sounds with rather long pauses in between. However, once we make this concession, the question becomes whether there is a great difference between tone pauses and picture pauses. Thus, after all it is quite intelligible that all $d'$-values and $AMMA_{\text{rhythm}}$ loaded upon a single factor in the VARIMAX analysis.

How all this again relates to our and other neurophysiological findings will be discussed in the next chapter.

# Chapter 7

# Relating Neuromagnetic Responses to Discriminative Abilities

## 7.1 Introduction

Having separately investigated the neurophysiology of duration discrimination in Chapters 2–5 and its psychophysics in Chapter 6 the aim of this chapter is to explore the relation between the two. Thus, this chapter investigates the transition from sensation to perception or, so to speak, from body to mind. The relevance but also the conceptual limitedness of correlations between sensational and perceptual data has already been introduced in Chapter 1 and will come up again in Chapter 8.

Given our data the relation between neurophysiology and psychometry can be investigated on two levels. The first level concerns possible psychophysical correlations for single tasks; i.e. the question becomes whether individual strategy or accuracy in performance covaries with a certain neuromagnetic response. The second level concerns the pattern found over all four tasks. Here the question is whether the distinctive features found for one task as compared to others are similar for the neuromagnetic and the psychometric data.

## 7.2 Material and Methods

As in the previous chapter, we exclusively used the data of the ten subjects which participated in all four MEG measurements to allow for the attempted direct comparisons between the tasks (that, by the same token, the following statistics become a little weak, was already discussed in the previous chapter).

For the recording and evaluation of the subjects behavioural responses—that is the discriminative ability $d'$ and the likelihood ratio $\beta$—see Chapter 6. Other than those two variables, which were recorded along with the neuromagnetic responses, the musical aptitude was not determined during a MEG measurement. Thus, the AMMA rhythm was not considered here, for it is not immediately linked to a MEG measurement as are $d'$ and $\beta$. For the same reason, only those neuromagnetic data were taken into account, which were recorded during the 'attend' conditions of Chapters 4 & 5 (and as modelled in the four-dipole analysis). Here the source strength of the sustained field and the parietal activation was derived as described in those chapters. Additionally, to get an estimate for the standard error of the parietal activation, bootstrapping was employed by drawing one-thousand re-samples to extract robust values. The difference between the resulting task-specific parietal activation was evaluated by a non-parametric analysis of variance (Friedman test). This test was followed by the Holm procedure for pairwise comparisons with an adjusted $\alpha$-value.

Pearson correlation coefficients were calculated to assess the relationship between sensational and perceptual variables. All statistical procedures were computed with the SAS® package (version 8).

## 7.3 Results

A significant psychophysical correlation was found between $d'$ and the mean dipole moment of the parietal sources for the tone task ($r = 0.73$, $p < 0.05$); i.e. a higher parietal activation went along with a better performance. However, since a correlation of $p < 0.05$ given a sample of ten subjects might not be very convincing, we investigated whether this correlation was independent of the source model and the type of stimulus (standards versus deviants). This was exemplarily done by considering the parietal responses to the deviant stimuli in the six-source model of Chapter 4 for all twenty subjects that participated in the tone task. Again the correlation was found to be significant ($r = 0.61$, $p < 0.01$).

Coming back to the initial sample ($N = 10$), no such correlation between parietal activation and discriminative ability was found for the other three tasks. The scatter plots for all four tasks are given in Fig. 7.1. Further, no correlation between the primary sensory responses (the auditory and visual sustained fields) and the discriminative abilities was found. Furthermore, the likelihood ratio $\beta$ indicating the strategy of the subject during the task was found to be unrelated to all neuromagnetic responses. The complete correlation analysis for all four tasks is shown in Table 7.1.

| tone task | | $d'$ | $\beta$ |
|---|---|---|---|
| | $sustained\ field\,(mean)$ | $0.05, n.s.$ | $0.29, n.s.$ |
| | $parietal\ activation\,(mean)$ | $\mathbf{0.73, p < 0.05}$ | $0.13, n.s.$ |
| | $d'$ | | $0.46, n.s.$ |
| tone pause task | | | |
| | $sustained\ field\,(mean)$ | $0.12, n.s.$ | $0.31, n.s.$ |
| | $parietal\ activation\,(mean)$ | $0.04, n.s.$ | $0.56, n.s.$ |
| | $d'$ | | $0.35, n.s.$ |
| picture task | | | |
| | $sustained\ field\,(mean)$ | $0.43, n.s.$ | $0.60, n.s.$ |
| | $parietal\ activation\,(mean)$ | $0.27, n.s.$ | $0.18, n.s.$ |
| | $d'$ | | $0.60, n.s.$ |
| picture pause task | | | |
| | $sustained\ field\,(mean)$ | $0.20, n.s.$ | $0.33, n.s.$ |
| | $parietal\ activation\,(mean)$ | $0.39, n.s.$ | $0.50, n.s.$ |
| | $d'$ | | $0.43, n.s.$ |

***Table 7.1:*** *Magnitude of Pearson correlation coefficients and levels of significance for the relations between the following neuromagnetic and behavioural variables: the mean dipole moment of the sustained fields and the superior parietal lobe activity in the 'attend' condition, the discriminative ability ($d'$), and the likelihood ratio ($\beta$). A significant correlation was found between the activation of the parietal sources and the subjects' discriminative abilities for the tone duration task.*

In Fig. 7.2 we finally compared the course of the $d'$-values over the different tasks with that of the mean parietal source activation (now again referring to the $N = 10$ sample to allow for direct comparison over tasks). The two patterns agree in so far as the tone discrimination always exhibits the largest mean value which

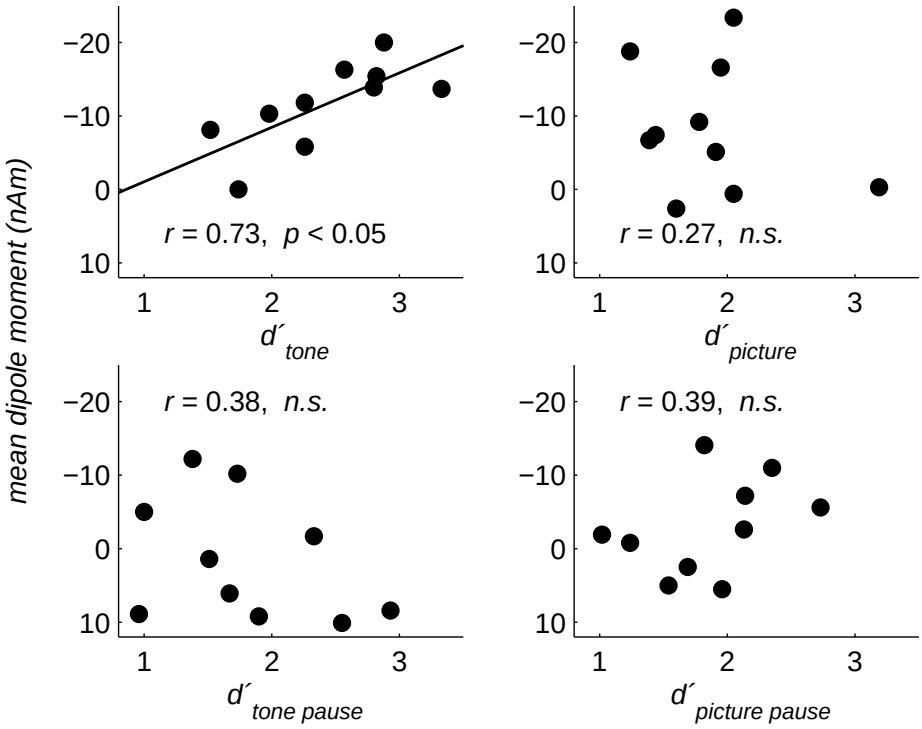


***Figure 7.1:*** *Shown are the scatter plots for the mean activation of the parietal dipoles against $d'$ for the different tasks. A significant correlation is only found for the tone duration task.*

separates from the standard error of the other tasks. Further, the small neuromagnetic responses for the two pause discrimination tasks as compared to the tone task matches the significantly poorer performance found for them. However, the two patterns disagree as far as the picture task is concerned. Whereas with respect to the discriminative performance, the picture task resembles the two pause but not the tone task, this is not the case for the parietal neuromagnetic responses. To gain further statistical evidence, a Friedman test was computed which revealed a significant overall effect in the parietal activation ($F_{3,27} = 10.92$; $p < 0.001$). The following Holm procedure showed that the tone and the picture task separate from the two pause tasks—see Table 7.2.

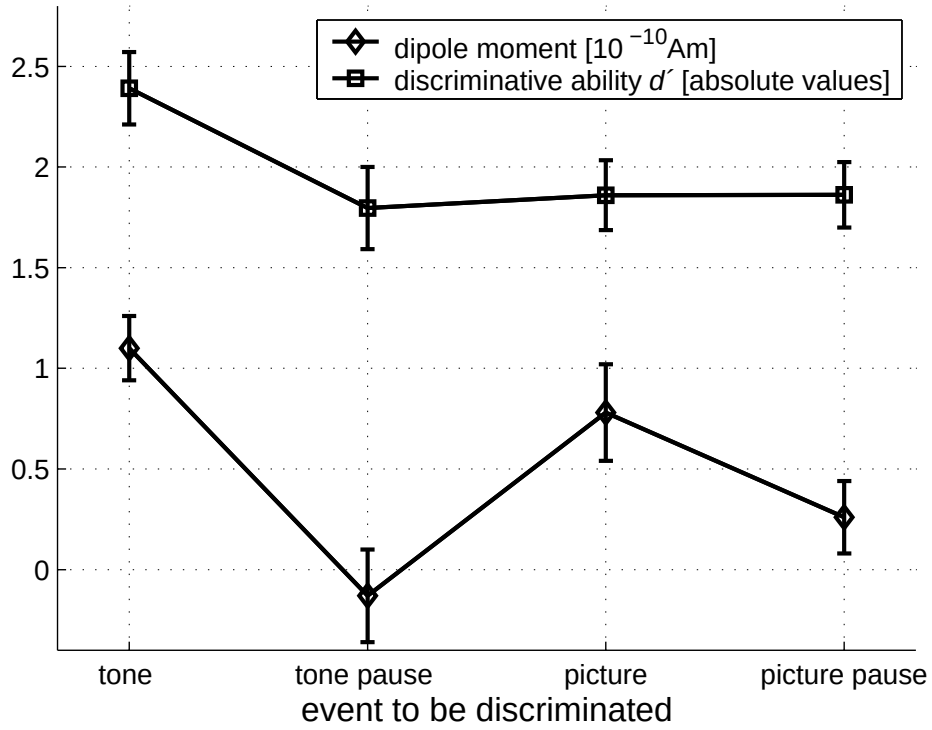


***Figure 7.2:*** *Comparison between the neuromagnetic responses in the 'attend' conditions and the psychometric results over the course of the different tasks. The plot shows the mean values and standard errors for the different d′-values (as already shown in Fig. 6.1) and for the strength of the activation of the mean parietal activity. Except for the picture duration discrimination, the pattern over the different tasks is the same. The tone discrimination gives rise to the strongest parietal activation and also leads the best discriminative performances. The neuromagnetic responses for the two pause discrimination tasks where considerably smaller and performance was significantly poorer.*

| parietal activation during | picture pause task | picture task | tone pause task |
|---|---|---|---|
| tone task | 0.05 | 0.56 | 0.05 |
| tone pause task | 0.22 | $< 0.01$ | |
| picture task | 0.05 | | |

***Table 7.2:*** *The Holm procedure for the task-specific parietal source activation separates the two pause tasks from the tone and the picture task. Given are the p-values for the pairwise comparisons (adjusted $\alpha$-value).*

## 7.4 Discussion

The aim of this chapter was to explore psychophysical correlation for duration discrimination tasks. Hence, to allow for a direct comparison, all neuromagnetic variables were derived from the MEG 'attend' sessions for which also the perceptual variables $d'$ and $\beta$ were calculated.

It was shown that the subjects' discriminative ability as measured by $d'$ correlated with the mean activation of the parietal sources for the tone task but not for the other three tasks (Fig. 7.1). Thus, the larger the parietal activation, the better the performance in the duration discrimination of tones. This correlation was found to be robust and not to be dependent upon the auditory stimulus type, since $d'_{\text{tone}}$ was significantly correlated also to the mean parietal activation in answer to the deviant stimuli (using the data of all twenty subjects of Chapter 4 here). This fits well with our findings of Chapter 4, where the time course for the activation of the parietal dipoles was shown to be prolonged for the deviants but otherwise looking exactly the same as for the standards (Fig. 4.6). Hence, the figure suggests that subjects with stronger parietal responses to standards should also have stronger responses to deviants. So the correlation to $d'_{\text{tone}}$ should be about the same for standards as for deviants, as indeed we found it to be.

The fact that Gaab et al. [29] report about a decrease in parietal BOLD responses with better task performance does not contradict our finding of a positive correlation with respect to neuromagnetic responses. They employed a pitch task and suggest that better performing subjects relied on short-term auditory memory storage rather than on sensory integration of information; i.e. that the better performing subjects had rather an increased primary sensory than a parietal activation. Thus, our finding is in agreement with their conjecture that parietal activation is needed for the integration of information, for other than their pitch task, our task asked for such an integration to enable the evaluation of the duration for a long lasting stimulus. The fact that for our task the temporal integration was more important than any particular feature extraction like pitch, might also account for the fact that we found no significant correlations between primary sensory activation and discriminative behaviour. The underlying assumption that the features of individual notes are analysed in the auditory pathway up to and including the auditory cortex, while higher-order auditory patterns and information are analysed by distributed networks in areas distinct from the auditory cortex is well supported in the literature as, e.g., by Griffiths [40].

Table 7.1 shows that $\beta$, reflecting subjects' performative strategy, is not significantly linked to neuromagnetic activation. Notably, in Chapter 6 we found that

$d'$ but not $\beta$ is correlated to $AMMA_{\text{rhythm}}$. Taken together this illustrates the following: discriminative psychometric variables ($d'$ and $AMMA_{\text{rhythm}}$) correlate with one another and to attention-specific neuromagnetic responses, while strategic psychometric variables ($\beta$) lack such a connection.

Finally, the fact that only the tone discrimination task shows such a significant correlation for the mean parietal activation is in part reflected by Fig. 7.2. Here it is the tone task which led to the largest neuromagnetic responses, in particular as compared to the two pause tasks; and a correlation between $d'$ and parietal activation seems cogent only if there is a prominent activation at all. The fact that no such correlation was found for the picture task means that apparently a high parietal activation is not a sufficient condition for a good performance. Thus, the 'good monitoring' of an incoming stimulus in the parietal cortex does not necessarily mean a good behavioural performance.

The next chapter summarises all empirical results and elaborates on the general perspective gained with respect to time (and music) perception and to some of the philosophical issues introduced in Chapter 1.

# Chapter 8

# Conclusion

## 8.1 Neurophysiological Results: Summary and Experimental Outlook

The main intention of this thesis was to investigate attentional effects within and outside the auditory cortex in a tone duration discrimination task together with its relation to behavioural responses. Here the MEG experiment revealed an augmented left sustained field and an enhanced source activation outside the auditory cortex. The latter indeed carried most of the attention-specific difference between tasks (Chapter 2). Knowing about the MEG's radial blindness (Appendix A), also EEG recordings were done to complement our data. The next step was to gain model-independent evidence for the location of this activation (Appendix B), which was done by conducting a functional magnetic resonance imaging (fMRI) experiment (Chapter 3). In very good agreement with the MEG data, the additional source activation was found to be located in the superior temporal lobe (Brodman area 7). Using the localisations thus gained, the MEG and EEG models were re-analysed to exploit their high temporal resolution as compared to the fMRI (Chapter 4). Again, the major attentional effect was found for the parietal source activation, while a minor effect was exhibited by the sustained field of the left hemisphere. The fact that this attention-specific enhancement within the auditory cortex could not be seen in the fMRI data is likely due to the difference in sensitivity of the two methods (Appendix B).

To allow for inferences concerning the dependence upon sensory input for the two activations, a discrimination task for tone pauses was implemented in both the MEG and the fMRI (Chapters 3 & 4). Whereas the attention-specific enhance-

ment of the auditory sustained field remained untouched, the parietal activation turned out to be sensory input-dependent; that is, dependent upon whether tones or the pauses in between were attended to. Since the duration of the parietal activation also turned out to be directly linked to the stimulus duration, a template comparison process could be excluded. This means that the parietal activation does not reflect the inner representation of a standard stimulus as a comparison for the actual incoming stimulus, but rather reflects the monitoring of the latter. Further, investigating the relation between the neuromagnetic activation and the behavioural responses, a significant correlation was found between the parietal activation and the accurateness in task performance: the better the parietal monitoring, the better the discrimination between standards and deviants (Chapter 7). The fact that the fMRI data for the pause task revealed a similarly centred but much more widespread parietal activation for the pause task might reflect the much higher difficulty of that task (all individual discriminative abilities dropped considerably as compared to the tone task). Lacking sensory input and hence lacking the focussed activation of the parietal duration monitoring mechanism, the pause task might 'force into the acquisition' of a larger cortical network from which temporal information can somehow be extracted. Notably, this fits with the network model of time perception as presented in Chapter 1, which maintained that the exact elements recruited in the representation of time are task-dependent [54], [32].

Apart from these results, which constituted the main focus of the present work, several other interesting findings concerning attention-specific brain activation occurred during the course of our investigations. For instance, the difference in the time course and the functional role played by the parietal and the primary sensory activation could be underpinned by further over task comparisons which concerned (i) the modality-specificity and the (ii) sensory input-specificity. The former was done by comparing auditory and visual data, the latter again by comparing duration tasks with and without sensory input (picture task versus its complementary pause task—see Chapter 5). Again, the parietal activation turned out to be sensory input-dependent; i.e. was considerably smaller during the pause task. Its activation during the picture task resembled that of the tone task; meaning that it was marked by an increasing activation lasting for the whole stimulus input. As for the auditory domain, the findings for the primary visual responses were task-independent. All attention-specific enhancements found in the picture task were also found for the picture *pause* task; namely an augmentation of the N145 and the visual sustained field. To our knowledge the latter effect was tested for the first time ever in the present study. Comparing the two

modalities, they thus agree in showing an attention-specific difference for the sustained field (though not with respect to its hemispheric asymmetry), but disagree in attentional effects upon earlier transient responses, which were only seen for the visual domain.

Altogether this suggested the following: first, an enhancement of primary sensory activation (though differing in details) is found when attention is payed to intervals of about 1 s duration, which are marked by sensory information for that modality. In our case this marking information was an ongoing stimulus for the tone and picture task, while for the two pause tasks it was the offset of the previous stimulus and the onset of the following one. Second, our visual data underpin the conjecture from above that the parietal activation reflects a monitoring process for attended intervals which encompass sensory input (tone and picture task). The fact that the activation broke down for both pause tasks showed its task-dependence but modality-independence. A further functional difference was found with respect to a frontal activation prominent in the fMRI data and then shown to be related to an electrophysiological P3 deflection. The fact that this transient response occurred about 300 ms after stimulus offset and that its amplitude was highly correlated to the actual detection of deviants, showed it to reflect an executive response. It does not monitor the duration of the input as does the parietal activation, but 'signalises' afterwards whether a behaviour response should occur or not. Notably, this P3 investigation illustrated nicely the difference between MEG and EEG when it comes to depicting radially orientated activation.

Further, the psychometric data and their possible correlations to the electrophysiological results could now be evaluated over different tasks and modalities (Chapter 6 & 7). Here the performance for the tone task was found to mark the individual best for all subjects over all tasks. Together with the aforementioned covariation between tone task performance and strength of parietal activation this suggested a distinctive role played by auditory input for the perception of time. Indeed the pattern of the behavioural responses and the parietal neuromagnetic activation over the four tasks agreed well with respect to the differences between the tone and the two pause tasks, though not with respect to the role played by the picture task. While psychometrically the picture tasks belonged to the pause tasks, the strength of the parietal activation rather resembles that of the tone task. However, one would not have expected that the amount of parietal activation is the single cause for a good task performance. Already from looking at our results concerning the frontal sources we know that further stages of processing are involved in between getting sensory input and giving behavioural output. Fi-

nally, we investigated the relation between subjects' musical aptitude and their task performances. Here a covariation was found for all tasks. This suggests that the rhythmic aptitude we assessed by means of the *Advanced Measures of Music Audiation* does not so much reflect an auditory-specific phenomenon. Its score is rather related to a more general ability in discriminating time intervals or, to put it more generally, in time perception. This fits well with the fact that the correlation between the discriminative ability and a neuromagnetic activation in the tone task was not found for a primary auditory activation but for an activation also prominent when performing a picture task.

Before presenting the overall view we gained with respect to (auditory) time perception, we should mention some issues that must be investigated to further complete our data and to test the hypotheses presented. First, fMRI experiments on pictures and picture pauses seem indicated to gain model-independent evidence on the existence and extension of the parietal network. Up to now the parallels between the additional activations for the auditory and the visual tasks were only inferred by means of model-dependent MEG data. By the same token, the hypothesis that pause tasks lead to the 'recruitment of wider cortical areas' would also be tested. Second, the duration-specificity could be tested in further studies by using different attentional tasks like, for instance, pitch or loudness discrimination. Third, the psychophysical findings of Chapters 6 & 7 ask for higher statistical power; i.e. more subjects have to be tested to confirm the correlations we found. Fourth, also the structure of the blood oxygenation level dependent (BOLD) response stemming from the the auditory cortex as found in Chapter 3 asks for further investigation. Our data suggest that for subjects having a prominent posterior duplication of Heschl's gyrus most hemodynamic activity occurs there. This impinges upon questions like finding a demarcation towards the Planum temporale and the differences between musicians and non-musicians, since it seems that such duplications are more prominent in the latter group.

Notably, this investigation of the difference between auditory attentional effects in musicians and non-musicians is where this whole project started about three years ago; and since the perception of time was shown to be pertinent to understand the perception of music (Chapter 1), we should briefly present the overall picture we gained from our and other neurophysiological and psychometrical findings.

## 8.2 The Perception of Time and Music

> *[...] gesetzt, es gelänge, eine vollkommen richtige, vollständige und in das einzelne gehende Erklärung der Musik, also eine ausführliche Wiederholung dessen, was sie ausdrückt, in Begriffen zu geben, diese sofort auch eine genügende Wiederholung und Erklärung der Welt in Begriffen oder einer solchen ganz gleichlautend, also die wahre Philosophie sein würde.* ([123], p. 369)
>
> Arthur Schopenhauer, *Die Welt als Wille und Vorstellung*

Many neurophysiological investigations concerning the differences between musicians and non-musicians were conducted during the last few years. For a comprehensive summary and its relation to the philosophical concerns discussed below and in Chapter 1 see [130]. For instance, Schneider et al. [122] showed that middle latency auditory responses (N19-P30, occurring about 19 and 30 ms after tone-onset) are significantly correlated to tonal musical aptitude as measured by the AMMA test. However, we found no correlation between the rhythmic aptitude and the auditory sustained field. This difference presumably reflects the different stages of sensory processing. The auditory cortex is known to have representations of structural features like energy onsets, temporal pitches or frequency glides [40], [91]. Those are indeed related to *tonal* sensation and thus render the findings of Schneider et al. sensible. As far as the perception of *duration or rhythm* is concerned, our results suggest that the parietal cortex plays a crucial role; and that is why a correlation to the subjects' rhythmic aptitude is found for the parietal activation and not for a primary auditory response.

The fact that a significant correlation between discriminative ability and parietal activation was found only for the tone task, still suggests a special role played by the auditory system for the sensation and perception of time. The latter is supported by the fact that only the auditory system shows a mismatch negativity, which is an automatic electrophysiological response in answer to deviant stimuli in an ongoing presentation (occurring about 100–200 ms after the deviant). In particular, a mismatch negativity appears in answer to duration deviants and its generators lie both within and outside the auditory cortex. The critical duration of this memory trace is a few seconds, meaning that a mismatch negativity will not occur for a deviant tone of, say, 12 s duration when standard tones endure for 10 s.

As argued for in [130], the time scale of the auditory memory trace is thus that of the specious present and the same we investigated in our experiments. Notably, it differs from the lower one which, for instance, Schneider et al. investigated. Further, also the upper boundary of the specious present, which from psychological investigations is assumed to be at about 2–8 s and to demarcate the transition towards long-term memory processing, is supported by neurophysiological investigations. The most interesting one in the present context is a study on visually evoked potentials by Elbert et al. [20]. They explored the maximal duration for an ongoing contingent negative variation (CNV), which is the same type of activation as our reported parietal response (this was discussed in Chapter 2). The CNV-wave was found to reduce considerably or to even be absent when subjects had to reproduce standard intervals of 4 s or more; whereas it was presented when the task was to reproduce standard intervals of 1, 2 and 3 s. This diminished activation co-occurred with a considerable decrease in task performance; that is subjects were found to be less able to reproduce standard intervals of 4 s or more. This is all grist to our mills. First, we also found the strength of our additional parietal CNV-like activation to be linked to accurateness in task performance. Second, it suggests that our parietal activation would break down for discrimination tasks on intervals longer than about 4 s and thus suggest the activation to be a phenomenon exclusively on the time scale of the specious present. Notably, this differs, for instance, from the nature of a P3 deflection, which occurs in pitch tasks, duration tasks like ours and also in word memory tasks. Thus, other than the parietal monitoring activation, the frontally localised P3 executive activation is not restricted to the specious present but occurs on all three time scales mentioned in Chapter 1.

Altogether, this suggests that the cortical processing of different auditory features at different sites reflects the different prominent time scales of time and music perception. On the scale of up to several dozens of milliseconds structural features like pitch are extracted during the processing up to the level of the auditory cortex [40]. Next, within the range of a few seconds parietal regions have shown to be important for the processing of perceived durations and the perception of rhythm (specious present). For longer intervals both the role played by long-term memory and by widespread cortical networks becomes increasingly important; with respect to music perception, this corresponds, e.g., to following a tune or even tracing the overall architecture of a given piece [67], [41].

## 8.3 The Philosophical Outlook

> *'If you knew Time as well as I do [...] you wouldn't talk about wasting* it. *It's* him. *[...] And ever since that,' the Hatter went on in a mournful tone, 'he won't do a thing I ask! It's always six o'clock now. [...] it's always tea-time, and we've no time to wash the things between whiles.'* ([13], pp. 97 & 99)
>
> Lewis Carroll, *Alice's Adventures in Wonderland*

Also philosophical evidence converges with our and other neurophysiological and psychometric findings that support the distinctive role played by the time scale of the specious present for the perception of time itself and for that of music.

As within neurophysiology, the interest in music within analytic philosophy largely increased over the last decade and once more an extended temporal window for the integration of auditory sensory information was argued for. This time the phenomenon was termed 'quasi-hearing' by Jerrold Levinson, who takes it to be the essential ingredient for the bulk of musical understanding [67]. As already mentioned in Chapter 1, what counts for the understanding of music also counts for the understanding of speech and moreover is deeply rooted in the nature of the specious present and the way we perceive time [131]. It seems that no theory of meaning can do without a theory of inner time-consciousness. Here Husserl's concept of a 'Zeithof' ('time halo' being his name for what we called the specious present) still seems to be a good starting point for developing an adequate account [52], [53]. This is nicely illustrated by his separation between 'presentation' and '*re*-presentation'. While the former means an ongoing integration of incoming information and is the defining characteristic of the 'Zeithof', the latter incorporates retrieval and memory processes which occur outside the 'Zeithof'—see Chapter 1. This point of view separates Husserl from most of his contemporaries, but it parallels our neurophysiological finding that the parietal activation, which is crucial for time perception, marks an ongoing monitoring and not a retrieval process. Thus, in a sense the time course of the parietal activation found in our studies reflects the ongoing integration of auditory information together with its presentative (as opposed to a representative) nature; and also other findings from neurophysiology concerning, for instance, the mismatch negativity fit well with Husserl's account [130]. Altogether this suggests that the

elaboration of the 'Zeithof' concept is a worthy enterprise for further research in both neurophysiology and philosophy.

Surely, Husserl himself would not be sympathetic to our move of applying his theory of a 'Zeithof' to neurophysiology. However, it is exactly this compatibility which is most striking and which might indeed argue against a strict priority of phenomenology over physiology, as Husserl would have argued for. By the same token, it would also argue against the opposite claim of a priority of science over philosophy as often implicit in the neurophysiological literature. Thus, perhaps Husserl traced some more basic pattern inherent in those different aspects of time and time perception.

Taking this striking convergence between neurophysiology, psychology and philosophy as arguing for a single underlying theory means the application of Occam's razor. Put bluntly in the present context, if there is one basic theory that could do the work of three, then take the basic theory. Although this procedure seems reasonable, it fails to answer questions concerning the status of this basic theory of time and time perception. Note that this parallels the discussion on psychophysical correlations in Chapter 1, where we said that a correlation itself does not explain anything about the difference between mental states and physical states. By the same token, one might ask whether a 'basic theory of time' really is one about physical time; whether it really is about physical and psychological time as experienced etc. Fortunately, we do not have to answer this question here; and perhaps the reader shares the feeling that a common approach for both the sensation and the perception of time at least glosses a little over the (im)pertinent mind-body bifurcation.

# Appendix A

# Methods I: Electro- & Magnetoencephalography

Electroencephalography (EEG) consists in the measurement of differences in the electric potential at the scalp and is a widely known and well established method of clinical diagnosis. A related method (though not clinically used in general) is magnetoencephalography (MEG), where extracranial magnetic fields are recorded. In both cases the measured signals are induced by the synchronous activity of neurons (mostly postsynaptic currents). Those are crucial for information processing inside our brains.

EEG and MEG experiments are of particular interest, for they have a temporal resolution lying in the range of neural activation; i.e. in the millisecond range. Whereas, for instance, the temporal sensitivity of functional magnetic resonance imaging (fMRI—introduced in Appendix B) is about three orders of magnitude lower. However, as will be shown below, compared to fMRI, EEG and MEG analyses have the draw back of being model dependent.

This chapter provides a basis for understanding the background of the magnetoencephalographic (MEG) investigations presented in Chapters 2, 4 & 5. Whereas the microscopic biological processes and technical devices for signal recording will be introduced only very briefly, the underlying electromagnetism and the different methods for MEG data analysis shall be discussed in a little more detail now.

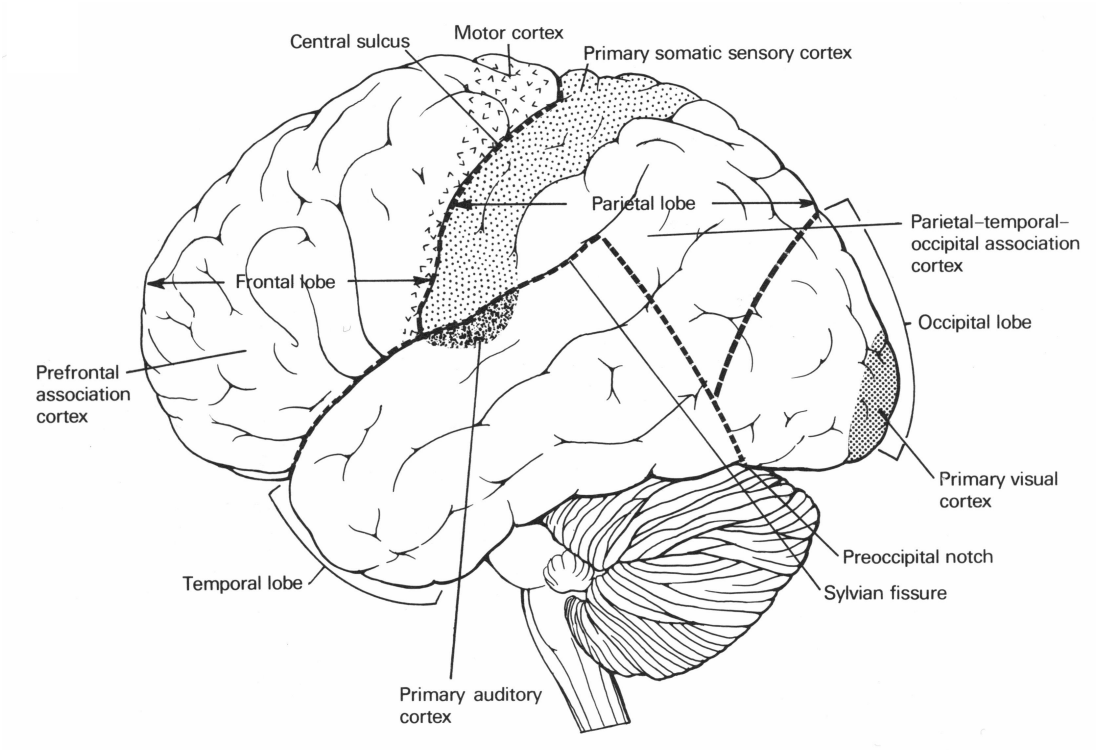


***Figure A.1:*** *Lateral (schematic) view of the human cortex (taken from [60]).*

## A.1 Neurophysiological and -anatomical Basics

The human brain has two hemispheres separated by a longitudinal fissure. Each hemisphere divides into a frontal, parietal, temporal and occipital lobe—see Fig. A.1. The areas most relevant to the present studies are the auditory cortex, the visual cortex and the parietal-temporal-occipital association cortex. The former two are so called sensory areas in which modality specific information processing happens as, e.g., pitch recognition. The aforementioned association cortex is responsible for higher sensory functions of the auditory, visual and somatosensory system. Presumably the integration of information taking place here forms a basis for more complex perceptions as, e.g., involved in attentional tasks.

The gray matter in the cortex consists mainly of neurons. There are about $10^{10}$ of them, connected among each other by about $10^{14}$ synapses—see Fig. A.2. The dendrites receive signals from other neurons through synapses. Active synapses give rise to postsynaptic potentials (PSPs) which in turn lead to current dipoles of $Q \approx 20$ fAm. Thus, the resulting fields decay like $1/r^2$, while the quadrupol fields evoked by action potentials (AP) decay with $1/r^3$ and thus contribute very little to the measured signal.

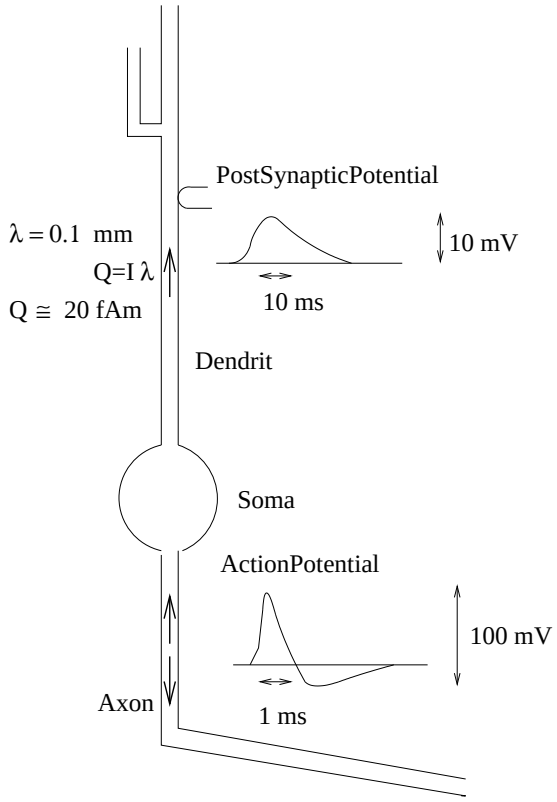


***Figure A.2:*** *Schematic picture of a neuron. Note the different time constants for the action potential and the postsynaptic potential.*

A typical current dipole moment measured in MEG is several tens of a nAm, that is there must be $10^6$ synchronously active synapses for a signal. In particular, it is the parallel alignment of pyramidal neurons within laminae III and IV of the gray matter that makes the net current flow to be about the sum of the current of all neurons. Some additional neurophysiological evidence on the origin of MEG (and fMRI) signals is given in Appendix B—see Fig. B.1 in particular.

The fact that depending upon the arrangement of the cortical neurons potentials and fields can neutralise each other is an instantiation of the well known inverse problem in electrodynamics (first shown by Helmholtz [49]). Thus, as discussed in detail below, there is no unique way to calculate the number and location of dipolar sources given an extracranial measurement (notwithstanding the number of sensors with which we measure).

Whereas the inverse problem applies to both EEG and MEG, only the MEG suffers from 'radial blindness'; this means that only the current components tangential to the head surface is accessible for the MEG (cf. Section A.3). It is

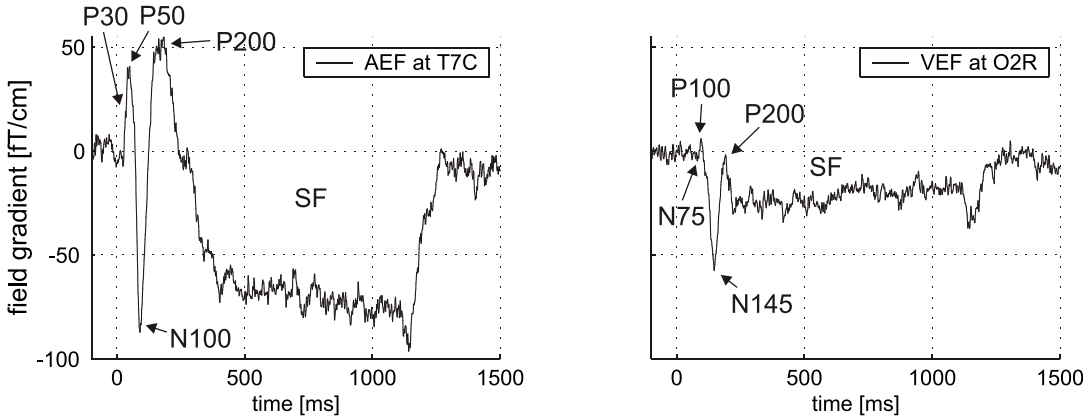


***Figure A.3:*** *Typical time courses of auditory and visually evoked responses are shown. Left: field gradient as measured near the auditory cortex and which was evoked by a sinusoidal tone enduring for one second (taken from our experiment of Chapter 2). Right: field gradient as measured near the visual cortex and which was evoked by a white circle also enduring for one second (taken from our experiment of Chapter 5).*

therefore that activity stemming from the auditory cortex can be measured excellently by the MEG, whereas the entwined surface of the visual cortex does not allow for such a complete access to activation. More details (and further references) about the morphology of the auditory cortex and its cytoarchitecture is given in my diploma thesis [129]. For the corresponding literature on the visual cortex see [112].

The responses measured by MEG are grouped according to the latency at which they occur. The early central auditory responses are evoked in the brainstem and hardly accessible by MEG (and not of further interest here). The middle latency auditory evoked fields (MAEFs) occur roughly after 8–50 ms post-stimulus onset, the late ones (LAEFs) after about 50–250 ms. The MAEFs and LAEFs get classified according to the latency and the polarity of the dominant EEG deflection, e.g. the negative response occurring after 100 ms post-stimulus onset is called N100 (sometimes an 'm' for neuro*magnetic* is added to distinguish it from a response measured by EEG). A typical time course of a magnetic field gradient as measured near the auditory cortex is given on the left in Fig. A.3.

The AEF-components relevant to the present study are the P30, P50, N100, P200 and the sustained field (SF). Since the former four responses occur only once at a fixed and short interval they are called 'transient'. The SF, however, as the name suggests, is a sustained response fully prominent after about 400–500 ms post-stimulus onset and enduring until 50–100 ms post-stimulus offset. Following the same nomenclature, the corresponding visually evoked responses (VEPs) are

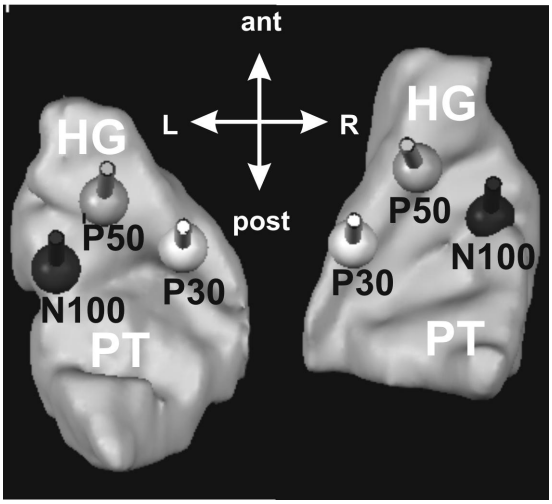


***Figure A.4:*** *Individual source locations for the auditory evoked responses in the human auditory cortex. The left and right Heschl's gyrus (HG) and Planum temporale (PT) is shown. Note that the location for the generators of the sustained field roughly agrees with that for the generators of the N100. This figure was kindly supplied by Peter Schneider (personal communication).*

the transients N75, P100, N145, P200 and a sustained field (SF). A typical time course of a visually evoked field as measured near the visual cortex is given on the right in Fig. A.3.

Since a MEG model encompassing three dipoles in each auditory cortex (as gathered from the fMRI experiment of Chapter 3) is employed in Chapter 4, the supposed location of the sources of the different AEF-components should be mentioned. Here intracranial, cytoarchitectural and MEG studies revealed the following positions (cf. [47], [75], [117], [97], [43], [121] and [69]): the P30 originates within the medial portion of Heschl's gyrus (HG), the P50 stems from a more lateral part of HG, while the N100 is generated in the Planum temporale (near the border to the HG). The SF, originally assumed to stem from the central portion of the HG, has recently been shown to consist of at least two generators with differing functionality [44]. The generator of interest to us is located near the HG in the Planum temporale; i.e. near the generator of the N100. All positions mentioned are indicated in Fig. A.4.

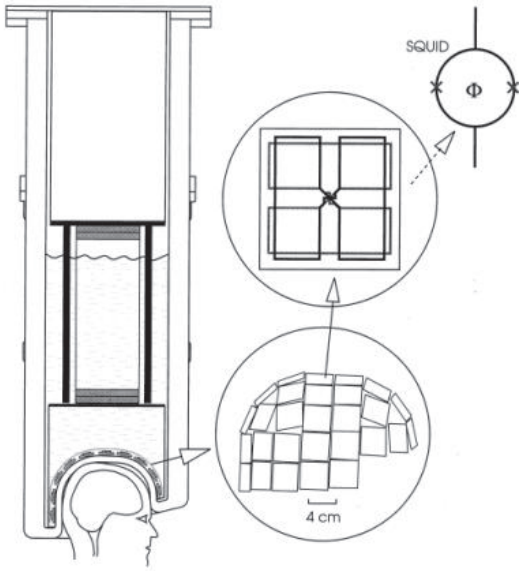


***Figure A.5:*** *Schematic setup of a MEG system. The dewar, filled with liquid helium to allow for superconductivity, is shown on the left. The enlargements on the right show the helmet-like arrangement of the sensor arrays, two orthogonally arranged 'figure-of-eight' gradiometers and a single SQUID.*

## A.2 Technical Basics

Notably, the extracranial magnetic fields we are talking about are of around 100 fT; i.e. they are about 8 orders of magnitude smaller than the magnetic field of the earth! The measurement of such weak fields became only possible through the development of very sensitive magnetometers, the so called 'SQUIDS'. To see how they work (and where the name comes from), we make a quick excursion into elementary quantum mechanics.

### SQUID Magnetometers

The SQUID magnetometers consist of closed superconductors interrupted by a thin normal conducting layer (Josephson junction), indicated by tiny crosses on the upper right in Fig. A.5.

Within the superconductor, electrons form Cooper pairs which condense and are the carriers of the current in the superconductor. The SQUID measures the phase difference of the wave function of a Cooper pair at the junction. This phase difference is given by:

$$\Delta\phi = \frac{-iq}{\hbar c} \oint_{\partial F} \vec{A}.d\vec{s} = \frac{-iq}{\hbar c}\Phi, \tag{A.1}$$

where $\Phi = \int_F \vec{B}.d\vec{f}$ is the magnetic flux and $q = 2e$ the charge of a Cooper pair.

The phase difference $2\pi$ is reached for a magnetic flux quant with the flux $\Phi_{\mathrm{m}}$:

$$\Phi_{\mathrm{m}} = \frac{\hbar c 2\pi}{2e} \approx 4 \cdot 10^{-7} \text{ gauss cm}^2 = 4 \cdot 10^{-15} \text{ T m}^2. \tag{A.2}$$

Phase differences $\Delta\Phi \ll \Phi_{\mathrm{m}}$ lead to detectable interference effects at the junction, hence the name **S**uperconducting **QU**antum **I**nterference **D**evice. The sensitivity is indeed in the femto-Tesla region, as can be seen from expression A.2.

### Experimental Setup

Subjects participating in our MEG experiments were placed under the dewar illustrated in Fig. A.5. To minimise external disturbances, the device is set up in a magnetically shielded room. The SQUIDS used are planar gradiometers and no magnetometers. The former have the advantage of being very sensitive to sources near the surface of the head—as, e.g., those stemming from the auditory cortex. Further, they are less sensitive to disturbing outer magnetic fields [143]. For instance, though the magnetic field of the earth is $10^8$ larger than the extracranial ones we are interested in, its gradient at the MEG dewar is vanishing. The fact that the gradiometers are thus also less sensitive for sources deep inside the head (brainstem activities, e.g.) is not really an *additional* draw back, since those sources appear to have mainly radial components from outside the scalp; i.e. are 'invisible' for the MEG anyway, as we will see now.

## A.3 Electrodynamic Basics

The classical introduction to the electromagnetism underlying MEG has been given in 1993 by Hämäläinen et al. [45]. The following presentation is mainly based upon this paper.

## Construction of Magnetic Fields and Potentials from Given Primary Currents

The frequencies involved are low enough to justify the quasi static approximation of the Maxwell equations, that is we start from:

$$\vec{\partial}\vec{D} = 4\pi\rho \tag{A.3}$$
$$\vec{\partial}\vec{B} = 0 \tag{A.4}$$
$$\vec{\partial} \times \vec{E} = 0 \tag{A.5}$$
$$\vec{\partial} \times \vec{H} = \vec{j}. \tag{A.6}$$

Further, we need:

$$\vec{j} = \sigma\, \vec{E}. \tag{A.7}$$

In the vacuum and the head we can put $\vec{B} = \vec{H}$.

Because of A.5 we can express $\vec{E}$ by the quasi static potential $\phi$:

$$\vec{E}(\vec{x}\,) = -\vec{\partial}\phi(\vec{x}\,). \tag{A.8}$$

We are interested in this potential $\phi$ at the scalp and on the magnetic field $\vec{B}$ outside the head. For further reference we denote ...

- ... the interior of the head by $G$,
- ... the surface of the head (i.e. the scalp) by $\partial G$.

Within an array of (mostly synaptic) cells flows a well localised current with a current density $\vec{j}_{\mathrm{p}}$. It is called the primary current. Since the brain is conducting, the potential difference created by the primary current leads to a current distributed over the whole brain, the so called volume current with current density $\vec{j}_{\mathrm{v}}$.

The primary current $\vec{j}_{\mathrm{p}}$ together with the volume current $\vec{j}_{\mathrm{v}}$ create a magnetic field $\vec{B}$. It can be calculated with the help of Maxwell's equations. Using A.4 $\vec{B}$ can be expressed as the rotation of a vector potential:

$$\vec{B} = \vec{\partial} \times \vec{A}, \tag{A.9}$$

which can be chosen to fulfill the Coulomb gauge

$$\vec{\partial}\vec{A} = 0. \tag{A.10}$$

Then A.6 becomes

$$\vec{\partial}^{\,2}\vec{A} = -\vec{j}, \tag{A.11}$$

with a solution vanishing at $|\,\vec{x}\,| \to \infty$:

$$\vec{A}(\vec{x}\,) = \frac{1}{4\pi}\int_G d^3x' \frac{\vec{j}(\vec{x}\,')}{|\vec{x}-\vec{x}\,'|}. \tag{A.12}$$

If the current distribution vanishes sufficiently fast the magnetic field is obtained from A.6 as A.11 leads to the standard solution:

$$\vec{B}(\vec{x}\,) = \frac{1}{4\pi}\Big[\vec{\partial}\times\int_G d^3x' \frac{\vec{j}(\vec{x}\,')}{|\vec{x}-\vec{x}\,'|} = \frac{1}{4\pi}\int_G d^3x' \frac{[\vec{j}(\vec{x}\,')\times(\vec{x}-\vec{x}\,')]}{|\vec{x}-\vec{x}\,'|^3}. \tag{A.13}$$

Putting the rotation in $\vec{B} = \vec{\partial}\times\vec{A}$ inside the integral, switching from $\vec{\partial}$ to $\vec{\partial}'$ and performing a partial integration one arrives at the following form:

$$\vec{B}(\vec{x}) = \frac{1}{4\pi}\int d^3x' \frac{1}{|\vec{x}-\vec{x}\,'|}\vec{\partial}'\times\vec{j}(\vec{x}\,'). \tag{A.14}$$

Because of A.7 and A.8 the total current is

$$\vec{j}(\vec{x}) = \vec{j}_{\rm p}(\vec{x}) + \vec{j}_{\rm v}(\vec{x}) = \vec{j}_{\rm p}(\vec{x}) - \sigma(\vec{x})\vec{\partial}\phi(\vec{x}). \tag{A.15}$$

Simple manipulations lead to

$$\vec{\partial}\times\vec{j} = \vec{\partial}\times(\vec{j}_{\rm p} + \phi\vec{\partial}\sigma), \tag{A.16}$$

that is besides the primary current the volume current contributes to the magnetic field as $\vec{j}_{\rm eff} = \phi(\vec{x}\,')\vec{\partial}'\sigma(\vec{x}\,')$. Inserting this into A.14 and partial integration yields finally to the result:

$$\vec{B}(\vec{x}) = \frac{1}{4\pi}\int d^3x' \frac{\Big(\vec{j}_{\rm p}(\vec{x}\,') + \phi(\vec{x}\,')\vec{\partial}'\sigma(\vec{x}\,')\Big)\times\Big(\vec{x}-\vec{x}\,'\Big)}{|\vec{x}-\vec{x}\,'|^3}. \tag{A.17}$$

If it where not for the space dependence of the conductivity $\sigma$ the contribution of the volume current would vanish. Even if we assume a homogeneous conductivity inside the head, there is a dependence on $x$, since outside the head the conductivity is zero.

The potential $\phi$ is related to the primary current $\vec{j}_{\mathrm{p}}$ through A.15 and $\vec{\partial}.\vec{j} = 0$, a consequence of A.6. It yields:

$$\vec{\partial}.(\sigma\vec{\partial}\,\phi) = (\vec{\partial}\sigma).(\vec{\partial}\phi) + \sigma\vec{\partial}^2\phi = \vec{\partial}.\vec{j}_{\mathrm{p}}. \tag{A.18}$$

Outside the head the conductivity is zero. Because of the continuity of the current components the current normal to $\partial G$ inside $G$ is zero and therefore

$$\hat{n}_{\partial G}.\vec{\partial}\phi = 0 \qquad \text{on } \partial G, \tag{A.19}$$

where $\hat{n}_{\partial G}$ is the normal on the scalp $\partial G$.

Thus we can calculate the potential from A.18 and the boundary condition A.19. From the potential and with A.17 we can calculate the magnetic field.

If the volume element, where $\vec{j}_{\mathrm{p}} \neq 0$, is small we can replace it by

$$\vec{j}_{\mathrm{p}}(\vec{x}) \approx I\ \vec{l}\ \delta(\vec{x} - \vec{x}_Q) = \vec{Q}\ \delta(\vec{x} - \vec{x}_Q). \tag{A.20}$$

Here $\vec{x}_Q$ is the position where the current density is different from zero, $I$ is the current strength and $\vec{l}$ is the direction vector of the current density. $\vec{Q}$ is called the current dipole moment,

$$\vec{Q} = \int d^r x'\ \vec{j}_{\mathrm{p}}(\vec{x}\,'). \tag{A.21}$$

The contribution of a primary current described by the current dipole $\vec{Q}$ at position $\vec{x}_Q$ is thus (cf. A.17):

$$\vec{B}_{\mathrm{p}}(\vec{x}) = \frac{1}{4\pi}\frac{\vec{Q}\times(\vec{x} - \vec{x}_Q)}{|\vec{x} - \vec{x}_Q|^3}. \tag{A.22}$$

The results obtained above can be summarized as follows. The potential and the magnetic field at any position outside and on the surface of the head can be calculated from $\vec{j}_{\mathrm{p}}$ and depend linearly upon it:

$$\phi(\vec{x}) = \int d^3x' \; \vec{\mathcal{L}}^{\mathrm{pot}}(\vec{x},\vec{x}\,').\vec{j}_{\mathrm{p}}(\vec{x}\,'), \tag{A.23}$$

$$\vec{B}_\alpha(\vec{x}) = \int d^3x' \; \vec{\mathcal{L}}_\alpha(\vec{x},\vec{x}\,').\vec{j}_{\mathrm{p}}(\vec{x}\,'), \tag{A.24}$$

where $\vec{\mathcal{L}}$ is the lead field vector depending only upon the geometry and conductivity of the head.

We have the important theorem:

**Theorem:** The magnetic field outside the head is uniquely determined by the component $B_n(\vec{x}) = \hat{n}_{\partial G}.\vec{B}(\vec{x})$ with $\vec{x} \in \partial G$, that is the normal component of $\vec{B}$ on the surface of the head.

**Proof:** Be $G'$ the complement of $G$, that is the space outside the head. In $G'$ we have $\vec{j} = 0$ and hence $\vec{\partial} \times \vec{B} = 0$. Therefore, in $G'$ we can express $\vec{B}$ through a scalar potential $\phi_{\mathrm{M}}$:

$$\vec{B} = \partial\phi_{\mathrm{M}}. \tag{A.25}$$

Because of A.4 we have in $G'$,

$$\vec{\partial}^{\,2}\phi_{\mathrm{M}} = 0. \tag{A.26}$$

The solution is determined by the Neumann boundary condition on the surface of $G'$, i.e. the scalp and infinity. At infinity everything is assumed to be zero (shielding!), so that the normal derivative at the scalp determines $\phi_{\mathrm{M}}$ and thus $\vec{B}$ in $G'$. The solution is given by:

$$\phi_{\mathrm{M}}(\vec{x}\,) = -\frac{1}{4\pi}\int_{\partial G} d^2a' \; G_{\mathrm{N}}(\vec{x},\vec{x}\,').\hat{n}_{\partial G}.\vec{\partial}\phi_{\mathrm{M}}(\vec{x}\,'). \tag{A.27}$$

$G_{\mathrm{N}}$ is the Greens function satisfying the Neumann condition

$$\hat{n}_{\partial G}.\vec{\partial}\,'G_{\mathrm{N}}(\vec{x},\vec{x}\,') = 0; \quad \vec{x}\,' \in \partial G. \tag{A.28}$$

The normal derivative $-\hat{n}_{\partial G}.\vec{\partial}\phi_{\mathrm{M}}(\vec{x}\,')$ is just $B_n$, the component of $\vec{B}$ normal to the surface of the head.

**Spherically symmetric case**

**Theorem:** If the head is a spherically symmetric system, that is $\sigma(\vec{x}\,) = \sigma(|\vec{x}\,|)$ and $G$ is a sphere, the contribution of the volume current to the normal component of $\vec{B}$ on the surface of the head the volume current is zero.

**Proof:** For a spherically symmetric system we have $\sigma = \sigma(|\vec{x}\,|)$ and $\hat{n}_{\partial G} = \vec{\partial}\,|\vec{x}\,|\,\vec{x}\,/\,|\vec{x}\,| \equiv \hat{x}$.

We have $\partial\sigma(|\vec{x}\,|) = \sigma'(|\vec{x}\,|)\hat{x}$, where $\sigma'$ is the derivative of $\sigma(|\vec{x}\,|)$ with respect to $|\vec{x}\,|$.

We thus deduce from A.17 the contribution of the volume current:

$$\vec{B}^{\,\mathrm{V}}(\vec{x}) = \frac{1}{4\pi}\int d^3x'\phi(|\vec{x}\,|)\sigma(|\vec{x}\,|)(\vec{x}' \times \vec{x})\frac{1}{|\vec{x} - \vec{x}\,'|^3}, \tag{A.29}$$

which evidently is orthogonal to $\vec{x}$ and thus to $\hat{x}$. Thus $B_n^{\mathrm{V}} = \hat{x}.\vec{B}^{\,\mathrm{V}} = 0$ and therefore only the primary current contributes to the normal component.

For a current dipole we have:

$$B_r(\vec{x}) \equiv \vec{B}(\vec{x}).\hat{x} = -\frac{1}{4\pi}\frac{\vec{Q}.[\vec{x} \times \vec{x}_Q]}{|\vec{x} - \vec{x}_Q|^3} \tag{A.30}$$

According to the theorem derived above the radial component of the magnetic field is thus exclusively determined by the primary current and no detailed knowledge of $\sigma(|\vec{x}\,|)$ is necessary. This is a big advantage of the MEG. Even if the spherically symmetric approximation might not be very trustworthy, it is quite good if the source is near the surface of the head (like the auditory cortex) and if the local curvature is taken into account. However, it also has an important and unpleasant consequence:

If a current dipole is in radial direction, that is if $\vec{Q} = |\vec{Q}|\hat{x}_Q$ then $\vec{B}(\vec{x}) = 0$ outside the head.

The proof is simple. One sees easily from A.30 that $B_r = 0$ on the surface of the head in that case and therefore the Neumann boundary volume problem has only the trivial solution $\vec{B} = 0$. This 'radial blindness' of the MEG is nicely illustrated in Chapter 4 when investigating a frontal P3 deflection which was exclusively visible within our EEG data.

Note that the primary current leads to tangential magnetic field components but that these are compensated by the volume current.

### The Inverse Problem

The problem to obtain potentials or fields from given sources is straightforward. Mathematically and physiologically much more interesting is the so called inverse problem, namely to obtain information about the primary current from measured potentials or fields on the surface of a body. It has been shown already in 1853 by Hermann von Helmholtz that this problem has no unique solution [49].

That this is the case follows from the fact that there can be non-vanishing primary currents which lead to no signal outside the body. We have seen already in the previous section that in the spherically symmetric case a radial current dipole $\vec{Q} = |\vec{Q}\,|\hat{x}$ cannot create a magnetic field outside the head. There are also currents which do not create a potential at the scalp; and there even exist currents that leave neither an electric nor a magnetic signal outside the head. Therefore, the solutions found for EEG and MEG data sets are never unique. As mentioned above, fortunately in the auditory cortex (other than in the visual) nearly all primary currents seem to be parallel to the surface of the head and thus accessible to MEG measurements.

## A.4 Modelling

Given the inverse problem, there are different ways to model MEG data which often lead to different results. In this section three ways of modelling are briefly introduced, namely the (RAP) MUSIC algorithm (together with the principal component analysis), discrete dipole source fitting and minimum norm solutions. As we will see, it is in particular the allowance for modelling over different activity-specific epochs which makes the latter method by far the most sensible one for the analysis of our MEG data presented in Chapters 2 & 5.

### Principal Component Analysis (PCA) and (RAP-)MUSIC Algorithm

Let us consider MEG data $\vec{B}$ as recorded by $N$ magnetometers. In fact the signal is not measured continuously but with a certain samplerate $1/T$. Thus, we shall denote the reading of magnetometer $i$ at time point $j$ by $B_{ij}$. Further, there will inevitably be some noise contributing to the reading $b_i$ of each magnetometer. Denoting the noise by $b_i^{\text{noise}}$ we can thus write the MEG data as follows:

$$B_{ij} = \begin{pmatrix} b_{1j} \\ \dots \\ b_{Nj} \end{pmatrix} = \begin{pmatrix} b_{1j}^{\text{signal}} + b_{1j}^{\text{noise}} \\ \dots \\ b_{Nj}^{\text{signal}} + b_{Nj}^{\text{noise}} \end{pmatrix}. \tag{A.31}$$

Assuming that $r < N$ sources imping upon our magnetometers, each source will contribute to the $i$th magnetometer reading by a topography $\vec{l}_i$. Again, for all magnetometers we can write those sensitivity distributions as a lead field matrix $\mathcal{L} \in [N \times r]$ (cf. equation A.24):

$$\mathcal{L} = [\vec{l}_1, \dots, \vec{l}_r]. \tag{A.32}$$

The measured signal at a certain magnetometer is the sum of all source contributions plus noise. From A.24 and A.20 we thus get:

$$B_{ij} = b_{ij}^{\text{signal}} + b_{ij}^{\text{noise}} = \mathcal{L}_{ik} Q_{kj} + b_{ij}^{\text{noise}}; \quad k = 1, \dots, r. \tag{A.33}$$

Here and in the following the Einstein rule is assumed; i.e. indices appearing twice are summed over. The autocorrelation of the measured sampled signal gives the so called product moment matrix $R \in [N \times N]$:

$$R_{ij} = B_{il} B_{jl}. \tag{A.34}$$

A principle component analysis (PCA) now consists in calculating the eigenvectors and eigenvalues of $R$. The eigenvectors thus define the topographies (channel configurations) that contribute to the measured signal and their respective eigenvalues give an estimate of the strength with which they do so.

Going from the PCA analysis to the multiple signal classification (MUSIC) algorithm two additional assumptions are made; namely that the contribution from the sources and noise are orthogonal to each other [88]. Additionally we must know the number of sources $r$. Given all this, the data will separate into a $r$-dimensional signal subspace and a $(N - r)$-dimensional noise-only subspace. Thus, equation A.34 yields:

$$R_{ij} = R_{ij}^{\text{signal}} + R_{ij}^{\text{noise}}; \quad \text{with} \quad R_{ij}^{\text{signal}} = \mathcal{L}_{ik} (Q_{kl} Q_{ml}) \mathcal{L}_{jm}. \tag{A.35}$$

The MUSIC algorithm now scans a discrete lattice with one or more dipoles to find the location(s) for which the principal angle between the array manifold vector $\vec{l}_i$ and the noise only subspace is maximum.

The difference between MUSIC and RAP (recursively applied and projected) MUSIC is the way the signal subspace is treated once a first source is found. While MUSIC finds $r$ local maxima for the whole subspace, RAP MUSIC removes the component of the signal subspace that is spanned by each source [89]. Thus, it calculates $r$ global maxima over their respective modified signal subspaces.

In particular, (RAP) MUSIC can be applied to the paired data sets of studies on attention in an interesting way. For instance, one could obviously take the signal subspace of the 'non-attend' condition and remove it from the signal subspace of the attend condition, so that RAP MUSIC would calculate the sources of the task-specific activity [23]. However, this shows a main draw back of both the PCA and the (RAP) MUSIC algorithm, since not all task-specific activity will be orthogonal to the one from the 'non-attend' condition (just think of an enhancement of a given 'non-attend activity'). Indeed this problem is a general one for the PCA and the (RAP) MUSIC algorithm, since also single data sets will often show activities which are linear dependent to some extent. An additional problem of (RAP) MUSIC is the calculation of adequate source localisations in cases where a topography stems from a simultaneous bilateral activation. Both problems will be illustrated below and shown in Fig. A.7.

## Discrete Dipole Source Fitting

While (RAP) MUSIC first separates the measured time-sampled field into signal and noise, we shall now start directly from the lead field matrix $\mathcal{L}_{ik}$ and the current dipole moments $Q_{kj}$. This is a sensible assumption if the signal-to-noise ratio is sufficiently high. Thus, as compared to equation A.33 we only consider $b_{ij}^{\text{signal}}$ now. Thus, if again $B_{ij}$ denotes the reading of magnetometer $i$ at time point $j$ we get:

$$B_{ij} = b_{ij}^{\text{signal}} = \mathcal{L}_{ik} Q_{kj}; \quad k = 1, \ldots, r, \tag{A.36}$$

where $r$ is the number of the assumed current dipoles.

By applying the Moore-Penrose pseudo-inverse $\mathcal{L}^{-1}$ to both sides of A.36, the time course of the source activities can be calculated from the measured magnetic field. Now one typically uses an algorithm which iterates source locations and orientations in order to find the configuration that best explains the measured data; i.e. that shows the smallest discrepancy between the observed and the calculated data. Normally this is done by using the $L_2$-norm, so that in the end

the model's residual variance gets minimised [116], [118]. Of course, given the experimental noise, only a limited amount of dipoles makes sense, since more dipoles lead to more free parameters and therefore always lead to a solution with an excellent fit. This solution might then be very far from the true one. Note, however, that is not different for the (RAP) MUSIC algorithm where one has to determine the rank of $\vec{\mathcal{L}}$ at the beginning; i.e. one also has to 'guess' the number of sources $r$ and a higher number will also result in a smaller residual variance of the model.

There are several heuristics that considerably improve and validate discrete dipole fitting. Before coming to those, however, we shall briefly introduce a third method for modelling MEG data; namely the minimum norm solution.

## Minimum Norm Solutions

Both (RAP) MUSIC and dipole source fitting both use discrete equivalent dipoles for analysing MEG data. One might argue, however, that a distributed source model is closer to reality and thus should be preferred.

Such a model also starts from the sum of the right hand side of equation A.36, where $r$ now goes, say, from 1 to 10,000 instead of from 1 to 4. The number of dipoles in a typical minimum norm solution thus exceeds the number of MEG sensors. Thereby we are left with an underdetermined problem, that is we have to place additional constraints to find a solution. Now, and this is where the name 'minimum norm solution' comes from, one possibility is to choose the solution for which the norm of the activities of all sources exhibits its minimum.

A major problem inherent in minimum norm solution is the smearing of focal activity [50]. As a matter of fact, it also led to rather poor results given the MEG data of the present work; data, for which we shall now compare the different ways of modelling (MUSIC, dipole fitting, minimum norm) more systematically.

## Comparison of Methods for the Data at Hand

Let us start by a heuristic from which all methods of modelling can profit; namely considering anatomical and physiological studies. Often those are used *post-hoc* to validate the adequateness of a certain model. However, given our rather complex MEG data of Chapters 2 & 5, such an anatomically sensible model could only be gathered by dipole fitting together with performing PCAs. Fig. A.6 shows such

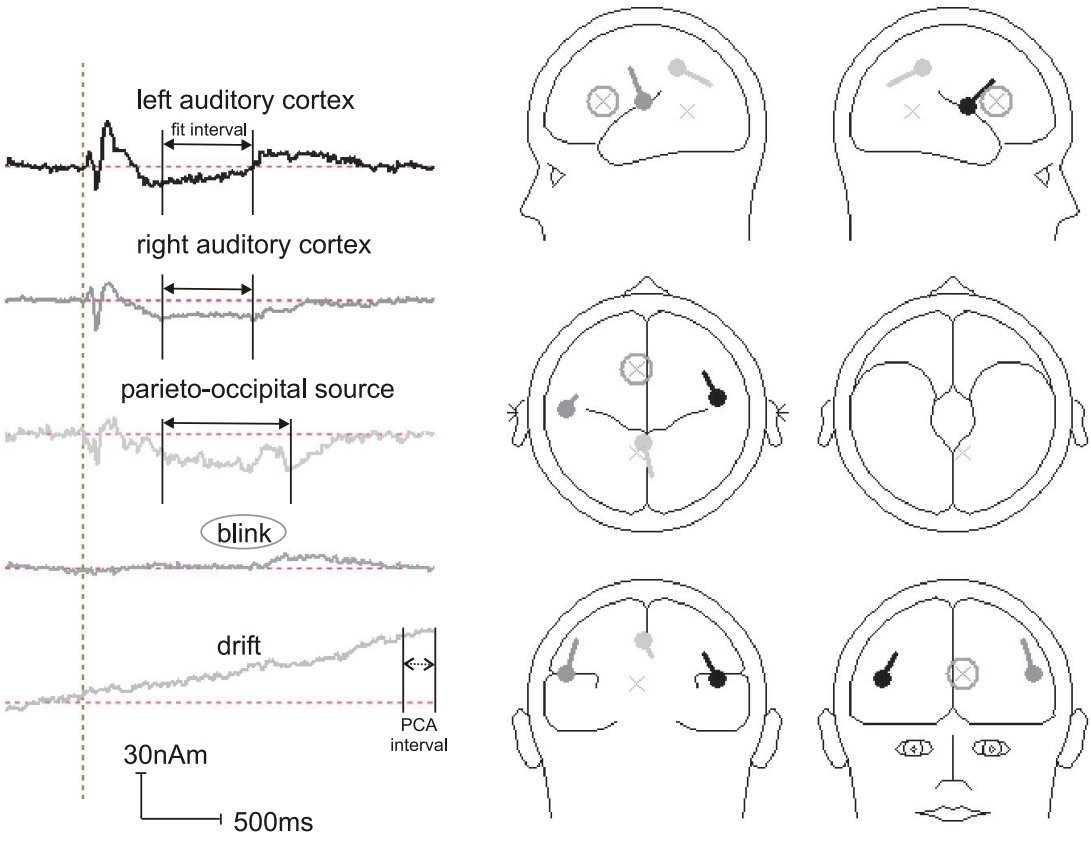


***Figure A.6:*** *Fitting of dipoles and principal component analysis as conducted with BESA2000® for single subject data from the 'attend' condition of Chapter 2. The drift and the subject's eye-blink have been removed from the signal space by a PCA component. Then the three dipoles have been fitted over the respective epochs of their main activation.*

a discrete dipole model (as done with BESA2000®) for a single subject's 'attend' condition of Chapter 2.

First, the drift was modelled by introducing the first PCA component as computed over an interval for which on average no event-related brain activation occurs—see Fig. A.6. Note that we could not get rid of this drift by a simple high-pass filtering of 3 Hz, say, for this would have considerably diminished the activities we are mainly interested in; namely the SF and the additional slow wave stemming from the parietal region.

Second, we averaged the subject's eye-blinks in the continuous MEG raw data and afterwards performed a PCA. The first component of it was then implemented as a spatial component into the averaged data for the auditory evoked responses (i.e. into the source analysis shown in Fig. A.6). This method gets discussed in

Chapter 2 in a little more detail.

Third, the dipole fitting was carried out with different fit intervals for the different activities. The generators of the SF were fitted for the 'non-attend' condition. Then they were introduced into the shown 'attend' condition where the additional dipole for the parietal region was added—cf. A.6).

Let us now compare this to the standard RAP MUSIC algorithm the results of which (for the same measurement) are shown in Fig. A.7. A rather poor localisation for one source obviously would have followed from assuming the auditory activation to stem from two topographies, given that the signal spaces spanned by the activities of the left and right auditory cortex are not linear independent. Hence, the more prominent activity would be modelled by the source of the first topography; and since RAP MUSIC now removes this topography the main activation stemming from the other auditory cortex—due to its highly correlated activity—gets removed as well. However, RAP MUSIC allows to force the calculation of two sources for each topography. This has indeed been done for the analysis shown in Fig. A.7; i.e. it was explicitly stated that the first topography is the result of *two* sources.

Indeed, rather than with the generators in the auditory cortex, RAP MUSIC had some severe problems with the additional source. As explained above, a high-pass filtering could not be used so that RAP MUSIC failed to separate the activity of the third source from the drift. This can be seen from the third source waveform in Fig. A.7. Indeed this is also the main problem of the minimum norm solutions for the given kind of data.

Thus, dipole modelling turned out to be the best way to analyse our data. Admittedly, however, things might be different if one could make use of high-pass filtering. The way dipole modelling is implemented in the software used, allows for the most freedom in modelling. It allows to make use of the main advantages of dipole fitting and of calculating PCA components; and in particular it allows to apply those tools over different source-specific epochs. Of course, one could think about how to apply minimum norm solutions or RAP MUSIC only to certain epochs of a given data set, putting the solutions together again etc. However, this is not our aim here.

Last but not least something should be added on the critique that in dipole modelling one could always add another source and thereby improve the models residual variance. We already mentioned that anatomical knowledge can be used to validate a dipole model. Also individual channel waveforms can provide additional evidence for a source and its location.

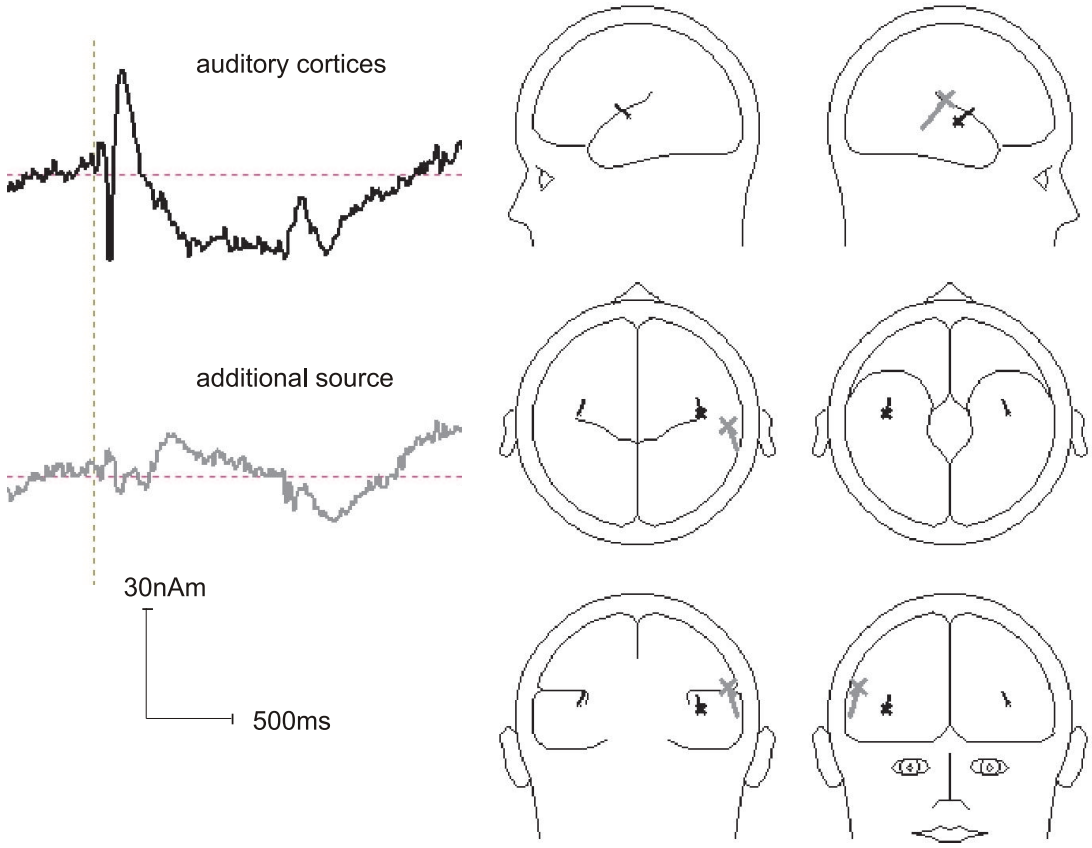


***Figure A.7:*** *RAP MUSIC analysis of the same data set as in the previous figure. The number of sources prescribed to the first signal space dimension (i.e. the first topography found by RAP MUSIC) was two.*

Further, the resulting source waveform also is a good indication of whether brain activation or noise got modelled; e.g. a well-defined transient response found over several subjects is very unlikely to result from uncorrelated noise. Furthermore, also the behaviour of the residual variance itself can sometimes be a good indication of the sensibleness of an additional dipole. We have brought forward such an argument in Chapter 2. There we found a highly significant interaction between the number of dipoles used in our models and the experimental condition ('attend' versus 'non-attend'). Though a decrease in residual variance when including an additional dipole is trivial, this interaction between adding a source and considerably improving only the model for the 'attend' condition is not. If the third dipole modelled only noise, then the decrease in the residual variance would be expected to be the same for both conditions. Since, however, this is not the case and the residual variance for the two dipole model was the same for both conditions, we have strong evidence that an additional (attention-specific)

source is involved here.

Albeit these heuristic improvements, one must not forget that all MEG analysis is model-dependent, for the inverse problem remains, of course. Thus, although we possess some well established methods of modelling, it would be desirable to have a model-independent way of localising cortical activity. Such a method is given by functional magnetic resonance imaging (fMRI), and a brief overview of the physics and neurophysiology underlying it is provided now in Appendix B.

# Appendix B

# Methods II: Nuclear Magnetic Resonance Imaging Techniques

Semi-classically speaking, **M**agnetic **R**esonance **I**maging (MRI) and **f**unctional MRI (fMRI) are based upon the measuring of the precession of nuclear spins.

While MRI more or less measures the amount of water in the brain tissue, fMRI records its haemodynamic response. The first method allows to get high resolution 3D data sets of the human brain; like those we used in Chapter 2 to learn about the cortical location of the third source from our MEG dipole model. The second method was made use of in Chapter 3, where we aimed at finding the location of the third source in a model-independent way.

This chapter introduces some basic principles of the physics underlying (f)MRI and explains certain issues concerning the data acquisition and analysis. The fact that MRI can be used to access the brain anatomy is quite straightforward and will become clear while we discuss the physical background. The way the haemodynamic responses relate to MEG data, however, is not that obvious. Thus, since we made use of this relation in Chapter 4, we first have to focus on the connection between haemodynamics and neural activity.

## B.1 Neurophysiological Basics

Although the human brain accounts for only about 2% of the total body mass, it consumes 20% of the body's glucose and oxygen. These are delivered by the blood supply through a rich network of vessels, from which the brain receives

about 20% of the whole cardiac output [33]. As we shall see now, blood flow and energy metabolism inside the brain are tightly linked to neural activity. Indeed it is this connection that legitimates our procedure of Chapter 4, where we used activations seen in the fMRI data as seeds for MEG dipoles and thus supposed a similar type of response to be measured by both techniques.

So how do neural activity and blood flow relate to one another and how can fMRI measure that? All metabolic changes in neurones that accompany neurotransmitter release are energy-requiring. Indeed energy requirement and oxygen consumption are virtually the same because about 90% of the glucose is aerobically metabolised [72]. Thus, energy production inside the brain depends ultimately upon oxygen metabolism, and there is thus a greater local demand for delivery of oxygen with increased synaptic activity. To meet this increased metabolic demand, neuronal activation is accompanied by increased local blood flow. Approximately half of the energy produced by this consumption supports electrophysiological function, whereas the other half is used for cellular homeostatic activities. At rest an average human brain of 1 kg consumes oxygen at a rate of about 35 ml/s [72]. More details on brain energy metabolism and haemodynamic responses are given in [33].

**B**lood **O**xygenation **L**evel **D**ependent (BOLD) fMRI images signal contrast arising from changes in the local magnetic susceptibility. The latter is an index of the extent to which an applied magnetic field is distorted as it interacts with a material. Blood can be considered simply as a concentrated solution of haemoglobin. However, its oxidised and reduced form have widely differing magnetic properties. When bound to oxygen, haemoglobin only has paired electrons and thus hardly influences the local magnetic field. Whereas deoxygenated haemoglobin contains unpaired electrons and thus has a strong magnetic moment whereby it strongly influences the local magnetic field.

Given an increased blood flow, we have an oversupply of oxygen in the venous blood and the concentration of deoxygenated haemoglobin decreases. Hence, also the unsteadiness in the local magnetic field decreases. This gives rise to increased signals from the water in both the blood vessels and the surrounding brain tissue (the first is connected to the relaxation time $T_2$, the latter to $T_2^*$, cf. below). BOLD fMRI concentrates on the radio frequency signal, which is sensitive to changes in the local magnetic field ($T2^*$). Thus, although one measures the signals from protons, fMRI provides information about the local blood flow. Measuring the radio frequency signal after presenting a certain stimulus and subtracting the same signal when measured after no stimulus, one gets the specific difference between the deoxygenated and oxygenated haemoglobin due to

this stimulus. Thus, in fMRI one measures the blood circulation which in turn gives us information about neural activity. Therefore, the difference shows the brain regions which are particularly active when the given stimulus occurs.

However, it should be emphasised that although the general principles of the relation between haemodynamic response and neural activity are known, the precise mechanisms are not. Since for the present work it is, however, important to show that MEG and fMRI data are compatible, we shall briefly introduce some empirical evidence supporting that both techniques measure the same kind of activation.

This compatibility between fMRI and MEG data was established via the recording of local field potentials (LFP) and multi-unit activity (MUA). Both methods use electrodes inside the brain for measuring neural activity; but while MUA records action potentials, LFP records postsynaptic potentials. When studying neural mass actions via LFPs a current source density (CSD) analysis proved very helpful [87]. The CSD is defined as the second spatial derivative of the voltage across the electrode sites used for recording LFPs.

The close connection between auditory evoked potentials and CSDs in the macaque monkey was shown by the investigations of Steinschneider et al. [136]. The main result is given in Fig. B.1. Note the correspondence between the CSD and the AEP in laminae III and IV. That the early positive response (P1) in monkeys corresponds to the human P50 was established by [19]. Thus, these results support our claim of Appendix A, that in our MEG experiments we measure activation in exactly these laminae.

The fact that also the fMRI ultimately measures postsynaptic (rather than action) potentials was shown by Logothetis et al., who found a correlation between the BOLD response and the LFPs [72], [74]. Their main result is presented in Fig. B.2. Indeed for stimulation frequencies lower than 0.16 Hz they were able to estimate neural responses by a deconvolution of the BOLD response [73].

Thus, altogether the studies of Steinschneider et al. and Logothetis et al. showed the compatibility of MEG and fMRI data which both ultimately measure postsynaptic activity. By the same token our procedure of Chapter 4, where we used source locations gathered from fMRI data as seeds for MEG dipole models, is legitimised. However, before comparing fMRI and MEG any further, something must be said on the basic physical properties of matter which allow for magnetic resonance imaging in the first place.

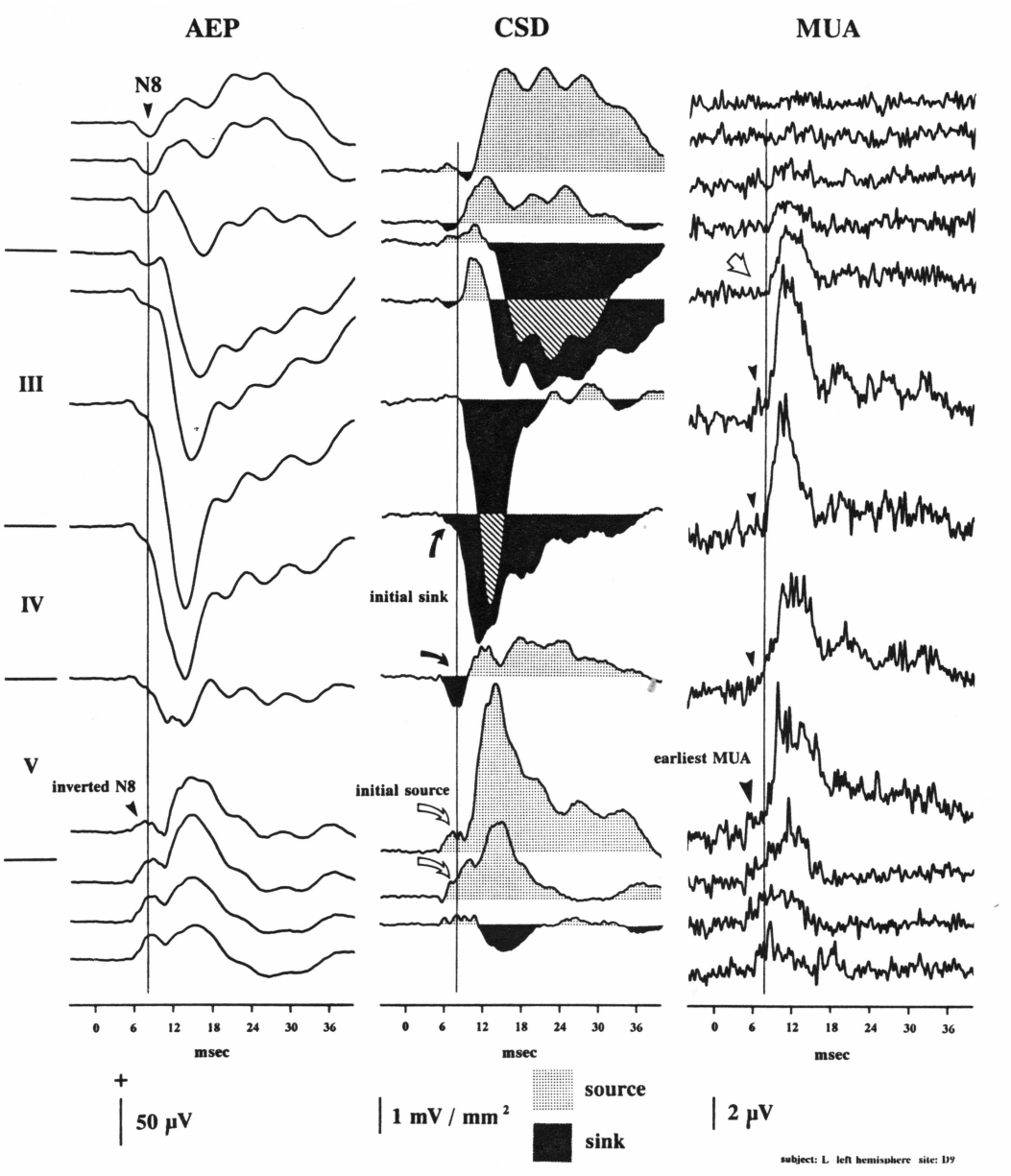


***Figure B.1:*** *Patterns of click-evoked auditory evoked potentials (AEP), current source densities (CSD) and multi-unit activity (MUA) recorded within the primary auditory cortex of a macaque monkey (taken from [136]). The initial sink is simultaneous with the N8 deflection and located in lamina IV. Later current sinks are located in laminae III and IV. They have prominent superficial sources, and reflect the current flows generating the early positive components of the AEP. The correspondence between monkey and human AEP was shown by [19].*

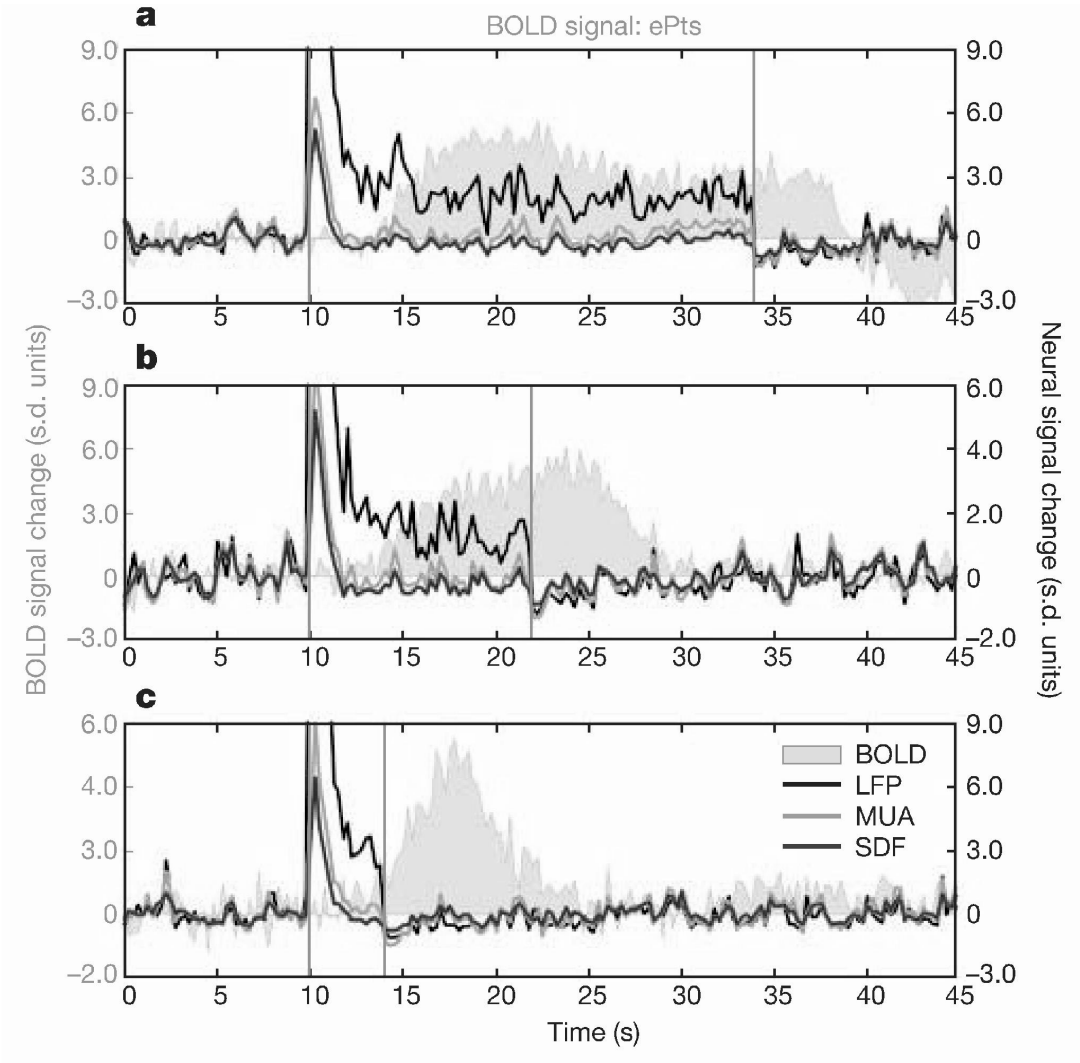


***Figure B.2:*** *Simultaneous neural and haemodynamic recordings from a cortical site of macaque monkeys showing transient neural responses (taken from [74]). Fig. a–c: responses to a pulse stimulus of 24, 12 and 4 s. Both single- and multi-unit responses (MUA) adapt a couple of seconds after stimulus onset. The signal exhibiting the highest correlation with the BOLD response is the local field potential (LFP).*

## B.2 Physical Basics

### Nuclear Magnetism

The main ingredients of matter, that is electrons, protons and neutrons, have a spin and with it a magnetic moment. The numerical values for protons and electrons are:

$$\begin{aligned} \text{electron} \quad & \mu_B = e\hbar/(2m_e) = 5.8 \times 10^{-11}\,\text{MeV T}^{-1}, \\ \text{proton} \quad & \mu_p = 2.8e\hbar/(2m_p) = 8.8 \times 10^{-14}\,\text{MeV T}^{-1}. \end{aligned}$$

A spin either aligns itself parallel (magnetic quantum number $m = -1/2$) or antiparallel ($m = +1/2$) to a given external magnetic field $\vec{B}_0$. The energies of these levels are $W_- = -\mu B_0$ and $W_+ = +\mu B_0$. The ratio between the number of parallel ($N_-$) and antiparallel ($N_+$) aligned spins in thermal equilibrium is given by:

$$\frac{N_+}{N_-} = \frac{e^{-W_+/(kT)}}{e^{-W_-/(kT)}} = e^{-2\mu B_0/(kT)} \tag{B.1}$$

At room temperature $kT \approx 1/40\,\text{eV}$, so that for the magnetic field of the earth (1 gauss = 1/10000 T) for a proton this ratio is $e^{-7.0\times10^{-10}} \approx 1 - 7.0 \times 10^{-10}$. Given a magnetic field of 1.5 T it is $e^{-1.1\times10^{-5}} \approx 1 - 1.1 \times 10^{-5}$. Thus, only about 11 spins in every 1,000,000 contributed to the net magnetic moment we made use of in our fMRI experiment of Chapter 3.

Transitions between the two energy states accompany absorption or emission of the energy:

$$\Delta W = 2\mu B_0. \tag{B.2}$$

We can identify this transition with a frequency $\omega_0$, the so called Larmor frequency:

$$\omega_0 = \frac{2\mu}{\hbar} B_0 = \gamma B_0, \tag{B.3}$$

where $\gamma$ denotes the gyromagnetic ratio ($\mu = \gamma J = \gamma m\hbar$). Protons forming the nucleus of hydrogen, for instance, exhibit a resonance frequency of $\nu_0 = \omega_0/(2\pi) \approx 43\,\mathrm{MHz}$ given an external field of $1\,\mathrm{T}$ [59].

Such a transition can be induced by a high frequency signal which turns the spins so that the equilibrium state will get lost and the net tissue magnetisation is rotated by a certain angle and starts to nutate on the transverse plane. When the signal is turned off, the magnetisation is subject only to the static field $B_0$ and gradually returns into its equilibrium state. Thereby energy of the same radio wave frequency $\nu_0$ is emitted. In an MRI experiment this signal leads to an induced voltage in a receiver coil from which an image is reconstructed (see below).

## Relaxation Processes

Within our brains protons are never in isolation but in a chemical environment. Thus, the magnetic field at their position is not only dependent upon the external field $B_0$ but also upon the surrounding. Further, the intensity of those signals depends upon the number of protons contributing. Thus, nuclear magnetic resonance allows to investigate the amount of protons of a certain surrounding. In particular, the human brain can thus be scanned for the concentration of protons in pure water. This allows to distinguish cerebrospinal fluid (water content: 97.5%) from gray and white matter (77.4%) and from bone (12.2%).

Further, the environment has a huge influence on the relaxation; i.e. the time constant in which the excited spins emit their signal or get out of phase. The chemical environment can thus also be accessed by selecting special relaxation times, which in turn are of different importance for MRI and fMRI.

First, we have the spin-lattice relaxation time, denoted by $T_1$. Due to Brownian motion of surrounding molecules (lattice) the equilibrium magnetisation (direction of $B_0$) is exponentially rebuilt. The water inside the cerebrospinal fluid exhibits a larger $T_1$-value than the water inside the gray matter, which in turn is larger than the $T_1$-value stemming from the water inside the white matter. Thus, in a standard $T_1$-weighted MRI scan cerebrospinal fluid will appear quite dark, while white matter will appear rather bright and gray matter somewhere in between. Thus, $T_1$-weighted scans are particularly useful for anatomical images and are exactly the type we used in Chapter 2 to anatomically locate the third source of the MEG dipole model. Of course, the different signal intensities also

depend upon the repetition time of the radio-wave pulse $T_{\mathrm{R}}$; the most trivial case being $T_{\mathrm{R}} > T_1$, for which most of the contrast gets lost.

Second, there occurs a spin dephasing in the plane perpendicular to $B_0$ which results from mutual interactions between the spins. Hence it is called spin-spin relaxation and is usually denoted by $T_2$. It is based upon the fact that any energy transitions of a nucleus will change the local field at nearby nuclei, which in turn alters the protons' precession; i.e. it follows a loss of coherence. Other than $T_1$, $T_2$ is larger for white matter than for gray matter; i.e. in a $T_2$-weighted MRI scan, the gray matter will appear brighter. In fact, the relaxation time $T_2$ is a crude idealisation, for it assumes an ideal homogenous magnetic field. Inside the brain, however, we have local inhomogeneities which lead to additional dephasing. This is accounted for by assuming an *effective* spin-spin relaxation time $T_2^* < T_2$.

## Principles of Imaging

The magnetic field at the nucleus is determined primarily by the strong magnetic field that is applied to the sample in the imaging experiment—in our case 1.5 T, see Chapters 2 & 3. Imaging the location of resonating nuclei in a sample is made possible by the superimposing small magnetic field gradients like $G_x = \partial B/\partial x$ of usually less than 100 mT/m.

The relative positions of molecules along the smaller gradient field can now be measured from differences in resonance frequency, since the resonance (Larmor) frequency of a proton is proportional to the whole applied field strength (static plus gradient field). So now we have:

$$\omega_0 = \gamma B_0 \quad \longrightarrow \quad \omega_0(x) = \gamma B_0 + \gamma G_x x. \tag{B.4}$$

In practice, however, one is not measuring the nuclear magnetic resonance signal $I$ as a function of $\omega_0$, but the temporal development of the free inductive decay; i.e. $I(t)$. Via a Fourier transformation this can, however, easily be translated back into frequency space:

$$I(\omega_0) = \int dt I(t) e^{i\omega t}. \tag{B.5}$$

$I(\omega_0)$ gives the number of nuclei contributing to a certain frequency and hence the number of nuclei at a certain location in $x$.

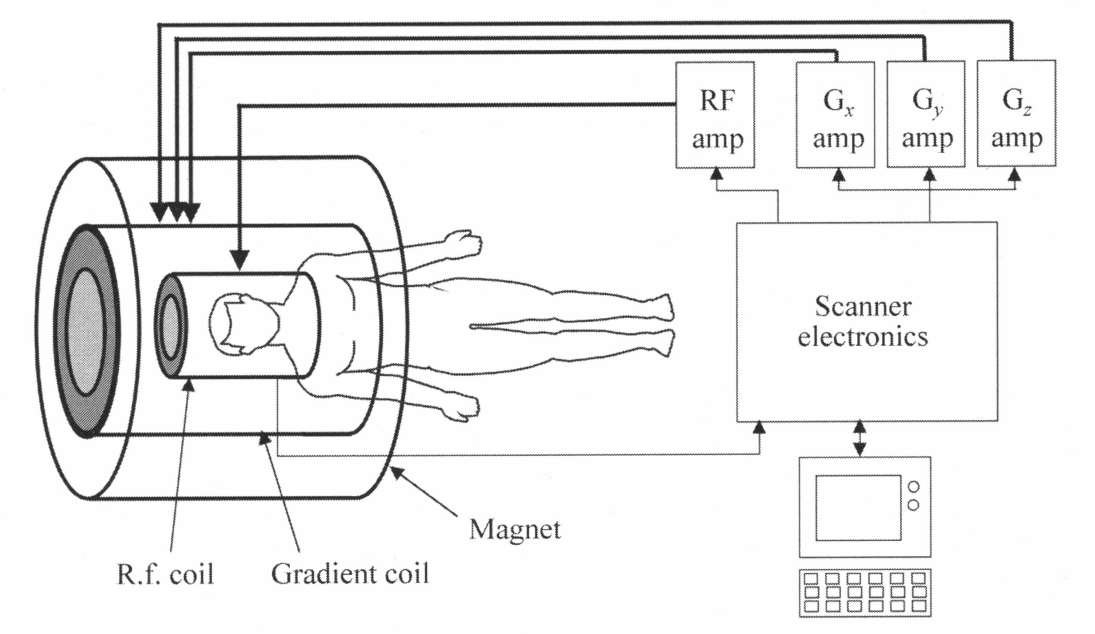


***Figure B.3:*** *Schematic picture of a MRI scanner (taken from [59]). A large static magnetic field is applied to get a sufficient net magnetic moment from the nuclear spins of the brain tissue. The excitation of these spins is then induced by signals from the radio frequency (RF) coil. The application of the three gradient coils allows for a 3D spatial reconstruction of the recorded resonances.*

This, however, only describes the basic principles for a single spatial dimension. How the application of gradients in all three directions in space can provide 3D information gets discussed, for instance, in [59]. Here we shall only add a block diagramme of a scanner as used for (f)MRI experiments—cf. Fig. B.3.

## B.3 Common Brain Space and Statistics

This section discusses two particular problems concerning the analysis of fMRI data. This seems worthwhile for it explains in some more detail the procedures used in Chapter 3. First, we consider the anatomical compatibility of individual fMRI data sets; i.e. the question how different images of (one or more) brains can be mapped. Second, we discuss different ways of fixing the significance level for the statistical evaluation of fMRI data.

## Common Brain Space

Obviously, when conducting a fMRI experiment one is interested in relating the changes in the functional image to some brain structure; i.e. to some structural image of the (individual) brain. This is possible by using a common brain space.

The most well-known common brain space was developed by Talairach and Tournoux [137]. It aims at a common coordinate frame for expressing relative neuroanatomical positions in any brain by a simple geometric parcellation of the brain according to major anatomical landmarks. The common brain used by our fMRI analysis software (SPM2) is the Montreal Neurological Institute (MNI) average brain. It is based upon 152 MRI scans which got matched by warping one brain geometry into that of another which is done by computing a nine parameter affine transformation.

It is important to recognise that different common brain spaces, like, e.g., the MNI average brain and the Talairach brain, exhibit different shapes, so that there are different relations between specific structures and given coordinate systems; i.e. there will usually be no linear transformation rule between different brain spaces. The method used in Chapter 3 to get from MNI to Talairach coordinates was taken from [9]. Here, the aforementioned affine transformation was used to map the Talairach brain onto the MNI brain, which led to the following transformation matrix:

$$\begin{pmatrix} x_{\mathrm{Tal}} \\ y_{\mathrm{Tal}} \\ z_{\mathrm{Tal}} \end{pmatrix} = \begin{pmatrix} 0.88 & 0 & 0 & -0.8 \\ 0 & 0.97 & 0 & -3.32 \\ 0 & 0.05 & 0.88 & -0.44 \end{pmatrix} \begin{pmatrix} x_{\mathrm{MNI}} \\ y_{\mathrm{MNI}} \\ z_{\mathrm{MNI}} \\ 1 \end{pmatrix}. \tag{B.6}$$

Some more information on the analysis of fMRI data can, for instance, be found in [81] and [134].

## Statistics

A statistical evaluation of a fMRI experiment starts off with the generation of a parameter-map of $T$-values on a voxel-by-voxel basis; i.e. the (multivariate) ratio of the mean signal intensity to its standard error is computed. This map is then used to identify those voxels which exceed a certain threshold and thus a certain level of significance. For example, in a given case $T > 3$ might correspond to $p < 0.001$.

A crucial difficulty, however, results from the fact that large numbers of voxels are being accessed simultaneously for changes, for this leads to a high number of false detections. If, for instance, the voxels have a side length of 2 mm, we end up with about $N = 140,000$ voxels for the whole human brain (taking an average volume of $1100\,\mathrm{cm}^3$). Thus, if the threshold for significance of change in each individual voxel is set to $p = 0.05$, then 7000 ($= 0.05 \times 140,000$) voxels would be 'active' by chance alone. Therefore, the significance level has to be corrected for $\alpha$-error inflation.

A very conservative way to account for these false detections is the Bonferroni correction which simply divides the threshold by the number of independent tests and which yields for our example:

$$p_{\text{corrected}} = p/N = 0.05/140,000 \approx 3 \times 10^{-7}. \tag{B.7}$$

Depending on the fMRI experiment (its aim as well as the data quality) this might indeed be a much too stringent level of significance. Notably, identifying the number of voxels with the number of independent tests neglects the fact that the $T$-value of each voxel is highly correlated with that of its neighbours. Hence, the correction will become more adequate to a given set of fMRI data if instead one starts from the number of 'resolution elements'. Together with some other statistical refinements this leads to the so called random field theory—for further details and references see [8]. Another way to get a Bonferroni or Bonferroni-like correction less conservative is to start from a certain region of interest. Assume we are interested in the activity of the primary auditory cortices. Then we could reasonably restrict our statistical evaluation to two spherical volumes of perhaps a radius of $r = 2\,\mathrm{cm}$. Thereby we would end up with only about 3% of all the measured voxels. Hence, $p_{\text{corrected}}$ would increase for about two orders of magnitude and become much less conservative.

A different way to correct for false detections is to set an extent threshold for activations to count as significant. So, for example, one might say that at least $2^3 = 8$ adjacent voxels should extend a certain threshold before the activation is assumed to be significant. This amounts to employ a spatial low-pass filtering (without well defined standard filter properties though). This is a sensible method given that an activation normally is not bound to a single voxel of, say, $2 \times 2 \times 2\,\mathrm{mm}^3$—both due to the local extension of neural activity and to the spatial resolution of $T_2^*$ images.

The corrections of the significance level we employed in Chapter 3 were as follows. First, we used the just suggested extension threshold of $2^3 = 8$ for all data; i.e.

individual as well as group results. Second, for the group data a Bonferroni-like correction for the whole brain was applied (using random field theory as mentioned above). This resulted in a $p_{\text{corrected}}$-value similar to that of equation B.7. For the given experiment this corresponded to a threshold of $T > 4.95$. The individual data have not been Bonferroni corrected. Here the level of significance was set to $p < 0.001$, which corresponded to a threshold of $T > 3.13$.

Thus, the corrections for the group data in Chapter 3 led to very conservative statistical decisions and the resulting contrasts do only show highly significant activations with very few false detections. In contrast, the presentation of the individual data is much less conservative as to show the inter-individual variability (in particular for the attention-specific activities). Hence, since these data were mainly given for matters of illustration, a higher false detection rate was accepted.

## B.4 Comparing (f)MRI with MEG

With regard to temporal resolution, the MEG has a big advantage. Ranging in the order of 1 ms its sensitivity is about three orders of magnitude higher than that of the fMRI. This is a consequence not of any technical limit but a principal one resulting from the time course of the haemodynamic response function. As shown in Fig. B.4 it occurs roughly between 2 and 12 s after the stimulus, peaks at about 5.5 s and has a full width at half maximum (FWHM) of about 6 s. Note that these time constants are considerably larger than those for the postsynaptic potentials as measured by the MEG—cf. Fig. A.2. This is in accordance with the aforementioned works by Logothetis saying that for stimulation frequencies higher than 0.2 Hz a reconstruction of the neural response from the BOLD response is not possible.

The main advantage of fMRI, however, is its lack of an inverse problem. fMRI data are model-independent so that, for instance, any significant BOLD response found in a group analysis actually depicts enhanced activation, whereas the mean of different individual MEG models does not necessarily do so. However, we must not forget that fMRI analyses crucially rely on the warping of brains to enable the comparison of functional with structural data. Further, the spatial accuracy of the $T2^*$ signals is rather bad, since haemodynamic responses are not spatially very specific and signal changes from draining veins spatially blur the activation response. As a first indication of the spatial accuracy of our fMRI data one might take the radius of the BOLD responses which is typically about 5 mm.

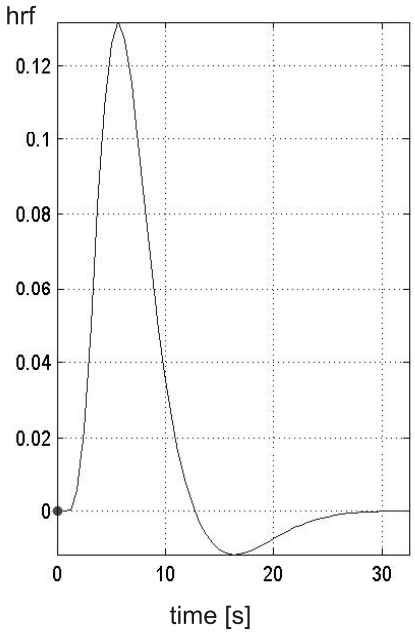


***Figure B.4:*** *Time course of the haemodynamic response function (hrf) as used in the fMRI analysis software SPM2. Note the resulting rather blurred nature of the response; the full width at half maximum (FWHM) is about 6 s.*

Thus, the fMRI data surely provide a lower resolution than the anatomical 3D MRI data sets we used as a post-hoc heuristic for checking MEG source location in Chapters 2 & 5. One way to access the spatial resolution of both fMRI and MEG is, of course, a comparison of the location we gathered for our additional parietal activity in the discrimination task on tone durations. There our fitted third MEG source of Chapter 2 showed a Euclidean distance from the two of the fMRI experiment of Chapter 3 of about 3 cm. This mainly resulted from the difference in the $x$-direction (we modelled one source, whereas the fMRI showed a bilateral activation). In the $yz$-plane the extension of the BOLD response matches the errorbars of the MEG localisations extremely well—cf. top row of Fig. 3.9 in Chapter 3. Thus, obviously the spatial accurateness of the MEG model crucially depends on the adequateness of the chosen number of dipoles. However, together with the given intracranial depth of the source(s) and the radial blindness of the MEG, the agreement between fMRI and MEG data is rather encouraging.

Indeed one must not expect a naive one-to-one correspondence between BOLD and MEG responses for all cases. This was seen explicitly for the frontal BOLD response which we assume to be related to the electrophysiological P3 deflec-

tion, but which does not show the target-specificity of the latter; meaning that the P3 but not the frontal BOLD response was prominent only in answer to deviants. However, our experiments show the extreme valuableness of employing both MEG/EEG and fMRI. Not only did we find very good agreement between fMRI and MEG data but also the analysis of one kind of data always contributed to a better understanding of the other. Thus, the fMRI supported the additional parietal source found in the MEG data, the time course of the MEG source waveforms underpinned the functional difference between the parietal and the frontal BOLD activation etc.

# Appendix C

# Methods III: Psychometry

In Chapter 6 we used signal detection theory and the *Advanced Measures of Music Audiation* (AMMA test) to assess subjects' performance during the MEG experiments and their musical aptitude. First, this appendix motivates and introduces signal detection theory in a little more detail. Second, the AMMA test will be introduced and an alternative way of evaluating it will be suggested. This alternative evaluation will be compared to the standard one using data gathered from 20 subjects.

## C.1 Evaluation of Discriminative Behaviour

During all four of our MEG experiments (discrimination of the duration of tones, silent periods, pictures and dark screens) subjects were asked to press a mouse button in response to a deviant; i.e. the longer target signal. There are four possible types of responses, which get classified and named in Table C.1.

The simplest idea for evaluating these responses would be to take the subjects' hit rate $p_{\text{hit}}$ as a measure for their discriminative abilities. However, as Fig. C.1

| stimulus | response | result | rate |
|---|---|---|---|
| deviant | yes | hit | $p_{\text{hit}}$ |
| deviant | no | miss | $p_{\text{missed}} = 1 - p_{\text{hit}}$ |
| standard | yes | false alarm | $p_{\text{false alarm}}$ |
| standard | no | correct rejection | $p_{\text{corr. rej.}} = 1 - p_{\text{false alarm}}$ |

***Table C.1:*** *Possible stimulus-response combinations and terminology according to signal detection theory [39].*

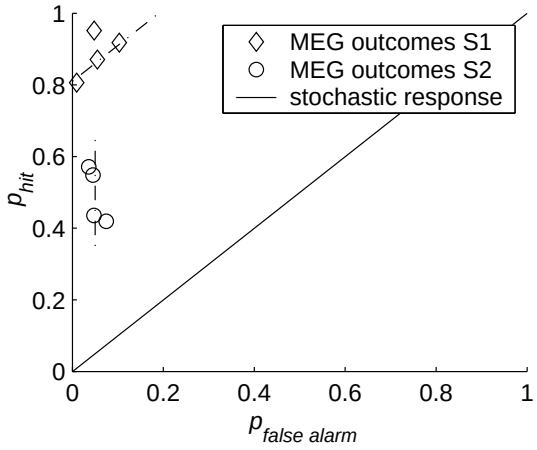


***Figure C.1:*** *Scatter plot for hit and false alarm rates of two subjects who participated in all MEG- and fMRI-measurements.*

suggests, $p_{\text{hit}}$ will not always be an appropriate variable for this. Indeed it would lead to appropriate results for subject 2 ($S2$) whose behavioural data more or less all lie on a vertical line; i.e. share roughly the same $p_{\text{false alarm}}$. However, $p_{\text{hit}}$ would be a rather bad variable for subject 1 ($S1$), because three data points for $S1$ are parallel to the line for which $p_{\text{hit}}$ matches $p_{\text{false alarm}}$; i.e. the line of a 'perfect' stochastic response (cf. Fig. C.1). Thus, points in a row parallel to that line rather seem to depict equally good performances and not varying ones as the difference in $p_{\text{hit}}$ would suggest. Hence, a method considering both $p_{\text{hit}}$ and $p_{\text{false alarm}}$ is needed.

Such a method is provided by signal detection theory, which was first used in a psychophysical context by Green and Swets [39] and which we shall introduce now.

## Signal Detection Theory

First we introduce an internal coordinate, the so called 'sensual continuum $x$'. The perception of deviants and standards is assumed to follow probability density functions of normal distributions in $x$, denoted by $\varphi_{\text{std}}(x)$ and $\varphi_{\text{dev}}(x)$. The standard deviation $\sigma$ is assumed to be the same for both distributions. In Fig. C.2 this is illustrated for a case matching our MEG experiments where 80% of the stimuli have been standards and 20% have been deviants.

The discriminative ability $d'$ (d-prime) of a subject is now given by the difference between the expectation values of the two distributions (normalised by their

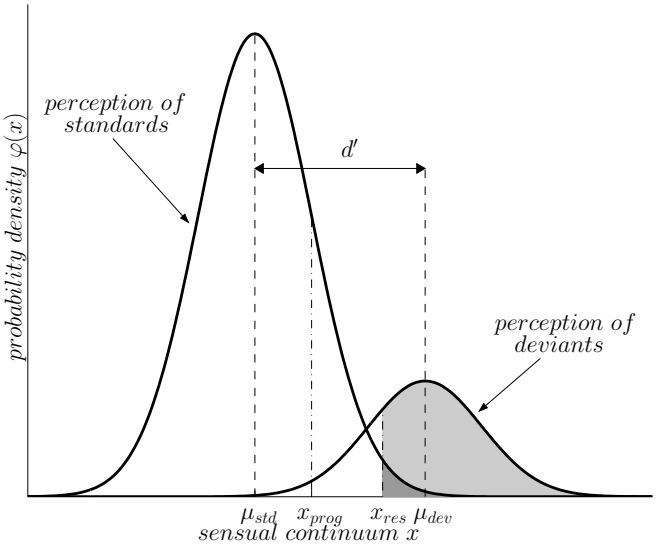


***Figure C.2:*** *Introduction of discriminative ability $d'$ (d-prime) and restrictiveness in strategy $\beta$ (likelihood ratio) as used in signal detection theory. The distribution of excitation for deviants and standards (both sharing the same standard deviation $\sigma$) is given along an internal coordinate, the so called 'sensual continuum x'. The subject is assumed to set a critical x-value ($x_{crit}$; two possible values are indicated by $x_{prog}$ and $x_{res}$) which establishes the boundary between judging the stimulus to be a standard ($x_{crit} < x_{prog}$; $x_{crit} < x_{res}$) or a deviant ($x_{crit} \geq x_{prog}$; $x_{crit} \geq x_{res}$—see the grey shaded area).*

standard deviation, cf. Fig. C.2):

$$d' := \frac{\mu_{\mathrm{dev}} - \mu_{\mathrm{std}}}{\sigma} \tag{C.1}$$

Rather than any expectation values it is $p_{\mathrm{hit}}$ and $p_{\mathrm{false\,alarm}}$ that can be gathered directly from the subjects responses. Thus, to make $d'$ experimentally accessible, we start from the expression:

$$p_{\mathrm{hit}} = 1 - \Phi(\frac{x_{\mathrm{crit}} - \mu_{\mathrm{dev}}}{\sigma}) = \Phi(\frac{\mu_{\mathrm{dev}} - x_{\mathrm{crit}}}{\sigma}), \tag{C.2}$$

where $\Phi$ denotes the probability ($\Phi(y) = \int_{-\infty}^{y} \varphi(y')\,dy'$) and $x_{\mathrm{crit}}$ the subject's boundary between judging a stimulus to be a standard ($x < x_{\mathrm{crit}}$) or a deviant ($x \geq x_{\mathrm{crit}}$). This yields:

$$\Phi^{-1}(p_{\mathrm{hit}}) = \frac{\mu_{\mathrm{dev}} - x_{\mathrm{crit}}}{\sigma}. \tag{C.3}$$

Thus, also making use of the analogous expression for $p_{\text{false alarm}}$, it follows that:

$$d' = \Phi^{-1}(p_{\text{hit}}) - \Phi^{-1}(p_{\text{false alarm}}). \tag{C.4}$$

Whereas $S2$ in Fig. C.1 always was very restrictive in his strategy, i.e. quite keen on not producing too many false alarms, $S1$ was much more progressive. Given his very high hit rate he was so to speak 'quite sloppy' in allowing for false alarms. Such a difference in strategy can also be illustrated by the help of Fig. C.2. Here the shaded area gives the positive responses of a subject using a restrictive criterion set at $x_{\text{res}}$, whereas a more progressive criterion is indicated by $x_{\text{prog}}$).

Signal detection theory also allows to derive a numerical value for the restrictiveness of the subject's strategy; namely the likelihood ratio $\beta$. Note that $x_{\text{crit}}$ itself would not be an adequate variable here, for the positions of the normal distributions vary between subjects. To account for this, $\beta$ is defined as the ratio of the probability densities at $x_{\text{crit}}$:

$$\beta := \frac{\varphi_{\text{dev}}(x_{\text{crit}})}{\varphi_{\text{std}}(x_{\text{crit}})} = \frac{e^{-\frac{(x_{\text{crit}}-\mu_{\text{dev}})^2}{2\sigma^2}}}{e^{-\frac{(x_{\text{crit}}-\mu_{\text{std}})^2}{2\sigma^2}}} = e^{-\frac{1}{2}\{[\Phi^{-1}(p_{\text{hit}})]^2-[\Phi^{-1}(p_{\text{false alarm}})]^2\}}. \tag{C.5}$$

It can be seen from Fig. C.1 that signal detection has a draw back if the sample size is too low (or the task is too easy). This is because if either $p_{\text{hit}}$ goes to one or $p_{\text{false alarm}}$ goes to zero, one runs into a singularity ($d'$ goes to infinity—cf. equation C.4). However, *as a matter of fact* this turned out to be no problem with the data at hand. No subject of the current MEG-studies ever ran into such a singularity. Admittedly, some low values in $p_{\text{false alarm}}$ occurred which seemed to make the resulting $d'$ too high. However, much more problems would have followed from simply using $p_{\text{hit}}$ as a psychometric measure, given that there have been subjects with equal $p_{\text{hit}}$ and yet quite different $p_{\text{false alarm}}$. Besides, in Chapter 7 individual behavioural data got compared to neuromagnetic ones. Knowing the probabilistic nature of neural responses, the compatibility of these two types of data was particularly ensured by signal detection theory, which employs Gaussian distributions as its basis—see [98] for a similar argumentation.

## C.2 Evaluation of Musical Aptitude (AMMA Test)

The *Advanced Measures of Music Audiation* (AMMA test; see [35]) was designed by Edwin E. Gordon and is a psychometric means to estimate individual rhythmic and tonal abilities. The test has a retest reliability of 0.89 and 0.90 for the tonal and the rhythmic score, respectively [36]. It is widely used at conservatories in the USA and has recently been introduced to neurophysiological research by Schneider et al. [122]. Given that we investigate the abilities in discriminating durations, we are interested in the rhythmic rather than the tonal aptitude.

According to Gordon, the AMMA test measures 'audiation', a potential or capacity to learn music. Thus, it does not measure musical training or personal achievement. How *aptitude* and *achievement* can be separated experimentally and in which ways the validity of the test was checked is discussed, e.g., in [36]. Some elaboration on the conceptually rather poor notion of 'audiation' I did elsewhere [131]. Moreover, Gordon maintains that the ability to 'audiate' can be influenced only until the age of nine years [35], which agrees with the fact that cortical plasticity is also prominent until about that age. Given that our investigations focus on time perception and rhythmic aptitude, it is worth mentioning that psychological reproduction and estimation studies found a stable temporal performance to be reached in infants at about eight years of age [85].

The AMMA test is conducted as follows: subjects are presented with 30 pairs of melodies and have to decide whether the two performances within each pair ...

- ... *vary tonally* (whether one or more tones changed in pitch),
- ... *vary rhythmically* (i.e. whether the duration of one or more tones or pauses changed), or
- ... *are the same.*

All pairs of melodies belong to exactly one of these three categories.

To calculate the standard rhythmic raw score $AMMA_{\text{rhythm}}$ the hits and false alarms with respect to rhythmically changed pairs are considered together with the correctly identified unchanged pairs. The according matrix is given in Table C.2 (with the bracketed values set to zero). An offset of 20 points is added in this standard procedure, which is to account for the fact that one could get

| subject's response | actual change | | |
|---|---|---|---|
| | none | rhythmic | tonal |
| none | +1 | (-1) | 0 |
| rhythmic | -1 | +1 | -1 |
| tonal | 0 | (-1) | 0 |

***Table C.2:*** *Possible melody pair-response combinations and evaluation for the AMMA rhythmic raw score. The entries in brackets mark the additional combinations taken into account for the alternative evaluation proposed in this chapter; in the standard evaluation they are set to zero.*

a maximal negative value of 20; namely if always answering 'rhythmic change' where indeed there was no change or a tonal one. The tonal raw score is calculated analogously. It should be added that quite sensibly this method differs from calculating $d'$, since 30 responses can hardly be viewed as constituting two normal distributions.

## Proposing a Re-Analysis

The draw back of this procedure is that it does not penalise responding 'no change' or 'tonal change' in those cases where there was indeed a change in rhythm. This leads to the rather absurd result that a completely untrained ear which hears no differences at all between the performances of each pair—and accordingly always responses with 'no change'—gains a raw score of 30 (offset of 20 plus 10 for the 10 pairs which indeed staid the same). His score would thus lie amidst that of professional musicians—cf. percentile ranks in the manual to the AMMA test. This biased result, however, gets ruled out if penalties in the just suggested way are added. This is shown by the entries in brackets in Table C.2. The corresponding offset for this procedure should then be 30 instead of 20, for now one can give up to 30 penalised responses. The score gathered from this re-evaluation will be called $rAMMA_{\text{rhythm}}$.

We calculated both $AMMA_{\text{rhythm}}$ and $rAMMA_{\text{rhythm}}$ for all 20 subjects who participated in the initial experiment on tone duration discrimination (cf. Chapters 2 & 4). As for the smaller ensemble ($N$=10) presented in Chapter 6, a significant correlation between the discriminative ability as measured by $d'_{\text{tone}}$ and $AMMA_{\text{rhythm}}$ score was found ($r = 0.54, p < 0.05$). The correlation between $d'_{\text{tone}}$ and the newly suggested $rAMMA_{\text{rhythm}}$ was found to be $r = 0.49, p < 0.05$. The Olkin procedure showed that this slight difference between the two correlations

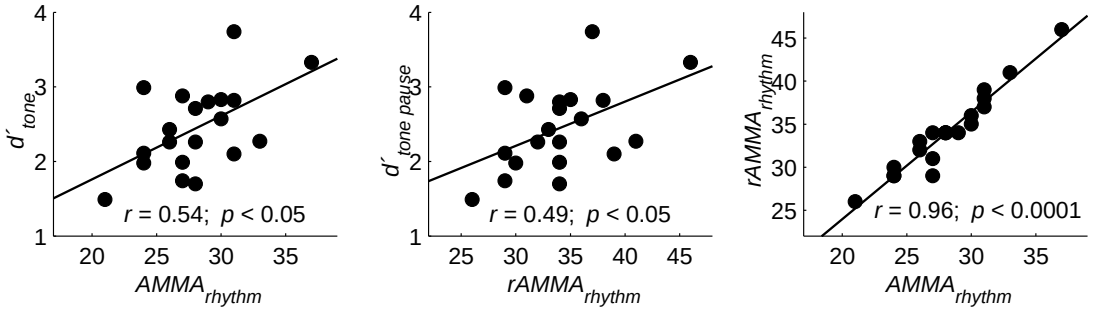


***Figure C.3:*** *Correlations between $d'_{tone}$ and subjects' rhythmic aptitude as evaluated according to the standard procedure ($AMMA_{rhythm}$; left subplot) and the renormalised one ($rAMMA_{rhythm}$; subplot in the middle). The correlation between the two evaluations is given in the subplot on the right. The plots show the data for all 20 subjects who participated in the initial experiment on tone discrimination.*

is not statistically significant ($z = 0.77, n.s.$). This was obviously due to the fact that the correlation between $AMMA_{\text{rhythm}}$ and $rAMMA_{\text{rhythm}}$ was highly significant ($r = 0.96, p < 0.0001$). The scatter plots of all three correlations are given in Fig. C.3.

Thus, the proposed re-evaluation did not show a considerable effect. The correlation to $d'_{\text{tone}}$ basically staid the same, which was not astonishing given the extremely high correlation between $AMMA_{\text{rhythm}}$ and $rAMMA_{\text{rhythm}}$. This has been the case since *as a matter of fact* no subject engaged in the described 'sounds-all-the-same-to-me' strategy. However, although the re-evaluation was empirically irrelevant in our case, it still is *theoretically* much more convincing and might become crucial for different data sets.

# Bibliography


[1] A. Angrilli, P. Cherubini, A. Pavese, and S. Manfredini. The influence of affective factors on time perception. *Perception & Psychophysics*, 59:972–982, 1997.

[2] M. Annett. A classification of hand preference by association analysis. *British Journal of Psychology*, 61:303–312, 1970.

[3] A. Augustinus. *Bekenntnisse – Confessiones*. Insel, Frankfurt (Main), 1987 [$\sim$ 400 AD].

[4] P. Belin, S. McAdams, L. Thivard, B. Smith, S. Savel, M. Zilbovicius, S. Samson, and Y. Samson. The neuroanatomical substrate of sound duration discrimination. *Neuropsychologia*, 40:1956–1964, 2002.

[5] V. Benussi. *Psychologie der Zeitauffassung*. Carl Winter, Heidelberg, 1913.

[6] P. Berg and M. Scherg. A multiple source approach to the correction of eye artifacts. *Electroencephalography & clinical Neurophysiology*, 90:229–241, 1994.

[7] R. A. Block. Models of psychological time. In R. A. Block, editor, *Cognitive Models of Psychological Time*, pages 1–35. Lawrence Erlbaum, Hillsdale (N.J.), 1990.

[8] M. Brett. Thresholding with random field theory. Available at `http://www.mrc-cbu.cam.ac.uk/Imaging`, 1999.

[9] M. Brett. The MNI brain and the Talairach atlas. Available at `http://www.mrc-cbu.cam.ac.uk/Imaging/mnispace.html`, 2002.

[10] D. V. Buonomano and U. R. Karmarkar. How do we tell time? *Neuroscientist*, 8:42–51, 2002.

[11] P. W. Burgess, A. Quayle, and C. D. Frith. Brain regions involved in prospective memory as determined by positron emission tomography. *Neuropsychologia*, 39:545–555, 2001.

[12] K. O. Bushara, R. A. Weeks, K. Ishii, B. Tian, J. P. Rauschecker, and M. Hallett. Modality-specific frontal and parietal areas for auditory and visual spatial localization in humans. *Nature Neuroscience*, 2:759–766, 1999.

[13] L. Carroll. *The Annotated Alice*. Penguin, London, 1970.

[14] J. T. Coull, R. S. Frackowiak, and C. D. Frith. Monitoring for target objects: activation of the right frontal and the parietal cortices with increasing time on task. *Neuropsychologia*, 36:1325–1334, 1998.

[15] J. T. Coull and A. C. Nobre. Where and when to pay attention: the neural systems for directing attention to spatial locations and to time intervals as revealed by both PET and fMRI. *The Journal of Neuroscience*, 18:7426–7435, 1998.

[16] N. Cowan. On short and long auditory stores. *Psychological Bulletin*, 96:341–370, 1984.

[17] A. R. Damasio. *Descartes' Error: Emotion, Reason and the Human Brain*. Grosset/Putnam, New York, 1994.

[18] A. Dittmann-Balcar, M. Juptner, W. Jentzen, and U. Schall. Dorsolateral prefrontal cortex activation during automatic auditory duration-mismatch processing in humans: a positron emission tomography study. *Neuroscience Letters*, 308:119–122, 2001.

[19] J. J. Eggermont and C. W. Ponton. The neurophysiology of auditory perception: from single units to evoked potentials. *Audiology & Neuro-Otology*, 7:71–99, 2002.

[20] T. Elbert, R. Ulrich, B. Rockstroh, and W. Lutzenberger. The processing of temporal intervals reflected by CNV-like brain potentials. *Psychophysiology*, 28:648–655, 1991.

[21] A. K. Engel and W. Singer. Temporal binding and the neural correlates of sensory awareness. *Trends in Cognitive Sciences*, 5:16–25, 2001.

[22] A. Engelien, W. Huber, D. Silbersweig, E. Stern, C. D. Frith, W. Doring, A. Thron, and R. S. Frackowiak. The neural correlates of 'deaf-hearing'

in man: conscious sensory awareness enabled by attentional modulation. *Brain*, 123:532–545, 2000.

[23] J. J. Ermer, J. C. Mosher, M. Huang, and R. M. Leahy. Paired MEG data set source localization using recursively applied and projected (RAP) MUSIC. *IEEE Transactions on Biomedical Engineering*, 47:1248–1260, 2000.

[24] A. M. Ferrandez, L. Hugueville, S. Lehéricy, J. B. Poline, C. Marsault, and V. Pouthas. Basal ganglia and supplementary motor area subtend duration perception: an fMRI study. *NeuroImage*, 19:1532–1544, 2003.

[25] P. C. Fletcher, C. D. Frith, S. C. Baker, T. Shallice, R. S. Frackowiak, and R. J. Dolan. The mind's eye: precuneus activation in memory-related imagery. *NeuroImage*, 2:195–200, 1995.

[26] P. C. Fletcher, C. D. Frith, P. M. Grasby, T. Shallice, R. S. Frackowiak, and R. J. Dolan. Brain systems for encoding and retrieval of auditory-verbal memory: an in vivo study in humans. *Brain*, 118:401–416, 1995.

[27] P. Fraisse. Perception and estimation of time. *Annual Review of Psychology*, 35:1–36, 1984.

[28] P. Fraisse. *Psychologie der Zeit*. Ernst Reinhard, Munich, 1985 [1957].

[29] N. Gaab, C. Gaser, T. Zaehle, L. Jäncke, and G. Schlaug. Functional anatomy of pitch memory—an fMRI study with sparse temporal sampling. *NeuroImage*, 19:1417–1426, 2003.

[30] V. Gallese, L. Fadiga, L. Fogassi, and G. Rizzolatti. Action recognition in the premotor cortex. *Brain*, 119:593–609, 1996.

[31] H.-G. Geißler. Zeitverarbeitung – Verarbeitungszeit: Temporale Invarianten und oszillatorische Mechanismen in Wahrnehmung und Gedächtnis. *Zeitschrift für Psychologie*, 208:129–168, 2000.

[32] J. Gibbon, C. Malapani, C. L. Dale, and C. R. Gallistel. Towards a neurobiology of temporal cognition: advances and challenges. *Current Opinion in Neurobiology*, 7:170–184, 1997.

[33] A. Gjedde. Brain energy metabolism and the physiological basis of the haemodynamic response. In P. Jezzard, P. M. Matthews, and S. M. Smith, editors, *Functional MRI: An Introduction to Methods*, pages 37–65. Oxford University Press, Oxford, 2001.

[34] J. Glicksohn. Temporal cognition and the phenomenology of time: a multiplicative function of apparent duration. *Consciousness and Cognition*, 10:1–25, 2001.

[35] E. E. Gordon. *Learning Sequences in Music*. GIA Publications, Chicago, 1997 [1980].

[36] E. E. Gordon. *Introduction to Research and the Psychology of Music*. GIA Publications, Chicago, 1998.

[37] C. L. Grady, J. W. van Meter, J. M. Maisog, P. Pietrini, J. Krasuski, and J. P. Rauschecker. Attention-related modulation of activity in primary and secondary auditory cortex. *NeuroReport*, 8:2511–2516, 1997.

[38] P. M. Grasby, C. D. Frith, K. J. Friston, C. Bench, R. S. Frackowiak, and R. J. Dolan. Functional mapping of brain areas implicated in auditory-verbal memory function. *Brain*, 116:1–20, 1993.

[39] D. M. Green and J. A. Swets. *Signal Detection Theory and Psychophysics*. Wiley, New York, 1966.

[40] T. D. Griffiths. The neural processing of complex sounds. *Annals of the New York Academy of Sciences*, 930:133–142, 2001.

[41] T. D. Griffiths. Functional imaging of pitch analysis. *Annals of the New York Academy of Sciences*, 999:40–49, 2003.

[42] T. D. Griffiths, S. Uppenkamp, I. S. Johnsrude, O. Josephs, and R. D. Patterson. Encoding of the temporal regularity of sound in the human brainstem. *Nature Neuroscience*, 4:633–637, 2001.

[43] A. Gutschalk, R. Mase, R. Roth, N. Ille, A. Rupp, S. Hähnel, T. W. Picton, and M. Scherg. Deconvolution of 40 Hz steady-state fields reveals two overlapping source activities of the human auditory cortex. *Clinical Neurophysiology*, 110:856–868, 1999.

[44] A. Gutschalk, R. D. Patterson, A. Rupp, S. Uppenkamp, and M. Scherg. Sustained magnetic fields reveal separate sites for sound level and temporal regularity in the human auditory cortex. *NeuroImage*, 15:207–216, 2002.

[45] M. Hämäläinen, R. Hari, R. J. Ilmoniemi, J. Knuutila, and O. V. Lounasmaa. Magnetoencephalography: theory, instrumentation, and applications to noninvasive studies of the working human brain. *Reviews of Modern Physics*, 65:413–497, 1993.

[46] M. Hampe. Der Körper von innen: Zur Wahrnehmung des Körpers in Spinozas Doppelaspekttheorie der Affekte. In A. Engstler and R. Schnepf, editors, *Affekte und Ethik: Spinozas Lehre im Kontext*, pages 129–148. Georg Olms, Hildesheim, 2002.

[47] R. Hari, M. Pelizzone, J. P. Mäkelä, J. Hallstrom, L. Leinonen, and O. V. Lounasmaa. Neuromagnetic responses of the human auditory cortex to on- and offsets of noise bursts. *Audiology*, 26:31–43, 1987.

[48] D. L. Harrington, K. Y. Haaland, and R. T. Knight. Cortical networks underlying mechanisms of time perception. *The Journal of Neuroscience*, 18:1085–1095, 1998.

[49] H. L. F. Helmholtz. Über einige Gesetze der Vertheilung elektrischer Ströme in körperlichen Leitern, mit Anwendung auf die thierisch-elektrischen Versuche. *Annalen der Physik und Chemie*, 89:211–233, 353–377, 1853.

[50] K. Hoechstetter. *Magnetic Source Imaging of Tactile Evoked Activity in the Human Secondary Somatosensory Cortex*. PhD Thesis, Faculty of Physics, Heidelberg, 2001.

[51] L. Hultin, P. Rossini, G. L. Romani, P. Högstedt, F. Tecchio, and V. Pizzella. Neuromagnetic localization of the late component of the contingent negative variation. *Electroencephalography & clinical Neurophysiology*, 98:435–448, 1996.

[52] E. Husserl. *Texte zur Phänomenologie des inneren Zeitbewußtseins [1893-1917]*. Felix Meiner, Hamburg, 1985.

[53] E. Husserl. *Vorlesungen zur Phänomenologie des inneren Zeitbewußtseins*. Max Niemeyer, Tübingen, 2000 [1928].

[54] R. B. Ivry. The presentation of temporal information in perception and motor control. *Current Opinion in Neurobiology*, 6:851–857, 1996.

[55] R. B. Ivry and R. E. Hazeltine. Perception and production of temporal intervals across a range of durations: evidence for a common timing mechanim. *Journal of Experimental Psychology: Human Perception and Performance*, 21:3–18, 1995.

[56] W. James. *The Principles of Psychology*. Holt, New York, 1950 [1890].

[57] L. Jäncke, S. Mirzazade, and N. J. Shah. Attention modulates activity in the primary and the secondary auditory cortex: a functional magnetic resonance imaging study in human subjects. *Neuroscience Letters*, 266:125–128, 1999.

[58] T. Jarvilehto, R. Hari, and M. Sams. Effect of stimulus repetition on negative sustained potentials elicited by auditory and visual stimuli in the human EEG. *Biological Psychology*, 7:1–12, 1978.

[59] P. Jezzard and S. Clare. Principles of nuclear magnetic resonance and MRI. In P. Jezzard, P. M. Matthews, and S. M. Smith, editors, *Functional MRI: An Introduction to Methods*, pages 67–92. Oxford University Press, Oxford, 2001.

[60] J. P. Kelly. Principles of the functional and anatomical organization of the nervous system. In E. R. Kandel and J. H. Schwartz, editors, *Principles of Neural Science*, pages 211–221. Elsevier, New York, 1985.

[61] K. A. Kiehl, K. R. Laurens, T. L. Duty, B. B. Forster, and P. F. Liddle. Neural sources involved in auditory target detection and novelty processing: an event-related fMRI study. *Psychophysiology*, 38:133–142, 2001.

[62] P. Lanz. *Das phänomenale Bewußtsein: Eine Verteidung*. Klostermann, Frankfurt (Main), 1996.

[63] N. S. Lawrence, T. J. Ross, R. Hoffmann, H. Garavan, and E. A. Stein. Multiple neuronal networks mediate sustained attention. *Journal of Cognitive Neuroscience*, 15:1028–1038, 2003.

[64] K.-M. Lee, K.-H. Chang, and J.-K. Roh. Subregions within the supplementary motor area activated at different stages of movement preparation and execution. *NeuroImage*, 9:117–123, 1999.

[65] M. I. Leon and M. N. Shadlen. Representation of time by neurons in the posterior parietal cortex of the macaque. *Neuron*, 38:317–327, 2003.

[66] C. M. Leonard, C. Puranik, J. M. Kuldau, and L. J. Lombardino. Normal variation in the frequency and location of human auditory cortex landmarks—Heschl's gyrus: where is it? *Cerebral Cortex*, 8:397–406, 1998.

[67] J. Levinson. *Music in the Moment*. Cornell University Press, Ithaca, 1998.

[68] B. Libet, C. A. Gleason, E. W. Wright, and D. K. Pearl. Time of conscious intention to act in relation to onset of cerebral activity (readiness-potential): the unconscious initiation of a freely voluntary act. *Brain*, 106:623–642, 1983.

[69] C. Liegeois-Chauvel, A. Musolino, J. M. Badier, P. Marquis, and P. Chauvel. Evoked potentials recorded from the auditory cortex in man: evaluation and topography of the middle latency components. *Electroencephalography & clinical Neurophysiology*, 92:204–214, 1994.

[70] D. E. Linden, D. Prvulovic, E. Formisano, M. Vollinger, F. E. Zanella, R. Goebel, and T. Dierks. The functional neuroanatomy of target detection: an fMRI study of visual and auditory oddball tasks. *Cerebral Cortex*, 9:815–823, 1999.

[71] R. Llinas, U. Ribary, D. Contreras, and C. Pedroarena. The neuronal basis for consciousness. *Philosophical Transactions of the Royal Society of London. Series B: Biological Sciences*, 353:1841–1849, 1998.

[72] N. K. Logothetis. The neural basis of the blood-oxygen-level-dependent functional magnetic resonance imaging signal. In A. Parker, A. Derrington, and C. Blackmoore, editors, *The Physiology of Cognitive Processes*, pages 62–116. Oxford University Press, Oxford, 2003.

[73] N. K. Logothetis. The underpinnings of the BOLD functional magnetic resonance imaging signal. *The Journal of Neuroscience*, 23:3963–3971, 2003.

[74] N. K. Logothetis, J. Pauls, M. Augath, T. Trinath, and A. Oeltermann. Neurophysiological investigation of the basis of the fMRI signal. *Nature*, 412:150–157, 2001.

[75] J. P. Mäkelä and R. Hari. Evidence for cortical origin of the 40 Hz auditory evoked response in man. *Electroencephalography & clinical Neurophysiology*, 66:539–546, 1987.

[76] J. A. Mangels, T. W. Picton, and F. I. M. Craik. Attention and successful episodic encoding: an event-related potential study. *Cognitive Brain Research*, 11:77–95, 2001.

[77] P. Maquet, H. Lejeune, V. Pouthas, M. Bonnet, L. Casini, F. Macar, M. Timsit-Berthier, F. Vidal, A. Ferrara, C. Degueldre, L. Quaglia, G. Delfiore, A. Luxen, R. Woods, J. C. Mazziotta, and D. Comar. Brain activation induced by estimation of duration. *NeuroImage*, 3:119–126, 1996.

[78] E. J. Maratos, R. J. Dolan, J. S. Morris, R. N. Henson, and M. D. Rugg. Neural activity associated with episodic memory for emotional context. *Neuropsychologia*, 39:910–920, 2001.

[79] A. Martinez, L. Anllo-Vento, M. I. Sereno, L. R. Frank, R. B. Buxton, D. J. Dubowitz, E. C. Wong, H. Hinrichs, H. J. Heinze, and S. A. Hillyard. Involvement of striate and extrastriate visual cortical areas in spatial attention. *Nature Neuroscience*, 2:364–369, 1999.

[80] D. W. Massaro. Preperceptual images, processing time, and perceptual units in auditory perception. *Psychological Review*, 79:124–145, 1972.

[81] P. M. Matthews. An introduction to functional magnetic resonance imaging of the brain. In P. Jezzard, P. M. Matthews, and S. M. Smith, editors, *Functional MRI: An Introduction to Methods*, pages 3–34. Oxford University Press, Oxford, 2001.

[82] W. C. McCallum. Potentials related to expectancy, preparation and motor activity. In T. W. Picton, editor, *Human Event-Related Potentials—EEG Handbook III*, pages 427–517. Elsevier, Amsterdam, 1988.

[83] J. M. E. McTaggart. *The Nature of Existence*. Cambridge, Cambridge University Press, 1968 [1927].

[84] D. H. Mellor. *Real Time II*. Cambridge, Cambridge University Press, 1998.

[85] J. A. Michon. The compleat time experiencer. In J. A. Michon and J. L. Jackson, editors, *Time, Mind, and Behavior*, pages 20–52. Springer, Berlin, 1985.

[86] J. A. Michon and J. L. Jackson. Introduction: the psychology of time. In J. A. Michon and J. L. Jackson, editors, *Time, Mind, and Behavior*, pages 2–17. Springer, Berlin, 1985.

[87] U. Mitzdorf. Current source-density method and application in cat cerebral cortex: investigation of evoked potentials and EEG phenomena. *Physiological Reviews*, 65:37–100, 1985.

[88] J. C. Mosher and R. M. Leahy. Recursive MUSIC: a framework for EEG and MEG source localization. *IEEE Transactions on Biomedical Engineering*, 45:1342–1354, 1998.

[89] J. C. Mosher and R. M. Leahy. Source localization using recursively applied and projected (RAP) MUSIC. *IEEE Transactions on Signal Processing*, 47:332–340, 1999.

[90] R. Näätänen. *Attention and Brain Function*. Lawrence Erlbaum, Hillsdale (NJ), 1992.

[91] I. Nelken, Y. Rotman, and O. Bar Yosef. Responses of auditory-cortex neurons to structural features of natural sounds. *Nature*, 397:154–157, 1999.

[92] I. Nenadic, C. Gaser, H.-P. Volz, T. Rammsayer, F. Häger, and H. Sauer. Processing of temporal information and the basal ganglia: new evidence from fMRI. *Experimental Brain Research*, 148:238–246, 2003.

[93] S. D. Newman, P. A. Carpenter, S. Varma, and M. A. Just. Frontal and parietal participation in problem solving in the Tower of London: fMRI and computational modeling of planning and high-level perception. *Neuropsychologia*, 41:1668–1682, 2003.

[94] T. Noesselt, S. Hillyard, M. Woldorff, A. Schoenfeld, T. Hagner, L. Jäncke, C. Tempelmann, H. Hinrichs, and H. J. Heinze. Delayed striate cortical activation during spatial attention. *Neuron*, 35:575–587, 2002.

[95] I. Olkin and M. Siotani. *Testing for the equality of correlation coefficients for various multivariate models (Technical Report)*. Laboratory for Quantitative Research in Education, Stanford University, 1964.

[96] C. Pantev, C. Eulitz, T. Elbert, and M. Hoke. The auditory evoked sustained field: origin and frequency dependence. *Electroencephalography & clinical Neurophysiology*, 90:82–90, 1994.

[97] C. Pantev, C. Eulitz, S. Hampson, B. Ross, and L. E. Roberts. The auditory evoked 'off' response: sources and comparison with the 'on' and the 'sustained' responses. *Ear & Hearing*, 17:255–265, 1996.

[98] A. J. Parker and W. T. Newsome. Sense and the single neuron: probing the physiology of perception. *Annual Review of Neuroscience*, 21:227–277, 1998.

[99] R. D. Patterson, S. Uppenkamp, I. S. Johnsrude, and T. D. Griffiths. The processing of temporal pitch and melody information in auditory cortex. *Neuron*, 36:767–776, 2002.

[100] T. B. Penney, L. G. Allan, W. H. Meck, and J. Gibbon. Memory mixing in duration bisection. In D. A. Rosenbaum and C. E. Collyer, editors, *Timing of Behavior: Neural, Psychological, and Computational Perspectives*, pages 55–80. MIT Press, Cambridge (Mass.), 1998.

[101] T. W. Picton and D. T. Stuss. Neurobiology of conscious experience. *Current Opinion in Neurobiology*, 4:256–265, 1994.

[102] T. W. Picton, D. L. Woods, and G. B. Proulx. Human auditory sustained potentials I: the nature of the response. *Electroencephalography & clinical Neurophysiology*, 45:186–197, 1978.

[103] H. Platel, C. Price, J. C. Baron, R. Wise, J. Lambert, R. S. Frackowiak, B. Lechevalier, and F. Eustache. The structural components of music perception: a functional anatomical study. *Brain*, 120:229–243, 1997.

[104] G. Plourde and T. W. Picton. Long-latency auditory evoked potentials during general anesthesia: N1 and P3 components. *Anesthesia & Analgesia*, 72:342–350, 1991.

[105] V. Pouthas, L. Garnero, A. M. Ferrandez, and B. Renault. ERPs and PET analysis of time perception: spatial and temporal brain mapping during visual discrimination tasks. *Human Brain Mapping*, 10:49–60, 2000.

[106] K. R. Pugh, B. A. Offwitz, S. E. Shaywitz, R. K. Fulbright, D. Byrd, P. Skudlarski, D. P. Shankweiler, L. Katz, R. T. Constable, J. Fletcher, C. Lacadie, K. Marchione, and J. C. Gore. Auditory selective attention: an fMRI investigation. *NeuroImage*, 4:159–173, 1996.

[107] S. M. Rao, A. R. Mayer, and D. L. Harrington. The evolution of brain activation during temporal processing. *Nature Neuroscience*, 4:317–323, 2001.

[108] M. Ratcliffe. Heidegger's attunement and the neuropsychology of emotion. *Phenomenology and the Cognitive Sciences*, 1:287–312, 2002.

[109] A. Revonsuo. Can functional brain imaging discover consciousness in the brain? *Journal of Consciousness Studies*, 8:3–23, 2001.

[110] D. A. Rosenbaum. Broadcast theory of timing. In D. A. Rosenbaum and C. E. Collyer, editors, *Timing of Behavior: Neural, Psychological, and Computational Perspectives*, pages 215–235. MIT Press, Cambridge (Mass.), 1998.

[111] G. Roth. *Fühlen, Denken, Handeln: Wie das Gehirn unser Verhalten steuert*. Suhrkamp, Frankfurt (Main), 2001.

[112] A. Rupp. *Evozierte Potentiale bei der sequentiellen Informationsverarbeitung und selektiven Aufmerksamkeit legasthener Kinder*. PhD Thesis, Faculty of Social and Behavioural Sciences, Heidelberg, 1998.

[113] A. Rupp, S. Uppenkamp, A. Gutschalk, R. Beucker, R. D. Patterson, T. Dau, and M. Scherg. The representation of peripheral neural activity in the middle-latency evoked field of primary auditory cortex in humans. *Hearing Research*, 174:19–31, 2002.

[114] G. Russell. *The Lydian Chromatic Concept of Tonal Organization*. Concept Publishing, New York, 1953.

[115] M. Satoh, K. Takeda, K. Nagata, J. Hatazawa, and S. Kuzuhara. Activated brain regions in musicians during an ensemble: a PET study. *Cognitive Brain Research*, 12:101–108, 2001.

[116] M. Scherg. Fundamentals of dipole source potential analysis. In F. Grandori, M. Hoke, and G. L. Romani, editors, *Advances in Audiology VI: Auditory Evoked Magnetic Fields and Electric Potentials*, pages 40–69. Karger, Basel, 1990.

[117] M. Scherg. *Akustisch evozierte Potentiale*. W. Kohlhammer, Stuttgart, Berlin, Köln, 1991.

[118] M. Scherg and P. Berg. New concepts of brain source imaging and localization. *Electroencephalography & clinical Neurophysiology (Supplement)*, 46:127–137, 1996.

[119] M. Scherg, J. Vajsar, and T. W. Picton. A source analysis of the human auditory evoked potentials. *Journal of Cognitive Neuroscience*, 1:336–354, 1989.

[120] M. Scherg and D. von Cramon. Two bilateral sources of the late AEP as identified by a spatio-temporal dipole model. *Electroencephalography & clinical Neurophysiology*, 62:32–44, 1985.

[121] P. Schneider. *Source Activity and Tonotopic Organization of the Auditory Cortex in Musicians and Non-Musicians*. PhD Thesis, Faculty of Physics, Heidelberg, 2000.

[122] P. Schneider, M. Scherg, H. G. Dosch, H. J. Specht, A. Gutschalk, and A. Rupp. Morphology of Heschl's gyrus reflects enhanced activation in the auditory cortex of musicians. *Nature Neuroscience*, 5:688–694, 2002.

[123] A. Schopenhauer. *Die Welt als Wille und Vorstellung*. Suhrkamp, Frankfurt (Main), 1995.

[124] R. I. Schubotz, A. D. Friederici, and D. Y. von Cramon. Time perception and motor timing: a common cortical and subcortical basis revealed by fMRI. *NeuroImage*, 11:1–12, 2000.

[125] S. J. Segalowitz, A. J. Wintink, and L. J. Cudmore. P3 topographical change with task familiarization and task complexity. *Cognitive Brain Research*, 12:451–457, 2001.

[126] W. Sellars. Time and the world order. *Minnesota Studies in the Philosophy of Science*, 3:527–616, 1962.

[127] W. Sellars. Foundations for a metaphysics of pure process. *The Monist*, 64:3–90, 1981.

[128] G. L. Shulman, A. P. Tansy, M. Kincade, S. E. Petersen, M. P. McAvoy, and M. Corbetta. Reactivation of networks involved in preparatory states. *Cerebral Cortex*, 12:590–600, 2002.

[129] N. Sieroka. *Einfluss auditorischer selektiver Aufmerksamkeit und musikalischer Begabung auf auditorisch evozierte Felder und Potentiale*. Diploma Thesis, Faculty of Physics, Heidelberg, 2002.

[130] N. Sieroka. Husserlian retentions and their neurophysiological counterparts. Manuscript, 2004.

[131] N. Sieroka. Quasi-hearing in Husserl, Levinson, and Gordon. *Journal of the British Society for Phenomenology (forthcoming)*, 2004.

[132] S. R. Simon, M. Meunier, L. Piettre, A. M. Berardi, C. M. Segebarth, and D. Boussaoud. Spatial attention and memory versus motor preparation: premotor cortex involvement as revealed by fMRI. *Journal of Neurophysiology*, 88:2047–2057, 2002.

[133] M. E. Smith and E. Halgren. Attenuation of a sustained visual processing negativity after lesions that include the inferotemporal cortex. *Electroencephalography & clinical Neurophysiology*, 70:366–369, 1988.

[134] S. M. Smith. Overview of fMRI analysis. In P. Jezzard, P. M. Matthews, and S. M. Smith, editors, *Functional MRI: An Introduction to Methods*, pages 215–227. Oxford University Press, Oxford, 2001.

[135] R. Srinivasan, D. P. Russell, G. M. Edelman, and G. Tononi. Increased synchronization of neuromagnetic responses during conscious perception. *Journal of Neuroscience*, 19:5435–5448, 1999.

[136] M. Steinschneider, C. E. Tenke, C. E. Schroeder, D. C. Javitt, G. V. Simpson, J. C. Arezzo, and H. G. Vaughan, Jr. Cellular generators of the cortical auditory evoked potential initial component. *Electroencephalography & clinical Neurophysiology*, 84:196–200, 1992.

[137] P. Talairach and J. Tournoux. *A Stereotactic Coplanar Atlas of the Human Brain*. Thieme, Stuttgart, 1988.

[138] M. Treisman. Temporal rhythms and cerebral rhythms. *Annals of the New York Academy of Sciences*, 423:542–565, 1984.

[139] M. Treisman. The perception of time: philosophical views and psychological evidence. In J. Butterfield, editor, *The Arguments of Time*, pages 217–246. Oxford University Press, Oxford, 1999.

[140] E. Tulving, S. Kapur, F. I. M. Craik, M. Moscovitch, and S. Houle. Hemispheric encoding/retrieval asymmetry in episodic memory: positron emission tomography findings. *Proceedings of the National Academy of Sciences of the United States of America*, 91:2016–2020, 1994.

[141] B. Turak, J. Louvel, P. Buser, and M. Lamarche. Event-related potentials recorded from the cingulate gyrus during attentional tasks: a study in patients with implanted electrodes. *Neuropsychologia*, 40:99–107, 2002.

[142] B. A. Vogt, D. M. Finch, and C. R. Olson. Functional heterogeneity in cingulate cortex: the anterior executive and the posterior evaluative regions. *Cerebral Cortex*, 2:435–443, 1992.

[143] J. Vrba. Squid gradiometers in real environments. In H. Weinstock, editor, *SQUID Sensors: Fundamentals, Fabrication and Applications*, pages 117–178. Kluwer, Dordrecht, 1996.

[144] M. G. Woldorff and S. A. Hillyard. Modulation of early auditory processing during selective listening to rapidly presented tones. *Electroencephalography & clinical Neurophysiology*, 79:170–191, 1991.

[145] W. Wundt. *Grundzüge der physiologischen Psychologie*. Wilhelm Engelmann, Leipzig, 1903 [1874].

[146] T. Yamazaki, K. Kamijo, A. Kenmochi, S. Fukuzumi, T. Kiyuna, Y. Takaki, and Y. Kuroiwa. Multiple equivalent current dipole source localization of visual event-related potentials during oddball paradigm with motor response. *Brain Topography*, 12:159–175, 2000.

[147] R. J. Zatorre and P. Belin. Spectral and temporal processing in human auditory cortex. *Cerebral Cortex*, 11:946–953, 2001.

[148] R. J. Zatorre, T. A. Mondor, and A. C. Evans. Auditory attention to space and frequency activates similar cerebral systems. *NeuroImage*, 10:544–554, 1998.

[149] A. Zeman. Consciousness. *Brain*, 124:1263–1289, 2001.

# Acknowledgements

I would like to thank all those who made the present studies feasible; Barbara Burghardt, Esther Tauberschmidt and Steffen Ritter for their help in conducting MEG recordings here in Heidelberg, Roland Rutschmann and Stefan Uppenkamp for their help in acquiring fMRI data in Oldenburg. The latter deserves additional thanks for answering all my questions concerning the analysis of those data and for his hospitality. Next, I would like to thank *all* those who participated in the experiments (notwithstanding whether their data fitted my ideas!)—in particular those who made it to the Northern German lowland with one of its natives (*Velen Dank ok für't Mitföhr'n no Ollenborg un do denn für't Untenannerklamüüstern vunne Toonläng'n*). Thanks to the DFG for the financial support.

There are many who contributed to the present work by means of discussions or helpful comments on earlier drafts (with apologies to Flann O'Brien: *Second thoughts can never be odd thoughts!*). In particular, I would like to mention Alexander Gutschalk, Karsten Hoechstetter, Nicole Ille and Peter Schneider. The one who deserves most thanks here is André Rupp, because he fought his way through the labyrinth of the thesis' first version (and back again!). His comments helped to get things into a concise form. Thanks also to my supervisors who left me free space to investigate things that seemed fruitful to me but who were there when asked for support (both material and intellectual). In particular, if today I have something like a comprehensive picture of what physics is about I largely owe it to Hans Günter Dosch.

Thanks to Tobi who shared my fate over the last few months; without him, I would not have known whom to moan to on Sundays (*You really should get a prize for this, Tobi!*). Finally, I am much obliged to my family. My parents deserve thanks for their constant interest in my work and the progress of my thesis. Most of all, however, I thank my beloved wife Pia for her never ending support in so many different ways (and in particular for *having given* comments on stile and grammar), and our dear children Simon and Tale for keeping me down to earth each day. I dedicate this thesis to you.